Aspects of Perturbative Quantum Field Theory

A Dissertation presented

by

Stanislav Srednyak

to

The Graduate School

in Partial Fulfillment of the

Requirements

for the Degree of

Doctor of Philosophy

in

Physics

Stony Brook University

May 2014

Stony Brook University

The Graduate School

Stanislav Srednyak

We, the dissertation committee for the above candidate for the

Doctor of Philosophy degree, hereby recommend

acceptance of this dissertation

George Sterman - Dissertation Advisor
Distinguished Professor, Department of Physics and Astronomy

Abhay Deshpande - Chairperson of Defense
Professor, Department of Physics and Astronomy

Raju Venugopalan
Senior Scientist, Department of Physics, Brookhaven National Laboratory and
Adjunct Professor, Department of Physics and Astronomy, Stony Brook University

Mikhail Movshev
Associate Professor, Mathematics Department

This dissertation is accepted by the Graduate School

Charles Taber
Dean of the Graduate School

Abstract of the Dissertation

Aspects of Perturbative Quantum Field Theory

by

Stanislav Srednyak

Doctor of Philosophy

in

Physics

Stony Brook University

2014

This thesis consists of three parts. The first is devoted to the calculation of multiplicity of two-gluon production in heavy ion collisions in the framework of Colour Glass Condensate. The second exhibits a finite basis for the perturbative correlation functions at a given loop order. The third demonstrates that the number of integrations in a perturbative amplitude can be reduced in half in even dimensions, and provides explicit formula for such a reduction in the (2,2) signature.

Acknowledgments

I thank Raju Venugopalan and BNL Physics Department for support of the research that led to Chapter 2, and George Sterman and YITP for support of the research that led to Chapters 3 and 4. During the research, I was supported by a SCIDAC grant, LDRD grant from BNL and NSF grants PHY-0969739 and -1316617.

Contents

Chapter 1

Introduction.

Quantum field theory is built around the notions of free particles and small couplings. This theory had initial success in the explanation of the anomalous magnetic moment of the electron (modern reference [1]). Perturbation theory was extensively developed and applied with great success to a variety of situations and experiments in quantum electrodynamics (QED), for example muon anomalous magnetic moment [2], radiative shift in energy levels [7], and Bhabha (e^+e^-) scattering .

Perturbation theory starts from the choice of a set of fields and a classical Lagrangian. For scalar theory with quartic potential it is

$$L_{\lambda\phi^4} = \int d^D x (\frac{1}{2}\phi\Box\phi - \frac{1}{2}m^2\phi^2 - \frac{\lambda}{4!}\phi^4) \ . \tag{1.1}$$

For gauge theories the classical Lagrangian of quantum chromodynamics (QCD) is

$$L_{QCD} = \int d^D x (-\frac{1}{4}F_a^{\mu\nu}F_{\mu\nu,a} + \sum_i \psi_i(\hat{D} + m_i)\psi_i) \ . \tag{1.2}$$

Here $F_{\mu\nu} = [D_\mu(A), D_\nu(A)]$ is the field strength tensor in adjoint representation of the gauge group, $\hat{D}(A) = \gamma^\mu(\partial_\mu + igA_\mu^{(F)}(x))$ is the covariant derivative in the fundamental representation, and the sum is over flavors of quarks. It is assumed that the metric is pseudoriemannian with signature $(+1, -1, -1, -1)$. For QED, the gauge field is an abelien $U(1)$ field, in QCD, it is a non-abelian $SU(3, C)$ field.

Canonical quantization then consists of declaring the fields to be operators acting on a formal Hilbert space. This space is constructed through the action of polynomials in field operators on the vacuum state $|0\rangle$. The choice of operators proceeds as follows. One starts with the free field, and expands it into plane waves. For the free scalar field in 4 dimensions the expansion is

$$\phi(x) = \int \frac{d^3\overline{p}}{(2\pi)^{3/2}\sqrt{2\omega_p}}(a(\overline{p})e^{-ipx} + a^*(\overline{p})e^{+ipx}). \tag{1.3}$$

This equation holds for the interacting theory in the infinite past. We therefore put subindex in, to refer to the coefficients a. The coefficients $a_{in}(\overline{p}), a_{in}^*(\overline{p})$ satisfy commutation relations

$$[a_{in}(\overline{p}), a_{in}(\overline{p'})] = 0, [a_{in}^*(\overline{p}), a_{in}^*(\overline{p'})] = 0, [a_{in}(\overline{p}), a_{in}^*(\overline{p'})] = \delta(\overline{p} - \overline{p'}). \tag{1.4}$$

Field operators evolve according to the equations of motion. For the scalar field above, it is

$$\Box\phi(x) + m^2\phi + \lambda\phi^3(x) = 0 \ . \tag{1.5}$$

The perturbative correlation functions are expectation values of time-ordered products of these evolving operators

$$G(x_1, ..., x_n) = \langle 0|T\phi(x_1)...\phi(x_n)|0\rangle \ . \tag{1.6}$$

We will concentrate on Fourier transforms of these functions

$$G(p_1, ..., p_n) = \int dx_1...dx_n e^{-ip_1x_1}...e^{-ip_nx_n}G(x_1, ..., x_n). \tag{1.7}$$

Feynman rules allow to write explicit expressions for these time ordered products in terms of multiple intgrals of certain rational functions. The central part of this construction is the propagator $G(x) = \langle 0|T\phi(0)\phi(x)|\rangle$, i.e., the causal Green's function

$$G(x) = \int \frac{d^4p}{(2\pi)^4}\frac{1}{p^2 - m^2 + i\epsilon}. \tag{1.8}$$

The functions $G(p_1, ..., p_n)$ can be expanded perturbatively in the coupling constant. Terms in this expansion are enumerated by Feynman graphs. In the case of $\lambda\phi^4$ theory these are 4-valent undirected graphs. To each momentun p_i there corresponds an external line in the graph. To each internal line in the graph there corresponds momentum over which we perform integrations. There is a factor of λ and a delta function for each vertex in the diagram. This reduces the number of integrals to the number of loops in the diagram, along with an overall momentum conservation delta function

The conclusion of the described procedure is that each term in the perturbative expansion can be written as the multiple integral

$$G^D(p_1, ..., p_n) = \int_{R^n} d^{4L}q \frac{1}{\prod_\alpha(k_\alpha^2 - m_\alpha^2 + i\epsilon)} \tag{1.9}$$

where

$$k_\alpha = \sum_i \eta_{\alpha i}q_i + \lambda_{\alpha r}p_r, \tag{1.10}$$

$$\eta_{\alpha i}, \lambda_{\alpha r} = +1, 0, -1 \tag{1.11}$$

and the integration is performed over the contour R^n. Here we still use the Minkowski metric and suppress overall factors. These integrals constitute the main object of study in parts 2 and 3 of this thesis.

In the application of the above procedures, cross sections are the squares of the on shell S-matrix amplitudes. Matrix elements of the S-matrix are the residues of the Green functions on the mass shell poles of their external lines

$$< p_1, ..., p_n, out|q_1, ..., q_m, in >= \prod_{i=1}^{M}[(-i)(2\pi)^{-3/2}Z^{-1/2}(p_i^2 - m_i^2)]$$
$$\times \prod_{j=1}^{n}[(-i)(2\pi)^{-3/2}Z^{-1/2}(q_j^2 - m^2)]G(p_1, ..., p_n; -q_1, ..., -q_m). \tag{1.12}$$

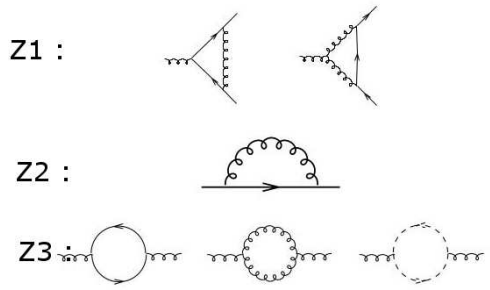

Figure 1.1: Lowest order diagrams giving contributions to the running coupling.

Here, Z is a factor that relates asymptotic non-interacting field with self-interacting field as the time goes to infinite past. Computationally, it is the residue of the two-point Green function $G(p)$ at $p^2 = m^2$. Thus it is possible to compute multiplicities in terms of residues at mass shell poles. This fact is used in the first part of the thesis.

The interpretation of UV divergences was a marked achievement in the development of QFT in 1950's. Two more developments were crucial for the establishment of the field theories of the standard model, including QCD. One was the realization that ghost fields are necessary for the quantization of gauge theories [10], and the other was the development of dimensional regularization [9]. Coupling constant renormalization factor is related to the renormalization factors Z_1, Z_2, Z_3 as

$$Z_g = \frac{Z_1}{Z_2} Z_3^{-1/2} \tag{1.13}$$

where Z_1 is the vertex renormalization factor, Z_2 is the fermion wave function renormalization factor, Z_3 is the gluon wave function renormalization factor (this factor includes ghost contribution). To the lowest order, they are the contributions from the diagrams on Figure 1.

Evaluation of these contributions gives the following result

$$Z_1 = -\frac{\alpha_s}{4\pi}\frac{1}{\epsilon}(C_A + C_F) + ... \tag{1.14}$$

$$Z_2 = -\frac{\alpha_s}{4\pi}\frac{1}{\epsilon}C_F + ... \tag{1.15}$$

$$Z_3 = \frac{\alpha_s}{4\pi}\frac{1}{\epsilon}(\frac{5}{3}C_A - \frac{4}{3}T_R n_f) + ... \tag{1.16}$$

where $\epsilon = 4 - D$ is the dimensional regularization parameter. The coefficient of the lowest order of the beta function

$$\mu^2 \frac{\partial \alpha_s(\mu)}{\partial \mu^2} = \beta(\alpha_s) \tag{1.17}$$

with

$$\beta = -\beta_0 \alpha_s^2 - \beta_1 \alpha_s^3 - ... \tag{1.18}$$

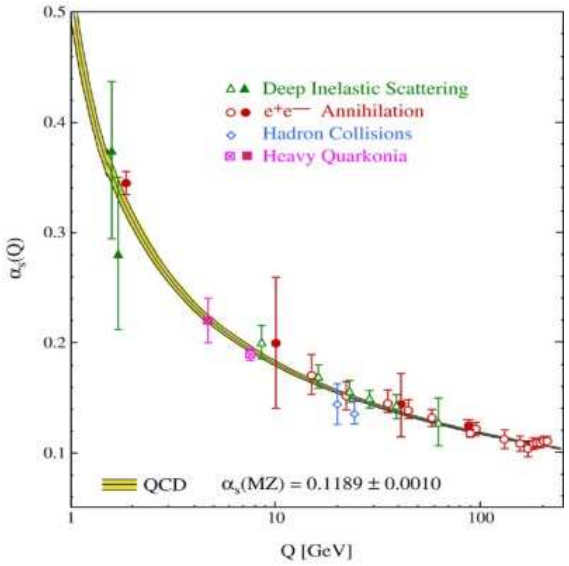

Figure 1.2: Coupling constant as function of renormalization scale. Theoretical calculations compared to the experiment [3].

where

$$\beta_0 = \frac{11C_A - 4T_R n_f}{12\pi} \ . \tag{1.19}$$

The observation that the first nonvanishing contribution to β has negative sign was of great importance for the establishment of QCD. Modern experiments [3] give the plot of $\alpha_s(\mu)$ shown at Figure 2.

The first part of the thesis, [4], is concerned with multiplicity calculation for the two particle spectrum. There is a remarkable ridge behaviour - the cross section has a jump at the zero angular separation that extends over a large rapidity interval. Colour Glass Condensate sums a subset of perturbative diagrams that are built from retarded Green's functions, and that are rooted on the strong colour fields spread around backward light cone, the latter having certain distribution. This distribution is taken to be Gaussian in this thesis.

The set up of just described calculation can be related to the Green's function formalism mentioned before. Suppose that the field on the light cone that gives initial conditions for colour fields is weak, so that one can use perturbative expansion. Then the solution of the classical Yang-Mills equations can be expanded in initial conditions. Terms in such expansion can be enumerated by directed trees, quite similar to Feynman diagrams, but now there are retarded Green's functions instead of causal ones, and the trees are rooted on the sources. These sources are subsequently averaged with certain distrubution (Gaussian in our case). The continuation of this line of research has been reviewed recently in Ref. [12].

The second [5] and third [6] part of the thesis are concerned with the study of purely perturbative Green's functions. At this moment perturbative causal Green's functions are known only in the form of integral representations. Due to $i\epsilon$ prescription, these integral representations amount to holomorphic functions defined on the compliment of Landau varieties in the space of complex external momenta. At present, only one loop multileg Green's

functions are relatively well understood [8].

At a given loop order, there are infinitely many Green's functions. They differ by the number of external legs. In the second part of this thesis it is shown that there is a finite basis of functions such that the original functions are expressed as linear combinations of the elements of this basis with coefficients rational in the external momenta. The explicit form of the rational coefficients is obtained. The functions in the basis are integrals of rational functions. In the case of scalar field theory, in the standard patch of compactified loop momenta space, these rational functions have constant numerator, and several quadratic and linear factors in the denominator. There is one quadratic factor for each line in a diagram obtained from the given one by amputating all external lines. There are up to $D+1$, where D is the dimension of space-time, linear factors for each such line. Thus, at the given loop order, there are finitely many basic functions. There is subtlety in choosing "contours" of integration in the basic functions, as the original contour intersects the zero sets of the linear factors. This question is not studied. It is our hope that there is a choise of "contour" (in fact, an equivalence class of contours) that do not intersect zero loci of the factors in the denominator of the basis functions, and which can be chosen as a representative for the integral.

The third part of the thesis demonstrates that the number of integrations, for a given diagram, can be reduced in half, assuming even dimensionality. This can be demonstrated ecplicitely, with a different from the usual choice of signature, i.e. (2,2)-signature. Then, using anliticity arguments, we suggest that the same conclusion is true for any choice of signature. The reduction is checked for box diagrams.

The thesis is concluded with some speculations on algebro-geometric and number-theoretic nature of perturbative amplitudes.

Chapter 2

Non-perturbative computation of double inclusive gluon production in the Glasma.

2.1 Introduction

At very high energies, the collision of two nuclei can be conveniently described as the collision of two Color Glass Condensates (CGCs) [13, 14, 15]. In this description, the wavefunctions of the nuclei are comprised of high occupation number classical gluon fields at small x coupled to static light cone color sources at large x. The separation between fields and sources evolves with energy; one obtains evolution equations for multi-parton correlations in the nuclear wavefunctions called JIMWLK renormalization group equations [14]. After the collision, the coherence of the nuclear wavefunction is lost; large x sources are no longer static and become sources for multi-particle production in the forward light cone [16]. For early times $\tau \sim 1/Q_{\rm s}$, where $Q_{\rm s}$ is the saturation scale, the non-equilibrium produced matter with high occupation number of order $1/\alpha_{\rm s}$ has remarkable properties [17, 18] and is termed the Glasma [19]. For reviews, see Ref. [20].

Recently, high energy factorization theorems were derived for inclusive multi-gluon production in a rapidity interval $\Delta y \lesssim 1/\alpha_{\rm s}$ [21, 22] in A+A collisions. The result can be expressed very compactly as [22]

$$\left\langle \frac{{\rm d}^n N_n}{{\rm d}^3\boldsymbol{p}_1 \cdots {\rm d}^3\boldsymbol{p}_n} \right\rangle_{\rm LLog} = \int \big[D\rho_1\big]\big[D\rho_2\big]\; Z_y\big[\rho_1\big]\, Z_y\big[\rho_2\big] \;\; \frac{{\rm d}N}{{\rm d}^3\boldsymbol{p}_1}\bigg|_{\rm LO} \cdots \frac{{\rm d}N}{{\rm d}^3\boldsymbol{p}_n}\bigg|_{\rm LO} \,. \tag{2.1}$$

The Z's are gauge invariant weight functionals that describe the distribution of color sources at the rapidity of interest. They are obtained in full generality by evolving the JIMWLK equations from an initial rapidity close to the beam rapidity. In the large $N_{\rm c}$ limit, the weight functionals Z can instead be obtained from the simpler mean field Balitsky–Kovchegov (BK) [23] equation. In this case, they can be represented as non-local Gaussian distributions in the sources [24]. For large nuclei, without significant small x evolution, one recovers the local Gaussian distributions of the McLerran-Venugopalan (MV) model [13]. We emphasize that the validity of eq. (2.1) is restricted to the kinematics where all the produced particles

are measured within a rapidity interval $\lesssim 1/\alpha_{\rm s}$ from each other, so that we can evaluate Z at this same rapidity $y_1 \approx \cdots \approx y_n \approx y$. The generalization to larger rapidity separations is non-trivial because one needs to account for the gluon radiation in the region between the tagged gluons. A formalism describing arbitrarily long range rapidity separations has been developed recently [25]. For simplicity, we shall not consider it further here.

The leading order single particle distributions in eq. (2.1) are given by

$$E_{\boldsymbol{p}} \frac{{\rm d}N}{{\rm d}^3\boldsymbol{p}}\bigg|_{\rm LO} \Big[\rho_1, \rho_2\Big] = \frac{1}{16\pi^3} \lim_{x_0 \to +\infty} \int {\rm d}^3\boldsymbol{x}\ {\rm d}^3\boldsymbol{y}\ e^{ip\cdot(x-y)}\ (\partial_x^0 - iE_{\boldsymbol{p}})(\partial_y^0 + iE_{\boldsymbol{p}}) \times \sum_\lambda \epsilon_\lambda^\mu(\boldsymbol{p})\epsilon_\lambda^\nu(\boldsymbol{p})\ A_\mu^{a,{\rm cl.}}[\rho_1,\rho_2](x)\ A_\nu^{a,{\rm cl.}}[\rho_1,\rho_2](y)\ . \quad (2.2)$$

For each configuration of sources ρ_1 and ρ_2 respectively, of each of the nuclei, one can solve classical Yang–Mills equations to compute the gauge fields $A_\mu^{\rm cl.}[\rho_1,\rho_2]$ in the forward light cone [26, 27, 28, 29, 30]. When our expression for the corresponding single inclusive distribution is substituted in eq. (2.1), and the distributions are averaged over with the distributions Z, one has determined from first principles (to all orders in perturbation theory and to leading logarithmic accuracy[1] in x), the n-gluon inclusive distribution in high energy A+A collisions at proper times $\tau \sim 1/Q_{\rm s}$. As noted previously, eq. (2.1) is valid only for $\Delta Y \lesssim 1/\alpha_{\rm s} \sim 3-5$ units of rapidity in A+A collisions at RHIC and the LHC respectively.

In the nuclei, before the collision, the typical range of color correlations is of the order of the inverse saturation scale $Q_{\rm s}^{-1}$, where ${Q_{\rm s}}^{-1} < {\Lambda_{\rm QCD}}^{-1}$. The saturation scale at a given transverse position in the nucleus depends on the two dimensional transverse projection of the nuclear matter distribution. In eq. (2.1), it appears in the initial conditions for the Z functionals; the energy evolution of the saturation scale is determined by the JIMWLK renormalization group equations. Because the saturation scales in the two nuclei are the only scales in the problem (besides nuclear radii), their properties determine the energy and centrality dependence of the inclusive observables.

The expression in eq. (2.1) is remarkable because it suggests that in a single event–corresponding to a particular configuration of color sources–the leading contribution is from n tagged gluons that are produced independently. The coherence in n-gluon emission is generated by averaging over color sources that vary from event to event. Because the range of color correlations in the transverse plane is of order $1/Q_{\rm s}$, the high energy factorization formalism suggests an intuitive picture of correlated multiparticle production arising from event by event fluctuations in particle production from $\sim R_A^2/1/Q_{\rm s}^2 = R_A^2 Q_{\rm s}^2$ color flux tubes of size $1/Q_{\rm s}$.

The color flux tubes, called Glasma flux tubes, are approximately boost invariant in rapidity because of the underlying boost invariance of the classical fields[2]. Besides providing the underlying geometrical structure for long range rapidity correlations, the Glasma flux tubes also carry topological charge [18], which may result in observable metastable CP-violating domains [31]. While eqs. (2.1) and (2.2) describe particle production from the Glasma flux

[1] Note that what we mean by leading log of x here means resumming the leading dependence in rapidity between the observed gluons and the projectiles; not between the different produced gluons.

[2] For rapidity separations $\gtrsim 1/\alpha_{\rm s}$, one expects significant violations of boost invariance from quantum corrections [25].

tubes, they do not describe the subsequent final state interactions of the produced gluons which become important for times $\tau \gg 1/Q_{\rm s}$.

If, as widely believed, the produced matter thermalizes by final state interactions, these will not significantly alter long range rapidity correlations because the effects of fragmentation, hadronization or resonance decays are typically restricted to $\Delta y \approx 1 \ll 1/\alpha_{\rm s}$. However, radial flow will have a significant effect on the observed angular correlations. This is because particles produced isotropically in a given flux tube will be correlated by the radial outward hydrodynamic flow of the flux tubes. Ideas on the angular collimation of particle distributions by flow were discussed previously in the literature [32, 33]. When combined with the long range rapidity correlations provided by the Glasma flux tubes, they provide a natural explanation [34, 35] of "ridge" like structures [36, 37] seen in the nearside spectrum of two particle correlated hadron pairs in A+A collisions. A similar structure is seen in three hadron correlations as well [38].

These structures were first seen in near side events with prominent jet like structures, where the spectrum of associated particles is observed to be collimated in the azimuthal separation $\Delta\varphi$ relative to the jet and shows a nearly constant amplitude in the strength of the pseudo-rapidity correlation $\Delta\eta$ up to $\Delta\eta \sim 1.5$ [36]. The name "ridge" follows from the visual appearance of these structures as an extended mountain ridge in the $\Delta\eta$-$\Delta\varphi$ plane associated with a narrow jet peak. This collimated correlation persists up to $\Delta\eta \sim 4$ [39]. An important feature of ridge correlations is that the above described structure is seen in two particle correlations without a jet trigger and persists without significant modification for the triggered events [40]. These events include all hadrons with momenta $p_T \geq 150$ MeV. In such events, a sharp rise in the amplitude of the ridge is seen [40, 41] in going from peripheral to central collisions. A number of theoretical models have been put forth to explain these ridge correlations [33, 42]. For a recent critical evaluation of these models, we refer the reader to Ref. [43].

In this paper, our primary purpose is to discuss how the Glasma flux tube picture arises *ab initio* from solving eqs. (2.1) and (2.2). In Ref. [34], it was argued that the two particle correlation function

$$C_2(\boldsymbol{p},\boldsymbol{q}) \equiv \left\langle \frac{{\rm d}^2 N_2}{{\rm d}y_p\, {\rm d}^2\mathbf{p}_T\, {\rm d}y_q\, {\rm d}^2\mathbf{q}_T} \right\rangle - \left\langle \frac{{\rm d}N}{{\rm d}y_p\, {\rm d}^2\mathbf{p}_T} \right\rangle \left\langle \frac{{\rm d}N}{{\rm d}y_q d^2\mathbf{q}_T} \right\rangle , \tag{2.3}$$

in the Glasma flux tube picture took on the simple geometrical form

$$\frac{C_2(\boldsymbol{p},\boldsymbol{q})}{\left\langle \frac{{\rm d}N}{{\rm d}y_p\, {\rm d}^2\mathbf{p}_T} \right\rangle \left\langle \frac{{\rm d}N}{{\rm d}y_q\, {\rm d}^2\mathbf{q}_T} \right\rangle} = \kappa_2\, \frac{1}{S_\perp Q_{\rm s}^2} , \tag{2.4}$$

where the right hand side of this relation is simply a non-perturbative constant κ_2 multiplied by the ratio of the transverse area of the flux tube to the transverse overlap area of the nuclei. This nice geometrical identity however is a conjecture based on a perturbative computation whose regime of validity is the kinematic region $p_T, q_T \gg Q_{\rm s}$, where one expects additional contributions, besides those arising from strong sources, to contribute significantly. Similar arguments, based on perturbative computations were used to generalize the result in eq. (2.4) to 3-particle correlations [44] and subsequently, even n-particle correlations [45]. In the latter

paper, it was shown that the general structure of n-gluon emissions is a negative binomial distribution.

Because the geometrical structure of the correlations is so striking and with manifest consequences, it is important to establish that is has a validity beyond perturbation theory. The perturbative expressions extended to lower momenta are strongly infrared divergent so it is not obvious whether they are regulated in that regime by the confinement scale of the order of $\Lambda_{\rm QCD}$ or instead a semi-hard scale of order $Q_{\rm s}^{-1}$ arising from the weak coupling albeit non–perturbative dynamics of the Glasma fields. We will tackle the problem head-on in this paper and investigate the form of eq. (2.3) in this paper. We will do so by solving the Yang–Mills equations in eq. (2.2) in full generality numerically on a space-time lattice. Our non-perturbative results from the lattice simulations are valid[3] in the entire kinematic domain of transverse momenta–from the smallest infrared scale given by the lattice size to the largest ultraviolet scale given by the lattice spacing. In physical units, these correspond to the inverse nuclear size and large momenta ($p_T, q_T \gg Q_{\rm s}$).

One can of course, on dimensional grounds, always express the r.h.s of eq. (2.4) as shown. However, κ_2 in general can depend on the dimensionless ratios $Q_{\rm s}/p_T$, $Q_{\rm s}/q_T$, the relative azimuthal angle $\Delta\varphi$ between the two gluons, and the dimensionless combinations $Q_{\rm s}R_A$ and $m/Q_{\rm s}$, where m is an infrared scale of order $\Lambda_{\rm QCD}$ and R_A is the nuclear radius. We will examine the dependence of κ_2 on these parameters carefully and discuss what they tell us about the structure of correlations. We find that the Glasma flux tube picture is valid; however, while the size of transverse correlations is still a semi-hard scale, it is not simply $Q_{\rm s}$ and does display some sensitivity to infrared physics. Our results are important for quantitative explanations of the ridge as resulting from Glasma flux tubes. In the semi-quantitative computation of Ref. [35], κ_2 was implicitly taken to be a free parameter and fit to the data–we will compare our result to this value. We will also compare our result to the value obtained by comparing the Glasma multiplicity distribution [45] to PHENIX data on multiplicity distributions at RHIC [46].

In section 2.2, we will review perturbative computations of multi-particle production in the Glasma. The non-perturbative computation will be discussed in Section 2.3. We will briefly outline the numerical approach, clearly stating the lattice parameters, their relation to physical parameters, and the approach to the continuum limit in the transverse and longitudinal co-ordinates. We will then systematically study the dependence of our results on the saturation scale, the nuclear size and the infrared cutoff m. In section 2.4, we will discuss the physical implications of our results and further refinements for quantitative comparison with experiment. We will end with a brief summary of our key results. Some details of the numerical computation are discusssed in an appendix.

2.2 Perturbative results for multi-particle production

The perturbative computation of two, three and n-gluon correlations in the Glasma have been discussed elsewhere [34, 44, 45]. For completeness, we will briefly review the results

[3]We emphasize however that at very large momenta there will be additional contributions to the distributions beyond the purely classical one discussed here.

here. The correlated two particle inclusive distribution can be expressed as

$$C(\boldsymbol{p},\boldsymbol{q}) = \frac{1}{4(2\pi)^6}\sum_{a,a';\lambda,\lambda'}\left\langle|\mathcal{M}^{aa'}_{\lambda\lambda'}(\boldsymbol{p},\boldsymbol{q})|^2\right\rangle - \left\langle|\mathcal{M}^{a}_{\lambda}(\boldsymbol{p})|^2\right\rangle\left\langle|\mathcal{M}^{a'}_{\lambda'}(\boldsymbol{q})|^2\right\rangle \ , \tag{2.5}$$

where the classical contribution to the amplitude for the production of a pair of gluons with momenta $\boldsymbol{p}$ and $\boldsymbol{q}$ is

$$\begin{aligned}\mathcal{M}^{aa'}_{\lambda\lambda'}(\boldsymbol{p},\boldsymbol{q}) &= \epsilon^{\lambda}_{\mu}(\boldsymbol{p})\,\epsilon^{\lambda'}_{\nu}(\boldsymbol{q})\,p^2q^2\,A^{\mu,a}(\boldsymbol{p})\,A^{\nu,a'}(\boldsymbol{q})\ ,\\ \mathcal{M}^{a}_{\lambda}(\boldsymbol{p}) &= \epsilon^{\lambda}_{\mu}(\boldsymbol{p})\,p^2\,A^{\mu,a}(\boldsymbol{p})\ .\end{aligned} \tag{2.6}$$

Here the ϵ's are the polarization vectors of the gluons and a, a' are the color indices of the gauge fields. The average $\langle\cdots\rangle$ in eq. (2.5) is an average over the color configurations of the two nuclei; this average will be discussed further shortly.

The gauge fields have a very non-trivial, non–linear dependence on the sources ρ_1 and ρ_2, which evolves as a function of the proper time τ. As mentioned previously, they can be determined by numerically solving Yang-Mills equations for $\tau \geq 0$ with initial conditions at $\tau = 0$ given by the gauge fields of each of the nuclei before the collision [26, 27, 29]. We will discuss these numerical solutions further in the next section. For large transverse momenta $p_T \gg Q_{\rm s}$, however, the equations of motion can be linearized and one can express the classical gauge fields produced in the nuclear collision as [17, 47, 48, 49]

$$p^2A^{\mu,a}(\boldsymbol{p}) = -if_{abc}\,g^3\int\frac{\mathrm{d}^2\mathbf{k}_T}{(2\pi)^2}\,L^{\mu}(\boldsymbol{p},\mathbf{k}_T)\,\frac{\rho_1^b(\mathbf{k}_T)\rho_2^c(\mathbf{p}_T-\mathbf{k}_T)}{\mathbf{k}_T^2(\mathbf{p}_T-\mathbf{k}_T)^2}\ . \tag{2.7}$$

Here f_{abc} are the SU(3) structure constants, L^{μ} is the well known[4] Lipatov vertex and ρ_1, ρ_2 are respectively the Fourier transforms of the color charge densities in the two nuclei [15].

From eq. (2.1), the average in eq. (2.5) corresponds to

$$\langle\mathcal{O}\rangle \equiv \int[D\rho_1\,D\rho_2]Z[\rho_1]Z[\rho_2]\,\mathcal{O}[\rho_1,\rho_2]\ . \tag{2.8}$$

In the MV model [13, 50]

$$Z[\rho] \equiv \exp\left(-\int\mathrm{d}^2\mathbf{x}_T\frac{\rho^a(\mathbf{x}_T)\rho^a(\mathbf{x}_T)}{2\,\mu_{_A}^2}\right)\ , \tag{2.9}$$

where ρ can be either ρ_1 or ρ_2. As we will discuss further in the next section, the color charge squared per unit area $\mu_{_A}^2$ can be expressed simply in terms of $Q_{\rm s}$. We will consider this Gaussian model in the rest of this paper[5]. For these Gaussian correlations, in momentum space,

$$\left\langle\rho^a(\mathbf{k}_T)\rho^b(\mathbf{k}'_T)\right\rangle = (2\pi)^2\mu_{_A}^2\,\delta^{ab}\delta(\mathbf{k}_T-\mathbf{k}'_T)\ . \tag{2.10}$$

[4]The components of this four vector are given explicitly by $L^+(\boldsymbol{p},\mathbf{k}_T) = -\frac{\mathbf{k}_T^2}{p^-}$, $L^-(\boldsymbol{p},\mathbf{k}_T) = \frac{(\mathbf{p}_T-\mathbf{k}_T)^2-{\mathbf{p}_T}^2}{p^+}$, $L^i(\boldsymbol{p},\mathbf{k}_T) = -2\,\mathbf{k}_T^i$.

[5]In the simplest treatment of small x evolution, based on the Balitsky-Kovchegov equation [23], $Z[\rho]$ can also be modelled by a Gaussian, albeit one with a non-local variance [49, 51].

Using eq. (2.7), (2.8) and (2.9) in eq. (2.5), one obtains [34],

$$C(\boldsymbol{p},\boldsymbol{q}) = \frac{S_\perp}{16\,\pi^7}\,\frac{(g^2\mu_{_A})^8}{g^4\,Q_{\rm s}^2}\,\frac{N_c^2(N_c^2-1)}{p_T^4\,q_T^4}\,. \tag{2.11}$$

It is instructive to express the result in eq. (2.11) in terms of the inclusive single gluon spectrum. This result, due originally to Gunion and Bertsch [52], has been been recovered previously in the CGC framework [17, 47, 53, 54] and is known to have the form

$$\left\langle \frac{{\rm d}N}{{\rm d}y_p\,{\rm d}^2\mathbf{p}_T}\right\rangle = \frac{S_\perp}{4\pi^4}\,\frac{(g^2\mu_{_A})^4}{g^2}\,\frac{N_c(N_c^2-1)}{p_T^4}\,\ln\left(\frac{p_T}{Q_{\rm s}}\right)\,. \tag{2.12}$$

Substituting eq. (2.12) on the r.h.s of eq. (2.11), one obtains

$$C(\boldsymbol{p},\boldsymbol{q}) = \frac{\kappa_2}{S_\perp Q_{\rm s}^2}\left\langle \frac{{\rm d}N}{{\rm d}y_p\,{\rm d}^2\mathbf{p}_T}\right\rangle\left\langle \frac{{\rm d}N}{{\rm d}y_q\,{\rm d}^2\mathbf{q}_T}\right\rangle\,, \tag{2.13}$$

which is the result we noted in eq. (2.4), with[6]

$$\kappa_2 \approx \frac{\pi}{(N_c^2-1)} = 0.4 \tag{2.14}$$

Identifying the theoretical error on κ_2 is difficult at this stage from the perturbative computation.

Computing κ_2 non–perturbatively by numerically solving the Yang–Mills equations is the primary objective of this paper. This quantity is not a pure number but can contain interesting structure. In the perturbative calculation, κ_2 is independent of the relative angle $\Delta\varphi$ at very large transverse momenta $p_T,\ q_T \gg Q_{\rm s}$. However, even in the perturbative calculations, one notices that there are finite azimuthal correlations between gluons as one goes away from the limit of asymptotically large transverse momenta. It is important to understand these correlations at momenta of interest to experiment to ascertain whether they have any phenomenological significance. Further, κ_2 can depend non-trivially on the transverse momenta of the pairs and on the energy and centrality of the nuclear collision. Finally, we want to determine whether κ_2 is infrared finite. This was the case for the analogous factor for the non-perturbative single gluon distribution at any finite time [26]; there is no guarantee that this should be the case for multi-gluon distributions.

Before we end this section, we should mention that perturbative computations were also performed for 3-gluon [44] and n-gluon correlations [45]. The result can be nicely summarized in terms of the cumulants of the multiplicity distribution as [45]

$$\left\langle \frac{{\rm d}^nN}{{\rm d}y_1\,{\rm d}^2\mathbf{p}_{T1}\cdots{\rm d}y_n\,{\rm d}^2\mathbf{p}_{Tn}}\right\rangle = \frac{(n-1)!}{k^{n-1}}\left\langle \frac{{\rm d}N}{{\rm d}y_1\,{\rm d}^2\mathbf{p}_{T1}}\right\rangle\times\cdots\times\left\langle \frac{{\rm d}N}{{\rm d}y_n\,{\rm d}^2\mathbf{p}_{Tn}}\right\rangle\,, \tag{2.15}$$

where

$$k = \zeta\,\frac{(N_c^2-1)Q_{\rm s}^2S_\perp}{2\pi}\,. \tag{2.16}$$

[6] In the computation of Ref. [34], there were numerical errors which gave a significantly larger perturbative estimate for κ_2.

Here ζ, is a non–perturbative coefficient[7] to be determined by numerical solutions of Yang-Mills equations. The expression in eq. (2.15) corresponds to a negative binomial distribution. One can extract ζ from fits to the multiplicity distribution data [46] and compare our non-perturbative result for κ_2 to this value thereby testing the validity of eq. (2.15) for the 2nd cumulant. Our approach can be straightforwardly be extended to higher cumulants but the computations are numerically intensive and will not be considered further here.

2.3 Non-perturbative computation

The two gluon cumulant, on dimensional grounds, can always be expressed in the form given in eq. (2.13). However, as we have noted previously, the dimensionless coefficient κ_2 can in general be a function of $Q_{\rm s}/p_T, Q_{\rm s}/q_T, \Delta\varphi, Q_{\rm s}R_A$ and $m/Q_{\rm s}$, where m is an infrared regulator scale that can be added to the MV model. If we assume that $m \sim \Lambda_{\rm QCD}$, the high energy asymptotics of our formalism is $m/Q_{\rm s} \ll 1$ and $Q_{\rm s}R_A \to \infty$. For A+A collisions at realistic RHIC and LHC energies, one expects $m/Q_{\rm s} \sim 0.2 - 0.1$ and $Q_{\rm s}R_A = 35 - 70$ respectively. We will return to the discussion of the infrared scale m later at the end of sec. 2.4.

For asymptotically large p_T, $q_T \gg Q_{\rm s}$, we anticipate, on the basis of our perturbative results, that $\kappa_2 \to$ constant. For p_T, $q_T \leq Q_{\rm s}$, we will determine the dependence of κ_2 on these ratios. In particular, we would like to determine whether the double inclusive gluon distribution is rendered infrared safe by the non-linearities of the Yang-Mills fields that may generate a mass scale (analogous to a plasmon mass) for finite times $\tau \gtrsim 1/Q_{\rm s}$.

2.3.1 Numerical approach

The numerical solutions of the classical Yang–Mills equations have been discussed at length elsewhere [26, 27, 29] and we will only outline the approach followed here for completeness. In the MV model [13], the Yang-Mills equations

$$[D_\mu, F^{\mu\nu}] = J^\nu. \tag{2.17}$$

have the source currents

$$J^\mu = \delta^{\mu+}\rho_1(\mathbf{x}_T, x^-) + \delta^{\mu-}\rho_2(\mathbf{x}_T, x^+), \tag{2.18}$$

where the color charge densities $\rho_{1,2}$ of the two nuclei are independent static color sources localized on the light cone $\rho_{1,2}(\mathbf{x}_T, x^\mp) \sim \rho_{1,2}(\mathbf{x}_T)\delta(x^\mp)$. They are distributed with the Gaussian probability distribution

$$\langle \rho^a(\mathbf{x}_T)\rho^b(\mathbf{y}_T)\rangle = g^2\mu_A^2\delta^{ab}\delta^2(\mathbf{x}_T - \mathbf{y}_T), \tag{2.19}$$

where $\mathbf{x}_T$ and $\mathbf{y}_T$ are vectors in the transverse plane. The initial conditions for the solutions of these equations in the forward light cone in the Fock–Schwinger gauge ($A^\tau = 0$) are given

[7] In the perturbative computation for the two and three particle correlations, this number was taken to be $\zeta = 2$.

by

$$\begin{aligned} A^i|_{\tau=0} &= A_1^i + A_2^i, \\ A^\eta|_{\tau=0} &= \frac{ig}{2}[A_1^i, A_2^i]\,, \end{aligned} \tag{2.20}$$

with

$$A_{1,2}^i = -\frac{i}{g} V_{1,2} \partial^i V_{1,2}^\dagger \text{ and } \boldsymbol{\nabla}_T^2 \Lambda_{1,2} = -g\rho_{1,2}\,. \tag{2.21}$$

where

$$V_{1,2} = \mathcal{P}_\mp\, e^{i\Lambda_{1,2}}. \tag{2.22}$$

It is convenient in the forward light cone to use the co-ordinate system $(\tau, \eta, \mathbf{x}_T)$, where $\tau^2 = t^2 - z^2$ and $\eta = 0.5\ln((t+z)/(t-z))$. The Yang-Mills equations in this co-ordinate system are manifestly boost invariant with the gauge fields independent of η, namely, $A^\mu \equiv A^\mu(\tau, \mathbf{x}_T)$. The symbol $\mathcal{P}_\mp$ denotes path ordering in the $\mp$ directions of the Wilson line $V_{1,2}$ respectively, which for nucleus 1 (nucleus 2) have an implicit dependence on x^- (x^+) in the solution. We will return to this point at the end of the subsection.

A subtle point we would like to emphasize is that the Wilson lines V, in the gauge field solution given by eq. (2.21) for nucleus 1 (nucleus 2) before the collision, are path ordered in x^- (x^+). This feature of the continuum solution is implemented by constructing the Wilson lines in consecutive steps representing a discretization of the longitudinal coordinate. On each lattice site $\mathbf{x}_T$ one constructs random color charges with a local Gaussian distribution

$$\left\langle \rho_k^a(\mathbf{x}_T)\rho_l^b(\mathbf{y}_T)\right\rangle = \delta^{ab}\delta^{kl}\delta^2(\mathbf{x}_T - \mathbf{y}_T)\frac{g^2\mu_A^2}{N_y}\,, \tag{2.23}$$

with the indices $k, l = 1, \ldots, N_y$ representing a discretized longitudinal coordinate. Numerical calculations of the single inclusive gluon distributions previously used $N_y = 1$, whereas the derivation of the analytical expression in eq. (2.21) required an extended source corresponding to the limit $N_y \to \infty$.

Our normalization is chosen to give

$$\sum_{k,l}\left\langle \rho_k^a(\mathbf{x}_T)\rho_l^b(\mathbf{y}_T)\right\rangle = \delta^{ab}\delta^2(\mathbf{x}_T - \mathbf{y}_T)g^2\mu_A^2. \tag{2.24}$$

The Wilson lines for the initial condition are then constructed from the sources eq. (2.23) by solving a Poisson equation and exponentiating it to give

$$V_{1,2}(\mathbf{x}_T) = \prod_{k=1}^{N_y} \exp\left\{-ig\frac{\rho_k^{1,2}(\mathbf{x}_T)}{\boldsymbol{\nabla}_T^2 + m^2}\right\}. \tag{2.25}$$

Here we have introduced an additional infrared regulator m into the MV model; some kind of infrared cutoff is required for inverting the Laplace operator. The single inclusive gluon distribution, integrated over transverse momenta, turns out to be weakly dependent on the infrared cutoff. One of the central aims of this paper is to study whether this is also the case for correlations. The parameter m plays an important role in the interpretation of our

results and we will return to it in our discussion of the results of our computations. We will return to the physical interpretation of the role of the parameter m later in our discussion. For large N_y the charge densities ρ_k in eq. (2.23) become small, and the individual elements in the product (2.25) approach identity. This is precisely the procedure that leads in the $N_y \to \infty$ limit to the continuum path ordered exponential in eq. (2.22).

The previous numerical computations of the single inclusive spectrum defined the gluon multiplicity in a manner that slightly deviates from the definition based on the LSZ formalism in eq. (2.2). In [29], taking advantage of the equipartition of energy in the classical theory, only the electric field parts of the numerical solution were used. Assuming a free dispersion relation the gluon multiplicity was taken to be

$$\frac{\mathrm{d}N}{\mathrm{d}^2\mathbf{k}_T\,\mathrm{d}y} = \frac{1}{(2\pi)^2}\frac{2}{|\mathbf{k}_T|}\mathrm{Tr}\left[\frac{1}{\tau}E^i(\mathbf{k}_T)E^i(-\mathbf{k}_T) + \tau E^\eta(\mathbf{k}_T)E^\eta(-\mathbf{k}_T)\right], \tag{2.26}$$

where the electric fields $E^i = \tau\dot{A}_i$ and $E^\eta = \dot{A}_\eta/\tau$ are time derivatives of the gauge potentials, defined here with the explicit factors of τ coming from the formulation of the theory in τ, η-coordinates. In Refs. [26, 27] the numerically obtained E- and A-fields were used to determine the dispersion relation of the interacting theory. This was then in turn used to determine the multiplicity, unlike the free dispersion relation assumed in eq. (2.2). In this work we use a definition that corresponds to eq. (2.2) and take the gluon spectrum as

$$\begin{aligned}\frac{\mathrm{d}N}{\mathrm{d}^2\mathbf{k}_T\,\mathrm{d}y} = \frac{1}{(2\pi)^2}\mathrm{Tr}\Bigg\{ & \frac{1}{\tau|\mathbf{k}_T|}E^i(\mathbf{k}_T)E^i(-\mathbf{k}_T) + \tau|\mathbf{k}_T|A_i(\mathbf{k}_T)A_i(-\mathbf{k}_T) && (2.27)\\ & + \frac{1}{|\mathbf{k}_T|}\tau E^\eta(\mathbf{k}_T)E^\eta(-\mathbf{k}_T) + \frac{|\mathbf{k}_T|}{\tau}A_\eta(\mathbf{k}_T)A_\eta(-\mathbf{k}_T) && (2.28)\\ & + i\Big[E^i(\mathbf{k}_T)A_i(-\mathbf{k}_T) - A_i(\mathbf{k}_T)E^i(-\mathbf{k}_T)\Big] && (2.29)\\ & + i\Big[E^\eta(\mathbf{k}_T)A_\eta(-\mathbf{k}_T) - A_\eta(\mathbf{k}_T)E^\eta(-\mathbf{k}_T)\Big]\Bigg\}, && (2.30)\end{aligned}$$

where the fields are evaluated in the 2-dimensional Coulomb gauge. The interference terms (2.29) and (2.30) are odd under the transformation $\mathbf{k}_T \to -\mathbf{k}_T$. They do not contribute when the gluon spectrum is averaged over the angle of $\mathbf{k}_T$, integrated over $\mathbf{k}_T$ or averaged over configurations of the sources. Thus neglecting them was justified when one was interested in the single inclusive gluon spectrum. In the case of two-gluon correlations they cannot, however, be neglected[8]. Due to these interference terms, the symmetry $n(\mathbf{k}_T) = n(-\mathbf{k}_T)$ does not hold configuration by configuration, but only on the average. Thus the correlation function $C(\mathbf{p}_T, \mathbf{q}_T) \neq C(\mathbf{p}_T, -\mathbf{q}_T)$. In particular, there is a peak in the correlation at $\mathbf{p}_T = \mathbf{q}_T$, which without the interference terms (2.29) and (2.30) would, by symmetry, imply a similar peak at $\mathbf{p}_T = -\mathbf{q}_T$. The main numerical effect of including these terms is that the backward peak at $\mathbf{p}_T = -\mathbf{q}_T$ is significantly depleted.

2.3.2 Parameters in the computation

From the discussion in the previous subsection, the parameters in the numerical lattice computation are

[8] We thank F. Gelis for pointing this out to us.

- $g^2\mu_A$, the root mean square color charge density.
- N_y, the number of points in the discretization of the longitudinal (x^- or rapidity) direction.
- The infrared regulator m. When $m = 0$, the Poisson equation is solved by leaving out the zero transverse momentum mode. This procedure corresponds to an infrared cutoff given by the size of the system.
- The lattice spacing a.
- The number of transverse lattice sites N_T, giving the transverse size of the lattice $L = N_T a$.

Of the dimensionful parameters a, $g^2\mu_A$ and m, only the dimensionless combinations $g^2\mu_A a$ and ma appear in the numerical calculation. The continuum limit $a \to 0$ is taken by letting $N_T \to \infty$ such that $g^2\mu_A a \to 0$ and $g^2\mu_A L = g^2\mu_A a N_T$ is a constant. This constant is determined by the physics input of the calculation. We have $\pi R_A^2 = L^2$ and, as we shall discuss in the next subsection, $g^2\mu_A$ is simply related to the saturation scale Q_s. The physical combination $Q_\mathrm{s}R_A$ relevant at RHIC and LHC energies will translate into corresponding values of $g^2\mu L$ in our computation. In sec. 2.4, we will explicitly translate our numerical results into physically relevant numbers. We note that there is another dimensionless combination $m/g^2\mu_A$-we will study the sensitivity of our results to this ratio.

2.3.3 Relating $g^2\mu_A$ and Q_s on the lattice

The root mean squared color charge density $g^2\mu_A$ that appears in our Glasma computations can be simply related to the saturation scale Q_s extracted from deeply inelastic scattering experiments. In these experiments, the cross section for a virtual photon scattering off a high energy hadron or nucleus is simply related to the dipole cross section of a quark-antiquark pair scattering off the hadron. This "dipole" cross-section is determined, in the CGC formalism, by the correlator of two Wilson lines in the fundamental representation of each of the nuclei before the collision as

$$\widetilde{C}^F(\mathbf{x}_T - \mathbf{y}_T) = \langle \operatorname{Tr} V^\dagger(\mathbf{x}_T) V(\mathbf{y}_T) \rangle \,, \tag{2.31}$$

with the expectation value $\langle\rangle$ evaluated with the distribution of the sources. For Gaussian correlators in the MV model of sources extended in the longitudinal direction,

$$\langle \rho^a(\mathbf{x}_T, x^-) \rho^b(\mathbf{y}_T, y^-) \rangle = g^2 \delta^{ab} \delta^2(\mathbf{x}_T - \mathbf{y}_T) \delta(x^- - y^-) \mu_A^2(x^-),$$

the Wilson line correlators can be computed analytically up to a logarithmic infrared cutoff that must be introduced in solving the Poisson equation in eq. (2.21). The result is

$$\widetilde{C}^F(\mathbf{x}_T) \approx N_c \exp\left(\frac{C_F}{8\pi} \chi \mathbf{x}_T^2 \ln(m|\mathbf{x}_T|) \right) , \tag{2.32}$$

with

$$\chi = g^4 \int dx^- \mu_A^2(x^-). \tag{2.33}$$

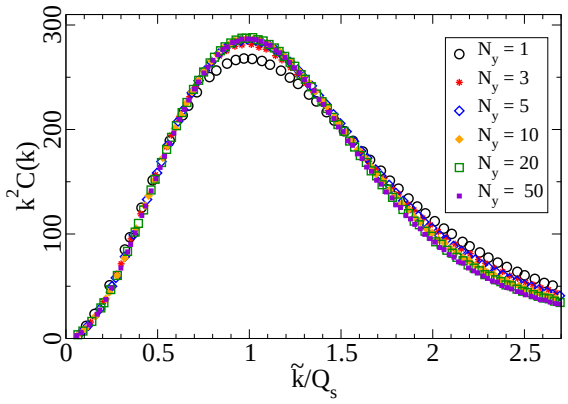

Figure 2.1: Adjoint representation Wilson line correlator for different N_y as a function of $\mathbf{k}_T/Q_{\rm s}$. From Ref. [55].

Alternately, the saturation scale $\tilde{Q}_{\rm s}$, in the fundamental representation, is defined as the momentum corresponding to the maximum of $\mathbf{k}_T^2\tilde{C}^F(\mathbf{k}_T)$, where $\tilde{C}^F(\mathbf{k}_T)$ is the Fourier transform of eq. (2.31). In this manner, one can relate the saturation scale to the root mean square color charge density.

The saturation scale defined previously is an inverse correlation length associated with the correlator of two Wilson lines in the fundamental representation. In a nuclear collision, it is the saturation scale in the adjoint representation that is relevant. It is defined, equivalently as the momentum corresponding to the maximum of $\mathbf{k}_T^2\tilde{C}^A(\mathbf{k}_T)$, where $\tilde{C}^A(\mathbf{k}_T)$ is the Fourier transform of the correlator of two adjoint Wilson lines

$$C^A(\mathbf{x}_T) = \langle V_{ab}(\mathbf{x}_T)V_{ab}(0)\rangle\,, \tag{2.34}$$

with

$$V_{ab}(\mathbf{x}_T) = 2\,{\rm Tr}\,\left[t^a V^\dagger(\mathbf{x}_T)t^b V(\mathbf{x}_T)\right]\,. \tag{2.35}$$

With some algebra, in the large N_c limit, the adjoint representation correlator can be related to a higher correlator of fundamental representation Wilson lines

$$C^A(\mathbf{x}_T) = \left\langle \left|\,{\rm Tr}\,\left[V^\dagger(\mathbf{x}_T)V(0)\right]\right|^2 - 1\right\rangle\,. \tag{2.36}$$

In the Gaussian MV model, one obtains

$$C^A(\mathbf{x}_T) \approx (N_c^2-1)\,\exp\left(\frac{N_c}{8\pi}\chi\mathbf{x}_T^2\ln(m|\mathbf{x}_T|)\right)\,. \tag{2.37}$$

The saturation scale $Q_{\rm s}$ in the adjoint representation, in identical fashion to the fundamental case, is defined as the momentum corresponding to the maximum of $\mathbf{k}_T^2\tilde{C}^A(\mathbf{k}_T)$, where $\tilde{C}^A(\mathbf{k}_T)$ is the Fourier transform of eq. (2.36). The adjoint Wilson line correlator is plotted in fig. 2.1 The two saturation scales are approximately related by the ratios of the Casimirs of the representations, namely, $Q_{\rm s}^2 \approx \frac{C_A}{C_F}\tilde{Q}_{\rm s}^{\,2}$.

Our definition of the saturation scale is not sensitive to the exact shape of the correlator for very large or small transverse momenta, and for a Gaussian correlator it reproduces the

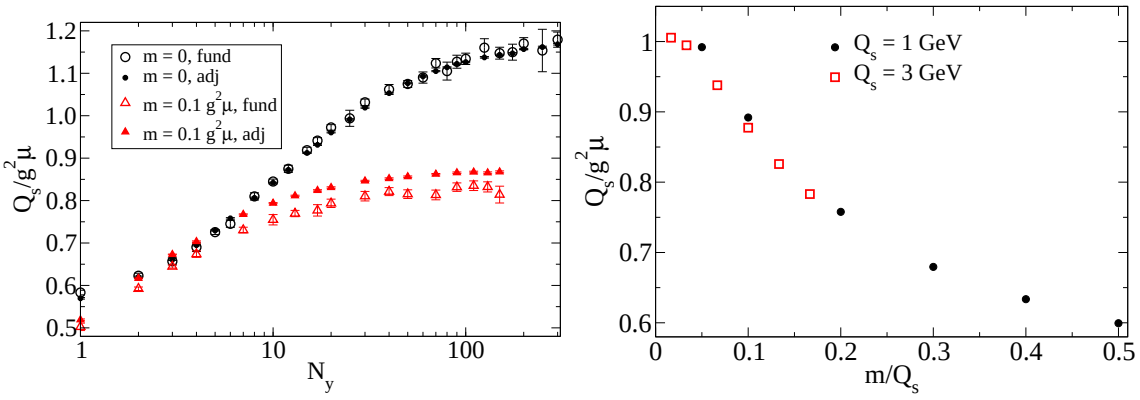

Figure 2.2: Left: $Q_{\rm s}/g^2\mu_A$ versus N_y. From Ref. [55]. Right: Dependence of the ratio $Q_{\rm s}/g^2\mu$ on $m/Q_{\rm s}$ for a fixed $Q_{\rm s} = 1$ GeV and $N_y = 50$. These are the conversion factors used to obtain the m-dependence of our results for fixed $Q_{\rm s}$ in fig. 2.9.

GBW saturation scale as $1/R_0^2 = \tilde{Q}_{\rm s}^{\,2}$. For small momenta, the fundamental and adjoint correlators look like Gaussians, which is the form used in the "GBW" fit of DIS data in Refs. [56]. For large momenta there is a power law tail $1/\mathbf{k}_T^4$ that differs from the original GBW fits, but resembles more closely the form required to match smoothly to DGLAP evolution for large Q^2 [57].

In Ref. [55], the relation between $Q_{\rm s}$ and $g^2\mu_A$ was studied extensively employing numerical lattice techniques. Discretizing the longitudinal distribution of sources as described in eq. (2.23) and constructing the Wilson line as in eq. (2.25), it was shown that $Q_{\rm s} \sim 0.57 g^2\mu_A$ for $N_y = 1$. This value was used in the numerical Glasma simulations of the single inclusive gluon spectrum. As we shall see in the following the gluon spectrum, when expressed in terms of the scaling variable $p_T/Q_{\rm s}$, is to a very good approximation independent of N_y. This is however not the case for the double inclusive spectrum, which will have a stronger dependence on N_y.

Due to the m-dependence of the single inclusive spectrum, the ratio κ_2 defined by eq. (2.4) will depend on m. To study this m-dependence for larger values of N_y (closer to the continuum limit in the longitudinal direction), we will need to invert the computation of $Q_{\rm s}$ as a function of $g^2\mu$ to obtain, as a function of $m/Q_{\rm s}$, the required values of $g^2\mu$ corresponding to a fixed value of $Q_{\rm s}$. The result of this exercise for $Q_{\rm s} = 1$ GeV and 3 GeV and using the numerical method employed in [55] is shown in fig. 2.2.

2.4 Results

We begin the discussion of our numerical results with the single particle spectrum because we are interested in the ratio of the double inclusive spectrum to the single particle spectrum squared. Some of the results for the single particle spectrum are new and have not been published elsewhere. We will then proceed to discuss the double inclusive spectrum and state our results for κ_2 defined in eq. (2.4).

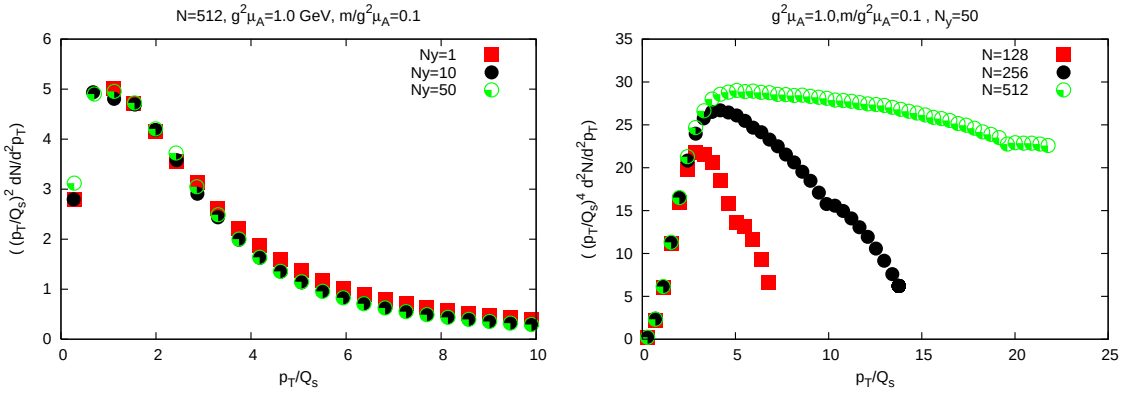

Figure 2.3: Left: The single particle spectrum (scaled by $(p_T/Q_s)^2$) for different N_y. Parameters are $g^2\mu = 1$ GeV, $N_T = 512$, IR cutoff fixed at $0.1g^2\mu$. Right: The single particle spectrum (scaled by $(p_T/Q_s)^4$) for different N_T. The continuum spectrum has a Q_s^4/p_T^4 behavior at $p_T \gg Q_s$; the convergence to this continuum behavior is clearly seen with increasing lattice size.

2.4.1 Single inclusive spectrum

The single inclusive multiplicity in A+A collisions was computed extensively previously by solving Yang-Mills equations numerically. We note that the single inclusive multiplicity computed gives excellent fits to the RHIC multiplicity data [28, 55] with values of Q_s for gold nuclei that agree to $\sim 10\%$ with those extracted from extrapolations of HERA data to RHIC [58]. In this sub-section, we will address some details of the computation that have not been presented previously and are relevant for the computation of κ_2.

In Ref. [55], the dependence of the single inclusive gluon distribution as a function of N_y was not computed. We have done it here and the result is shown in fig. 2.3. It shows that the single inclusive spectrum, scaled in units of $(p_T/Q_s)^2$, shows virtually no N_y dependence in particular for the moderate p_T region that dominates the integrated multiplicity. We may conclude that it has a weak dependence on N_y (for fixed m/Q_s) addressing a concern raised in Ref. [59]. The numerical single particle spectrum in the UV region is sensitive to the lattice spacing a, which, for a fixed value of Q_sR_A, translates into a dependence on the size of the lattice N_T. As shown in fig. 2.3, the spectrum approaches the continuum ultraviolet behavior of Q_s^4/p_T^4 with increasing lattice sizes from $N_T = 128^2$ to $N_T = 512^2$ lattices.

We studied the m/Q_s dependence of the single inclusive spectrum for a fixed large $N_y = 50$ and a 512×512 transverse lattice. The result is shown in fig. 2.4 (left). For small m/Q_s, the dependence of the spectrum on this quantity is quite weak-changing m/Q_s by a factor of 2 shows virtually no change in the spectrum. However, some dependence is seen when m/Q_s is increased, albeit the dependence is relatively weak in the $p_T \sim Q_s$ region which gives the dominant contribution to the integrated multiplicity. It should be kept in mind that the dependence of the spectrum on m/Q_s as shown is weaker than a logarithmic dependence even in the region where the dependence is the largest. It might seem counterintuitive that the value of an infrared scale m affects the gluon spectrum at such high momenta. One way to understand this is to keep in mind that the unitarity of the Wilson lines imposes a sum rule on their correlators, eqs. (2.31) and (2.36). Namely, because $\widetilde{C}^F(\mathbf{x}_T - \mathbf{y}_T = 0) = N_c$, the

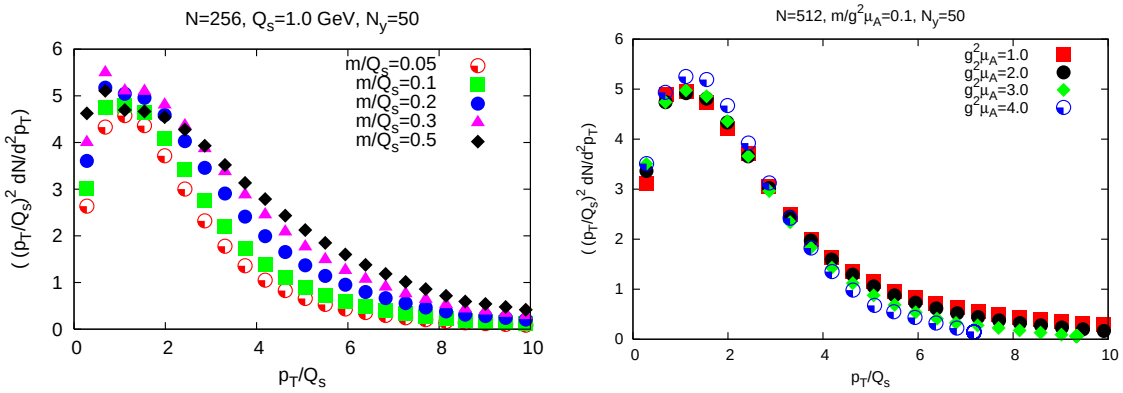

Figure 2.4: Left: The single particle spectrum for different m for $N_y = 50$, $N_T = 512$, and $Q_s = 1$ GeV. The spectrum is again scaled by $(p_T/Q_s)^2$. Right: The dependence of the single particle spectrum on $g^2\mu$ for a fixed $m/g^2\mu$.

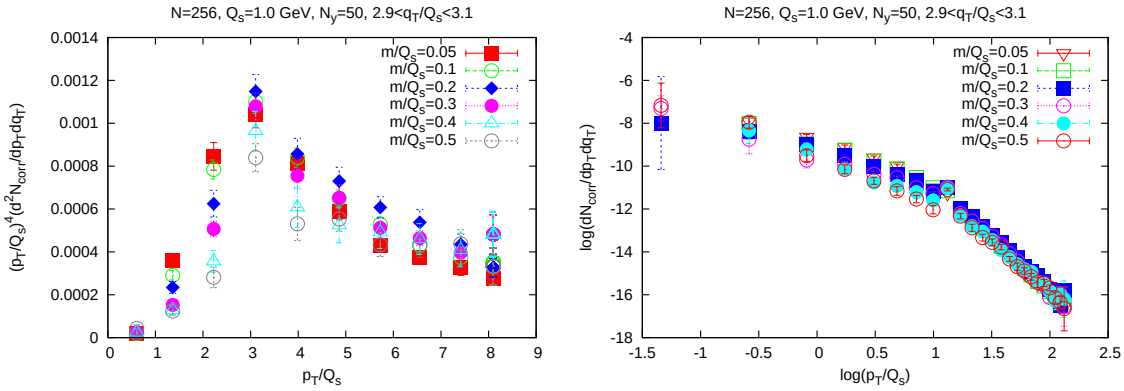

Figure 2.5: Sensitivity of the correlated part of the double inclusive spectrum to the value of IR cutoff m/Q_s. Left: Linear plot scaled by $(p_T/Q_s)^4$ to examine the anticipated perturbative behavior for large p_T. Right: Log-log plot of double correlated part of the double inclusive spectrum. The results are plotted for a small bin in q_T around $3\,Q_s$.

integral of the momentum space correlator $\int \mathrm{d}^2\mathbf{k}_T \widetilde{C}^F(\mathbf{k}_T) = (2\pi)^2 N_c$ is a constant. Thus a modification of the distribution in the infrared will also affect the UV behavior, which is also reflected in the gluon spectrum.

Finally, we plot in fig. 2.4 (right) the dependence of the single particle spectrum on the other dimensionless combination of scales $g^2\mu L$ for fixed $m/g^2\mu$. (This corresponds to a very good approximation to fixed m/Q_s.). Virtually no dependence is seen on this quantity, confirming the expectation that the single inclusive spectrum is completely insensitive to physics on scales corresponding to the size of the system. In summary therefore, the single particle spectrum is most sensitive to physics at the scale Q_s, weakly sensitive to physics on the scale m and completely insensitive to physics on the scale $1/R$.

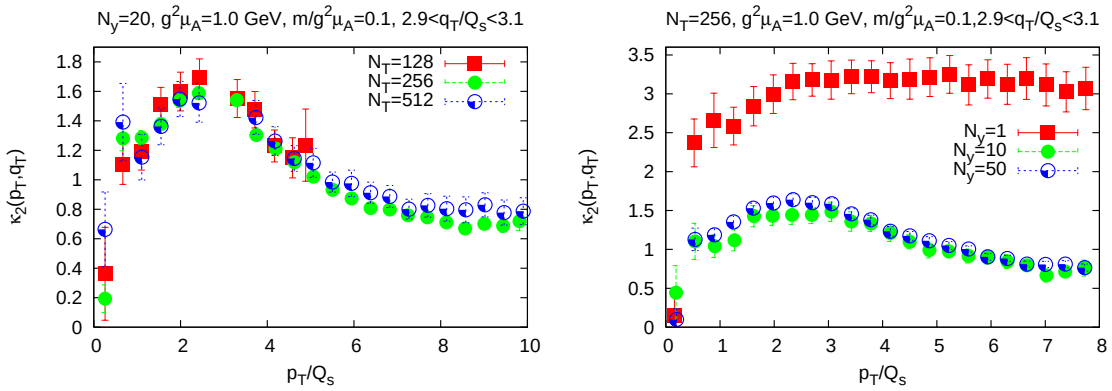

Figure 2.6: Left: Dependence of κ_2 on the transverse lattice size N_T as a function of p_T/Q_s for fixed q_T/Q_s. Right: Dependence of κ_2 on the number of points used in the construction of the path ordered exponential, N_y, as a function of p_T/Q_s for fixed q_T/Q_s.

2.4.2 Double inclusive spectrum

We now turn to the main focus of this study-the non-perturbative double inclusive gluon spectrum in A+A collisions. As in the single inclusive case studied in the previous section, we will first examine the sensitivity of the spectrum to the lattice parameters spelled out in section 2.3.2. Because the sensitivity of the single inclusive spectrum to these quantities is known to be weak, we will directly plot the dependence of κ_2 (see eq. (2.4)) on some of these quantities. After exploring the sensitivity of our results to lattice artifacts, we will quote results for the physical value of κ_2, and discuss the implications of our results.

In fig. 2.5, we plot the correlated part of the double inclusive spectrum as a function of p_T/Q_s, the momentum of one of the tagged gluons, while holding the transverse momentum q_T/Q_s of the other gluon fixed. The spectrum shown, plotted for different values of $m/g^2\mu$, is scaled by a factor $(p_T/Q_\mathrm{s})^4$ in fig. 2.5 (left). From the perturbative computation discussed in section 2.2, we expect this scaled spectrum to go to a constant value at large p_T/Q_s. We note that it does so approximately, keeping in mind that the spectrum at large p_T/Q_s is especially sensitive to lattice artifacts. We also note that the spectrum is weakly dependent on $m/g^2\mu$. In fig. 2.5 (right), we also plot the correlated double inclusive gluon spectrum as a log-log plot. In addition to the power law tail, we observe a qualitative change to a softer p_T spectrum for $p_T \leq 3Q_\mathrm{s}$.

2.4.3 Determining κ_2

In fig. 2.6, we study the dependence of κ_2 on the number of transverse $N_T \times N_T$ lattice sites and on N_y, the number of points in the longitudinal direction used to construct the path ordered Wilson lines. In the former case, hardly any dependence is seen thereby indicating a rapid convergence to the continuum limit. For longitudinal lattices, one observes a strong dependence for small N_y, but a rapid convergence thereafter, with virtually no N_y dependence seen for $N_y \geq 10$ onwards. The dependence of κ_2 on $g^2\mu L$ for a fixed value of $m/g^2\mu$ is shown in fig. 2.7. As anticipated, the dependence of κ_2 on $g^2\mu L$ is rather weak. This further confirms, as suggested previously, that the physics in the infrared is, for a finite m, insensitive

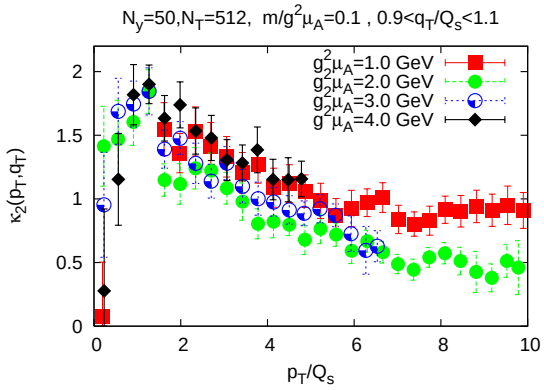

Figure 2.7: κ_2 for differing values of $g^2\mu L$ for a fixed $m/g^2\mu$ which is equivalent here to a fixed m/Q_s.

to the size of the system R_A.

Now that we have established the convergence of κ_2 as a function of N_y and N_T is robust, we should remind the reader that the continuum value of κ_2, being dimensionless, is most generally expressed as $\kappa_2(p_T/Q_\mathrm{s}, q_T/Q_\mathrm{s}, \Delta\varphi, Q_\mathrm{s}R_A, m/Q_\mathrm{s})$. In general κ_2 is a function of two 2-dimensional vectors. When one takes into account rotational symmetry, it is a function of three variables and there are many ways to plot such a function. The general structure is illustrated in fig. 2.8, where we show κ_2 as a function of $|\mathbf{p}_T - \mathbf{q}_T|$ and $|\mathbf{p}_T + \mathbf{q}_T|$. There is a delta-function peak at $\mathbf{p}_T = \mathbf{q}_T$ which is clearly visible. The peak is left out in the right hand plot of fig. 2.8 to better illustrate the remaining structure. As mentioned in sec. 2.3.1, there is also an enhancement in the correlation in the back-to-back configuration $\mathbf{p}_T = -\mathbf{q}_T$, which can be clearly seen in fig. 2.8.

We now address the dependence of κ_2 on m/Q_s. We saw in fig. 2.5 that the double inclusive spectrum had a weak dependence on $m/g^2\mu$, but the single inclusive spectrum had a slightly stronger dependence. The resulting effect on κ_2 is shown in fig. 2.9 as a function of p_T with q_T averaged over the interval $[2.9\,Q_\mathrm{s}, 3.1\,Q_\mathrm{s}]$ and as a function of the angle between $\mathbf{p}_T$ and $\mathbf{q}_T$. One observes that κ_2 decreases rapidly with increasing m/Q_s but converges to $\kappa_2 \sim 0.5$ for larger m/Q_s. The interpretation of the m/Q_s dependence of the results will be discussed further in the next section.

We can establish from the r.h.s. plot in fig. 2.9 that κ_2 is nearly constant as a function of $\Delta\varphi$; the strength of the correlation is only weakly dependent on the relative azimuthal angle between pairs of gluons. This result confirms the conjecture in Ref. [34]. Turning to the dependence of κ_2 on p_T/Q_s, q_T/Q_s, the dependence is not entirely flat as assumed in Ref. [34]; nevertheless, despite some structure, the variation of κ_2 with p_T/Q_s is on the order of 20% for $p_T/Q_\mathrm{s} \leq 4$.

Figures 2.10 and 2.11 show the effect of taking different configurations of the "trigger" and "associate" transverse momenta p_T and q_T. In fig. 2.10 (left) the momentum q_T is fixed to three different narrow bins and κ_2 is plotted as a function of p_T. Figure 2.10 (right) shows the dependence of κ_2 on the angle between $\mathbf{p}_T$ and $\mathbf{q}_T$ for three different combinations of p_T and q_T; either both around Q_s, both around $3\,Q_\mathrm{s}$ or one at Q_s and the other one at $3\,Q_\mathrm{s}$. In fig. 2.11, we show κ_2 for p_T and q_T having the same value, but with a finite angle between

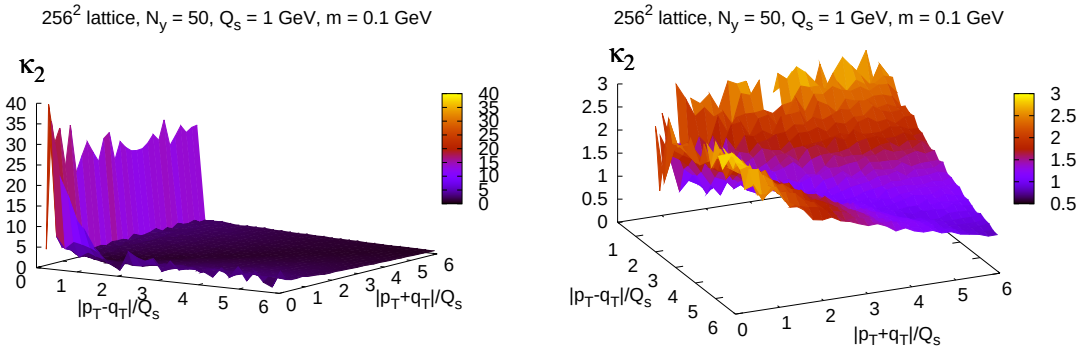

Figure 2.8: Three dimensional plot of $\kappa(|\mathbf{p}_T - \mathbf{q}_T|, |\mathbf{p}_T + \mathbf{q}_T|)$. The plot on the left shows the delta function peak at $\mathbf{p}_T = \mathbf{q}_T$. On the plot on the right this peak has been left out by reducing the range (the $|\mathbf{p}_T - \mathbf{q}_T|/Q_s$–axis starts from 0.1) to show the structure around the away-side, i.e. close to $\mathbf{p}_T = -\mathbf{q}_T$.

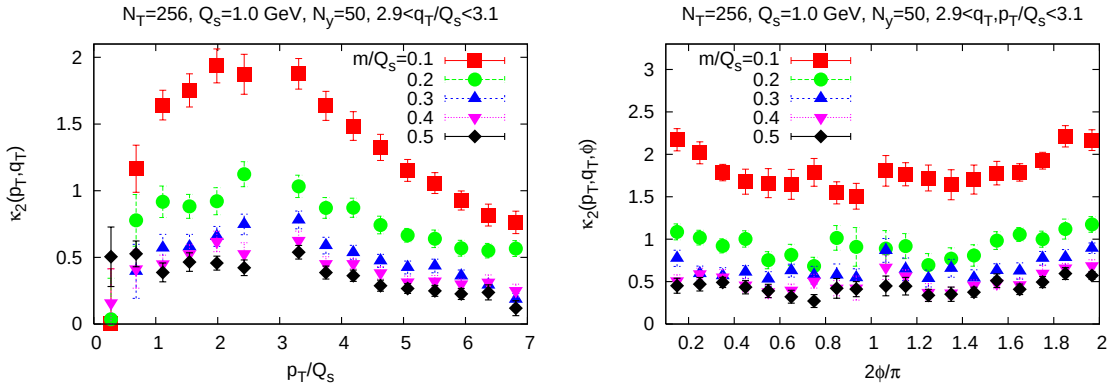

Figure 2.9: κ_2 for different values of m/Q_s with $Q_s = 1$ GeV, at $N_y = 50$. Left: κ_2 as a function of p_T for q_T in a small bin around $3\,Q_s$. Right: κ_2 as a function of $\Delta\varphi$ with both p_T and q_T in a small bin around $3\,Q_s$.

the vectors $\mathbf{p}_T$ and $\mathbf{q}_T$; showing a strong increase in the correlation for smaller values of the momenta.

2.5 Discussion and physical interpretation of results

We shall now discuss the physical implications of our numerical results for the double inclusive gluon distribution in the Glasma. In the Glasma flux tube picture [34], as noted in eq. (2.4) previously, it was conjectured that the correlated two gluon spectrum $C(\boldsymbol{p}, \boldsymbol{q})$ can be expressed as

$$\frac{C_2(\boldsymbol{p}, \boldsymbol{q})}{\left\langle \frac{\mathrm{d}N}{\mathrm{d}y_p\, \mathrm{d}^2\mathbf{p}_T} \right\rangle \left\langle \frac{\mathrm{d}N}{\mathrm{d}y_q\, \mathrm{d}^2\mathbf{q}_T} \right\rangle} = \kappa_2 \frac{1}{S_\perp Q_s^2}\,, \tag{2.38}$$

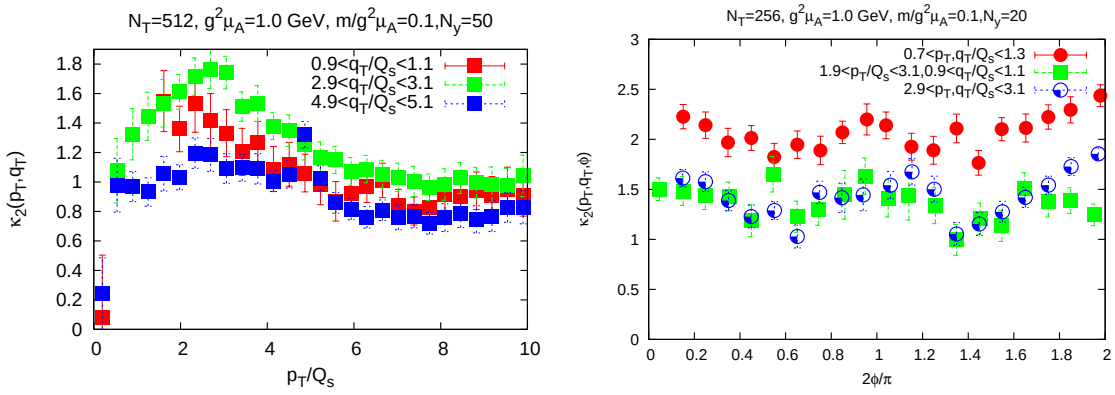

Figure 2.10: Left: κ as a function of absolute value of one of the momenta, the other being fixed to the specified value. Right: Angular dependence of κ at different absolute values of the momenta. Note absence of δ-function (point at $\Delta\varphi = 0$ outside plotted range on the y-axis) at unequal momenta.

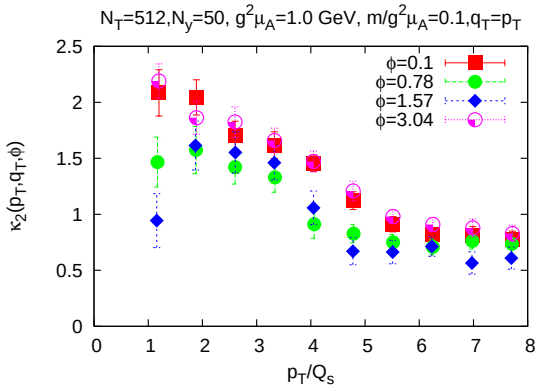

Figure 2.11: κ as function of momentum at equal momenta and specified angular separation.

where κ_2 is a non-perturbative constant which behaves parametrically as N_c^{-2}. The perturbative computation of κ_2 has a logarithmic dependence on p_T/Q_s and q_T/Q_s. Modulo this logarithm, one estimates perturbatively[9] that $\kappa_2 \sim 0.4$.

In comparing our non-perturbative results to the perturbative estimate, we first note that κ_2 is weakly dependent on $\Delta\varphi$ and p_T/Q_s, q_T/Q_s, just as conjectured in Ref. [34]. Our result for κ_2 is larger than the perturbative estimate, but it has a sensitivity, as shown in fig. 2.9, to m/Q_s. As noted previously, the double inclusive spectrum by itself has a relatively weak dependence on m/Q_s and the dependence on m/Q_s in the ratio κ_2 mostly comes from the single inclusive spectrum. Let us now discuss the physical interpretation of this dependence.

Recall that in our computation m appeared as a cutoff inserted into eq. (2.25) to invert the Laplace operator. It regulates the long distance Coulomb tails of the color field[10]. In the context of the MV model, this scale appears as an additional external parameter, whose value is not determined within the model itself. Thus it is not completely clear whether the scale m should be thought of as the confinement scale or a scale of order Q_s. In a straightforward implementation it is natural to think of m as a cutoff imposing color neutrality at the size of a nucleon. This is indeed the picture used for instance in Refs. [30].

This picture does not, however, take into account color screening effects coming from quantum evolution effects (virtual and radiative corrections) that are described by the JIMWLK and BK equations. At RHIC energies they may not be very important but will be extremely important at LHC energies. The effect of color screening of the correlators has been considered previously [60] (see also the discussion in Ref. [45]) and it is argued that quantum evolution effects regulate the infrared behavior of the color charge density correlator at a scale that is also parametrically of the order of Q_s. This is not a purely classical effect arising from non-linear Yang-Mills dynamics but from a combination of rescattering and quantum evolution effects. To determine the "correct" value of m in this context it is thus necessary to go beyond the MV model and include the effects of high energy evolution. A systematic numerical study of the two gluon correlation when high energy evolution effects are included is beyond the scope of this work.

A practical way to address this question in our simulation is to note that for a geometrical flux tube picture to be valid the two particle cumulant should be given by the size of the flux tube S_ft (representing the transverse range of color correlations) divided by the transverse area of the system times a number of order unity. We can make this logic explicit by expressing the size of the typical flux tube as

$$\frac{C_2(\boldsymbol{p},\boldsymbol{q})}{\left\langle \frac{\mathrm{d}N}{\mathrm{d}y_p\,\mathrm{d}^2\mathbf{p}_T}\right\rangle \left\langle \frac{\mathrm{d}N}{\mathrm{d}y_q\,\mathrm{d}^2\mathbf{q}_T}\right\rangle} = \frac{S_\mathrm{ft}}{S_\perp}\,, \tag{2.39}$$

where $S_\mathrm{ft} = \kappa_2(\cdots, m/Q_\mathrm{s})/Q_\mathrm{s}^2$. For the range of $m/Q_\mathrm{s} = 0.1$–0.5 considered, $\kappa_2 \approx 2$ - 0.5 converging rapidly to the latter value for increasing m/Q_s. The effective scale governing correlation strengths of unit strength is then $1/\sqrt{S_\mathrm{ft}} \approx 0.7$–$1.4\,Q_\mathrm{s}$. This scale, although not numerically very large, is nevertheless a semi-hard scale and corresponds to transverse distances much smaller than the nucleon size, thereby confirming the picture of early times

[9] On account of incorrect factors of 2 and π, the number quoted in Ref. [34] is an order of magnitude larger. The correct perturbative value (modulo logs) is quoted in Refs. [45, 44].

[10] The propagator for the 2 dimensional Laplace operator is a logarithm.

in the Glasma as classical field configurations that are coherent over transverse distances much smaller than a nucleon.

Let us then turn to a comparison with the RHIC data on two particle correlations. The experimentally observed quantity is $\Delta\rho/\sqrt{\rho_{\rm ref.}}(\Delta\varphi)$; in our framework, for $\Delta\varphi = 0$, it can be expressed as

$$\begin{aligned}\frac{\Delta\rho}{\sqrt{\rho_{\rm ref.}}}\,(\Delta\varphi = 0) &= \frac{dN}{dy}\cdot\frac{C_2(\boldsymbol{p},\boldsymbol{q})}{\left\langle\frac{{\rm d}N}{{\rm d}y_p\,{\rm d}^2\mathbf{p}_T}\right\rangle\left\langle\frac{{\rm d}N}{{\rm d}y_q\,{\rm d}^2\mathbf{q}_T}\right\rangle}\,(\gamma_B - \frac{1}{\gamma_B}) \\ &= \frac{K_N}{\alpha_{\rm s}}\,(\gamma_B - \frac{1}{\gamma_B}),\end{aligned} \tag{2.40}$$

where $K_N = \kappa_2/13.5$ for an SU(3) gauge theory and γ_B is the average radial boost in the framework of a blast wave model. From the RHIC data [40, 41], one can estimate that $\Delta\rho/\sqrt{\rho_{\rm ref.}}(\Delta\varphi = 0) = 1/\sqrt{2\pi\sigma_\varphi^2}$, with $\sigma_\varphi = 0.64$. Combining this with eq. (2.40), one obtains

$$\kappa_2^{\rm BW} \sim \frac{0.7}{(\gamma_B - \frac{1}{\gamma_B})}\,, \tag{2.41}$$

for $\alpha_{\rm s} = 0.5$ and where the superscript denotes that this is a crude estimate extracted from experiment using a blast-wave parametrization. For an average blast wave radial velocity $V_r = 0.6$, this gives $\kappa_2^{\rm BW} \sim 1.5$; for $V_r = 0.7$, one obtains $\kappa_2^{\rm BW} \sim 1$. There is considerable variation therefore in the value of $\kappa_2^{\rm BW}$ obtained from the ridge data due to the final state flow parametrization.

An alternative method to extract κ_2 is to compare the expression for the *negative binomial* multiplicity distribution (cf. eqs. (2.15)–(2.16) in the Glasma [45] to PHENIX data [46] on the same. From this comparison, one obtains

$$\kappa_2^{\rm NBD} \sim 3.9. \tag{2.42}$$

One sees therefore considerable variation in the extraction of κ_2 from experiment within the present framework. Within the many uncertainties, one can say at best it is a number of order unity. Our study suggests that a coherent picture of such correlations from RHIC and higher LHC energies can in principle provide unique information on color screening of strong fields at early times in heavy ion collisions.

An objective of this study is also to proceed in the opposite direction, namely, to determine κ_2 from a non-perturbative computation and use this as input into a dynamical space-time evolution model. As guide to this future program is the work in Ref. [61], where two particle correlations are extracted from the hydrodynamical evolution of flux tube structures in A+A collisions.

2.6 Summary

In this paper, we investigated the validity of the Glasma flux tube scenario of multi-particle correlations by performing a non-perturbative numerical computation of double inclusive gluon production in the Glasma. Our results were obtained by solving Yang-Mills equations

on a space-time lattice for Gaussian distributed color source configurations with a variance proportional to the saturation scale Q_s^2. Our results confirm key features of the Glasma flux tube scenario. Particles produced from coherent longitudinal electric and magnetic fields in transverse regions of size $\sim 1.4/Q_s$–$1/2\,Q_s$, much smaller than the nucleon size, have correlations of unit strength. As in the asymptotic perturbative estimates, particles produced from the flux tubes are uncorrelated in the relative azimuthal angle between the particles, the observed azimuthal collimation being produced later from radial flow. The correlations show non-trivial structure in p_T and q_T, which smoothly go over to perturbative results in the limit of $p_T/Q_s \gg 1$, $q_T/Q_s \gg 1$. Our results for the two particle correlation strength are consistent with estimates of the strength extracted from model comparisons to RHIC data. A useful extension of this work is to incorporate our results into more detailed hydrodynamical models of the space-time evolution of initial state correlations.

2.7 Lattice formulation

The Yang–Mills equations can be formulated as Hamilton's equations of motion. To preserve gauge invariance, they are solved numerically on a lattice where the degrees of freedom at a site i are the link variables

$$U_i(\mathbf{x}_T) = \exp\left[igaA_i(\mathbf{x}_T)\right], \tag{2.43}$$

where a is the lattice spacing on a transverse lattice. The appropriate discretized lattice (Kogut-Susskind) Hamiltonian in our case is given by

$$aH = \sum_{\mathbf{x}_T} \left\{ \frac{g^2 a}{\tau} \operatorname{Tr} E^i E^i + \frac{2N_c\tau}{g^2 a}\left(1 - \frac{1}{N_c}\mathrm{Re}\ \operatorname{Tr} U_\Box\right) + \frac{\tau}{a}\operatorname{Tr}\pi^2 + \frac{a}{\tau}\sum_i \operatorname{Tr}\left(\phi - \tilde{\phi}_i\right)^2 \right\}, \tag{2.44}$$

where E_i, U_i, π and ϕ are dimensionless lattice fields that are matrices in color space, with $E^i = E_a{}^i t_a$ etc. and the generators of the fundamental representation normalised as $\operatorname{Tr}(t_a t_b) = \delta_{ab}/2$.

The first two terms are the transverse electric and magnetic fields with the transverse plaquette defined as

$$U_\Box(\mathbf{x}_T) = U_x(\mathbf{x}_T) U_y(\mathbf{x}_T + e_x) U_x^\dagger(\mathbf{x}_T + e_y) U_y^\dagger(\mathbf{x}_T). \tag{2.45}$$

The last two terms are the kinetic energy and covariant derivative of the rapidity component of the gauge field $\phi \equiv A_\eta = -\tau^2 A^\eta$. The latter becomes an adjoint representation scalar following the assumption of boost invariance. For the parallel transported scalar field, we use the notation

$$\tilde{\phi}_i(\mathbf{x}_T) \equiv U_i(\mathbf{x}_T)\phi(\mathbf{x}_T + e_i)U_i^\dagger(\mathbf{x}_T). \tag{2.46}$$

In the Hamiltonian, eq. (2.44), there is a residual invariance under gauge transformations depending only on the transverse coordinates.

The Hamiltonian equations of motion are

$$\begin{aligned}
\dot{U}_i &= i\frac{g^2}{\tau}E^i U_i \text{ (no sum over } i), && (2.47)\\
\dot{\phi} &= \tau\pi, && (2.48)\\
\dot{E}^x &= \frac{i\tau}{2g^2}\left[U_{x,y} + U_{x,-y} - \text{ h.c. }\right] - \text{trace} + \frac{i}{\tau}[\tilde{\phi}_x, \phi] && (2.49)\\
\dot{E}^y &= \frac{i\tau}{2g^2}\left[U_{y,x} + U_{y,-x} - \text{ h.c. }\right] - \text{trace} + \frac{i}{\tau}[\tilde{\phi}_y, \phi],\\
\dot{\pi} &= \frac{1}{\tau}\sum_i \left[\tilde{\phi}_i + \tilde{\phi}_{-i} - 2\phi\right]. && (2.50)
\end{aligned}$$

Gauss's law, conserved by the equations of motion, is given by

$$\sum_i \left[U_i^\dagger(\mathbf{x}_T - e_i)E^i(\mathbf{x}_T - e_i)U_i(\mathbf{x}_T - e_i) - E^i(\mathbf{x}_T)\right] - i[\phi, \pi] = 0\,.$$

On the lattice the initial conditions (2.20) are

$$\begin{aligned}
0 &= \text{Tr}\left[t_a\left(\left(U_i^1 + U_i^2\right)\left(1 + U_i^\dagger\right) - \text{ h.c. }\right)\right], && (2.51)\\
E^i &= 0, && (2.52)\\
\phi &= 0, && (2.53)\\
\pi(\mathbf{x}_T) &= \frac{-i}{4g}\sum_i \Big[\left(U_i(\mathbf{x}_T) - 1\right)\left(U_i^{\dagger 2}(\mathbf{x}_T) - U_i^{\dagger 1}(\mathbf{x}_T)\right) && (2.54)\\
&+ \left(U_i^\dagger(\mathbf{x}_T - e_i) - 1\right)\left(U_i^2(\mathbf{x}_T - e_i) - U_i^1(\mathbf{x}_T - e_i)\right) - \text{ h.c. }\Big],
\end{aligned}$$

where $U_i^{1,2}$ in eq. (2.51) are the link matrices corresponding to the color fields of the two nuclei ($A_i^{1,2}$ in eq. (2.21)). The link matrix U_i, which corresponding to the $\tau \geq 0$ color field A_i, is determined by solving eq. (2.51).

Chapter 3

Partial Fractioning of Perturbative Amplitudes.

3.1 Introduction.

Tree and loop amplitudes and cross sections with multiple external lines in gauge and other field theories are the subject of wide attention [79], [63], [64]. Much of this work is based on analyticity properties of the integrals [65], [66], and on the identification of bases for integrals with fixed number of denominators [67].

If the number of loops is kept fixed, one might expect that the diagram function of a field theory, in some dimension d, would get progressively more complicated as the number of external lines is increased. For one loop, however, it has long been known that the number of denominators that are quadratic in the loop momentum can be reduced to no more than five for each loop [70] in four dimensions. This paper presents an alternative method for reducing a diagram with any number of loops and many external lines to a linear combination of integrals of limited complexity. These integrals correspond to vacuum bubble diagrams with the same number of loops as the original diagram and with up to $d+1$ denominators per line, d of which are linear in the loop momenta. The number of such diagrams increases linearly in $L-1$, independent of the number of external lines. Such integrals have $d+2$ poles per loop, to be compared to $2(d+2)$ poles in the integral of a standard diagram. The method of Ref. [71],[101] can then be applied to derive a further reduction to d denominators, at least in the one loop case. The reduction of the number of lines for single-particle irreducible diagrams is analogous to the recursive structure of gauge theory tree amplitudes, [76] and the underlying graphical identities are in fact related [68, 69].

The reduction is based on two fairly simple identities, which are presented in Section 2. The general formula for the class of what will be called "sufficiently dressed" diagrams is also presented there. For such diagrams the total number of denominators that depend on loop momenta q_i is $k(d+1)L$, with k a number that is defined by the theory and does not grow with d or L. For instance, for ϕ^3 theory k equals 3. Of these denominators, $k \times d \times L$ are linear, the others quadratic in q. In Section 3 it is shown how to extend the method to theories with spinors and vectors. The general result is that there is a basis for the integrals such that for each set of lines carrying a specific linear combination of loop momenta there

is only one quadratic and up to d linear factors in the denominator and up to $d+1$ linear factors in the numerator. It is possible to further reduce the number of linear denominators. The method for doing this is illustrated by a two-loop example in scalar theory in Section 4.

3.2 Identities.

We consider scalar integrals in d dimensions. To each diagram, we associate a vacuum bubble diagram, found by removing all external lines. In this section the method is presented in the case, when the diagram is "sufficiently dressed". A diagram is sufficiently dressed if there are at least d external lines emanating from each line in the corresponding bubble diagram. The reduction is performed for arbitrary complex masses and complex external momenta.

In the diagram, consider the set of denominators that corresponds to a given linear combination of loop momenta, q. This set of lines can be identified with a single line in the corresponding bubble diagram. The starting point of the reduction is the following identity, applied to any such set of lines,

$$\prod_{e=1}^{N_q} \frac{1}{(q+p_e)^2+m_e^2} = \sum_{e=1,\ldots,N_q} \frac{1}{(q+p_e)^2+m_e^2} \times \prod_{j=1,\ldots,N_q, j\neq e} \frac{1}{2q\cdot(p_j-p_e)+p_j^2+m_j^2-p_e^2-m_e^2} \ , \tag{3.1}$$

where N_q is the number of external lines attached to q, and p_e denotes the sum of external momenta carried on line e. This identity is valid as long as none of the denominators vanishes. The q, p_e are d-component momenta, and m_e are the (possibly complex) masses of the lines. Masses can be zero. The integral is regulated by off-shellness. This equation is valid for all $N_q > 1$.

Equation (3.1) is a consequence of the following identity which will be used repeatedly below,

$$\prod_{e=1}^{N} \frac{1}{s_e x + a_e} = \sum_{e=1}^{N} \frac{1}{s_e x + a_e} \prod_{f=1,\ldots,N, f\neq e} \frac{1}{s_f x + a_f}|_{x=X^e}, \quad s_e X^e + a_e = 0 \ . \tag{3.2}$$

In this equation, s_e, x, a_e are arbitrary complex numbers, considered for a generic point in the space $\{s_e, a_e, x\}$. The identity (3.2) is most easily proved by considering the integral

$$Int = \frac{1}{2\pi i} \int_C \frac{d\xi}{\xi} \prod_{e=1}^{N} \frac{1}{s_e(x+\xi)+a_e} \ , \tag{3.3}$$

where the contour of integration C encircles zero in a counter-clockwise sense. The integral over such contour is equal to the left hand side of Eq . (3.2). When a circle at infinity is added to such a contour, the integration can be closed on all the other poles of the integrand, giving in this way the sum of residues of the integrand other than from zero. This is equal to the right hand side of Eq . (3.2).

In particular, setting $s_e = s$ for all e and taking the limit $s \to 0$, the identity reduces to

$$\prod_{e=1}^{N} \frac{1}{a_e} = \sum_{e=1}^{N} \frac{1}{a_e} \prod_{f=1,\ldots,N,\neq e} \frac{1}{a_f - a_e} \ . \tag{3.4}$$

Taking $a_e = (q_e + p_e)^2 + m_e^2$ gives the identity Eq . (3.1).

We next assume that $N_q > d$. By further partial fractioning the product of linear factors in (3.1) can be further reduced, by using an identity whose proof will be given momentarily. For arbitrary $N_q > d + 1$ the identity is

$$\prod_{j\neq e}^{N_q} \frac{1}{2q\cdot(p_j - p_e) + p_j^2 + m_j^2 - p_e^2 - m_e^2} = \tag{3.5}$$
$$\sum_{j_1\neq\ldots\neq j_d\neq e} \Big(\prod_{s=1\ldots d} \frac{1}{2q\cdot(p_{j_s} - p_e) + p_{j_s}^2 + m_{j_s}^2 - p_e^2 - m_e^2}\Big) T^e_{j_1,\ldots,j_d}(p_{e'}) \ ,$$

where the factors $T^e_{j_1,\ldots,j_d}(p_{e'})$ are functions of external momenta only,

$$T^e_{j_1,\ldots,j_d}(p_{e'}) = \prod_{k\neq j_1,\ldots,j_d,e} \frac{1}{2Q_{j_1,\ldots,j_d}\cdot(p_k - p_e) + p_k^2 + m_k^2 - p_e^2 - m_e^2} \ . \tag{3.6}$$

In this expression, the d-dimensional vectors $Q_{j_1,\ldots,j_d}$ are the solutions of the following system of d linear equations, corresponding to the "missing" denominators in each of the terms on the right-hand side of Eq. (2),

$$2Q\cdot(p_{j_1} - p_i) + p_{j_1}^2 + m_{j_1}^2 - p_e^2 - m_e^2 = 0 \tag{3.7}$$
$$\ldots.$$
$$2Q\cdot(p_{j_d} - p_i) + p_{j_d}^2 + m_{j_d}^2 - p_e^2 - m_e^2 = 0 \ .$$

Thus the argument of $T^e_{j_1,\ldots,j_s}(p_{e'})$ represents masses and all momenta $p_{e'}$ that do not appear in the q-dependent denominators of that term. This sytem is to be solved at generic values of momenta and masses, i.e. symbolically. It is worth noting that solutions to Eq. (3.7) are analogous to the complex momenta that set internal lines of the S-matrix on shell in Ref. [76] and discussed diargammatically in Refs. [68, 69].

The proof of (3.5) again relies on the identity (3.2). In order to simplify the notation, we rewrite the identity to be proven in the form

$$F_N(\{l\},\{a\},q) = \prod_{e=1}^{N} \frac{1}{l_e\cdot q + a_e} = \tag{3.8}$$
$$\sum_{e_d\neq e_{d-1}\neq\ldots\neq e_1} \prod_{s=1,\ldots,d} \frac{1}{l_{e_s}\cdot q + a_{e_s}} T_{e_d,\ldots,e_1}(\{l\},\{a\}) \ ,$$

where $q \in C^d, l_e \in C^d, a_e \in C$ and

$$T_{e_d,...,e_1}(\{l\},\{a\}) = \prod_{f \neq e_d,...,e_1} \frac{1}{l_f \cdot Q + a_f} \ , \tag{3.9}$$

where Q is the solution of the system

$$l_{e_s} \cdot Q + a_{e_s} = 0 \ , s = 1, ..., d \ , \tag{3.10}$$

at a generic point in the parameter space.

For the proof of (3.8), single out a particular coordinate system in q-space and apply the identity (3.2) to the component q_d, to obtain

$$F_N(\{l\},\{a\},q) = \sum_{e_d=1}^{N} \frac{1}{l_{e_d} \cdot q + a_{e_d}} \prod_{f=1,...,N,\neq e_d} (\frac{1}{l_f \cdot q + a_f}|_{q_d = Q_d^{e_d}(\{l\},\{a\},q_{d-1},...,q_1)}) \ , \tag{3.11}$$

where $Q_d^{e_d}(\{l\},\{a\},q_{d-1},...,q_1)$ is the solution of $l_{e_d} \cdot q + a_{e_d} = 0$ considered as an equation for q_d. The identity (3.2) can be applied to the product under the sum with q_{d-1} singled out, with the result

$$\begin{aligned} F_N(\{l\},\{a\},q) = \sum_{e_d=1}^{N} & \frac{1}{l_{e_d} \cdot q + a_{e_d}} \\ & \times \sum_{e_{d-1}=1,...,N,\neq e_d} (\frac{1}{l_{e_{d-1}} \cdot q + a_{e_{d-1}}}|_{q_d = Q_d^{e_d}(\{l\},\{a\},q_{d-1},...,q_1)}) \\ \times \prod_{f=1,...,N,\neq e_d,e_{d-1}} & (\frac{1}{l_f \cdot q + a_f}|_{q_s = Q_s^{e_d,e_{d-1}}(\{l\},\{a\},q_{d-2},...,q_1) \ ,s=d,d-1}) \ , \end{aligned} \tag{3.12}$$

where $Q_s^{e_d,e_{d-1}} \ , s = d, d-1$ is the solution of the system $l_f \cdot q + a_f = 0 \ , f = e_d, e_{d-1}$, considered as equations for q_d, q_{d-1}. Continuing in this way, one may arrive at the following identity, valid for any $k, 1 \leq k \leq d$,

$$\begin{aligned} F_N(\{l\},\{a\},q) = \sum_{e_d=1}^{N} & \frac{1}{l_{e_d} \cdot q + a_{e_d}} \times \cdots \times \\ & \times \sum_{e_k=1,...,N,\neq e_d,...,e_{k+1}} (\frac{1}{l_{e_k} \cdot q + a_{e_k}}|_{q_r = Q_r^{e_d,...,e_{k+1}}(\{l\},\{a\},q_k,...,q_1), \ r=d,..,k+1}) \\ & \times \prod_{f=1,...,N,\neq e_d,...,e_k} (\frac{1}{l_f \cdot q + a_f}|_{q_s = Q_s^{e_d,...,e_k}(\{l\},\{a\},q_{k-1},...,q_1) \ ,s=d,...,k}) \ , \end{aligned} \tag{3.13}$$

where $Q_r^{e_d,...,e_k}(\{l\},\{a\},q_{k-1},...,q_1), r = d, ..., k$ is the solution of the system $l_{e_s} \cdot q + q_{e_s} = 0$ for $q_d, ..., q_k$. In particlular, for $k = 1$ the product under the iterated sum is independent of q. It will be denoted by $T_{e_d,...,e_1}(\{p\},\{a\})$. It coincides with the quantity defined in Eq. (3.9).

It is independent of the order of the indices $e_d, ..., e_1$. Thus, the identity (3.13) for $k = 1$ can be rewritten as

$$F_N(\{l\},\{a\},q) = \sum_{f_1\neq\ldots\neq f_d} T_{f_d,\ldots,f_1}(\{p\},\{a\}) \times \sum_{\{e_1,\ldots,e_d\}=\{f_1,\ldots,f_d\}} \frac{1}{l_{e_d}\cdot q + a_{e_d}} \times \cdots \times \times \left(\frac{1}{l_{e_1}\cdot q + a_{e_1}}\Big|_{q_r = Q_r^{e_d,\ldots,e_2}(\{l\},\{a\},q_1),\ r=d,..,2}\right) , \tag{3.14}$$

where the inner sum extends over permutations of the set $\{f_1, ..., f_d\}$. The inner sum is equal to $F_d(\{l_{f_1}, ..., l_{f_d}\}, \{a_{f_1}, .., a_{f_d}\}, q)$, as can be deduced from the identity (3.13) applied to this particular choice of the momenta l_e and scalars a_e, with $k = 1$, and $N = d$. This proves the identity (3.8), and hence Eq. (3.5)

Combining the two partial fractionings (3.1), (3.5), we see that, for $N_q > d$, the product of $N_q \geq d + 1$ denominators can be reduced to a sum of terms each of which has only $d + 1$ denominators, only one of which is quadratic,

$$\prod_e \frac{1}{(q+p_e)^2+m_e^2} = \sum_e \sum_{j_1,\ldots,j_d} \frac{1}{(q+p_e)^2+m_e^2} \times \prod_{s=1\ldots d} \frac{1}{2q\cdot(p_{j_s}-p_e)+p_{j_s}^2+m_{j_s}^2-p_e^2-m_e^2} T^e_{j_1,\ldots,j_d}(p_{e'}) \ . \tag{3.15}$$

We now embed this result in an arbitrary diagram. The integrand of an arbitrary 1PI Feynman scalar diagram can be written as

$$Integrand = \prod_{i=1}^{I} \prod_{e_i\in E_i} \frac{1}{(q_i+p_{e_i})^2+m_{e_i}^2} \ . \tag{3.16}$$

Here, $i = 1 \ldots I$ labels the lines of the corresponding bubble diagram and E_i labels the set of lines in the diagram associated with line i in the bubble diagram. All of the lines in E_i carry the same linear combination of loop momenta, q_i,

$$q_i = \sum_{\alpha=1}^{L} l_{i,\alpha} q_\alpha \ , \tag{3.17}$$

where L is the number of loop momenta. $l_{i,\alpha} \in \{0, 1, -1\}$ can be read from the bubble diagram in the standard way.

The partial fractioning formula (3.15) can be used to derive the following algebraic identity for the full integrand of any sufficiently dressed scalar integral

$$Integrand = \prod_{i\in I} \sum_{e_i\in E_i} \frac{1}{(q_i+p_{e_i})^2+m_{e_i}^2} \sum_{j_1^i,\ldots,j_d^i\in E_i} T^{e_i}_{j_1^i,\ldots,j_d^i}(p_{e_i'}) \times \prod_{s=1\ldots d} \frac{1}{2q_i\cdot(p_{j_s^i}-p_{e_i})+(p_{j_s^i})^2+(m_{j_s^i})^2-(p_{e_i})^2-m_{e_i}^2} \ , \tag{3.18}$$

where $T^{e_i}_{j^i_1,\ldots,j^i_d}(p_{e'_i})$ is obtained through the use of the prescription of Eq. (3.6) with p_e, p_j substituted accordingly. The order of operations is such that rightmost operations are done first. The argument $p_{e'_i}$ of T's signifies the dependence on other momenta from the line i.

The integrals of both sides of Eq. (3.18) are well-defined on any representative of the homology class in $H_{dL}(P^{dL} - \cup_i D^c_i)$ (D^c_i stand for the standard [65] compactifications of the zero sets of the Feynman denominators, and P^{dL} is the complex projective space) that does not intersect the zero loci of the linear factors. One such choice corresponds to the standard $i\epsilon$ prescription. Therefore we may extend the equality of integrands in (3.18) to an equality of integrals,

$$Integral = \int_\zeta (dq) \prod_{i\in I} \sum_{e_i\in E_i} \frac{1}{(q_i + p_{e_i})^2 + m^2_{e_i}} \sum_{j^i_1,\ldots,j^i_d} T^{e_i}_{j^i_1,\ldots,j^i_d}(p_{e'_i}) \tag{3.19}$$
$$\times \prod_{s=1\ldots d} \frac{1}{2q_i\cdot(p_{j^i_s} - p_{e_i}) + (p_{j^i_s})^2 + (m_{j^i_s})^2 - (p_{e_i})^2 - m^2_{e_i}} \ .$$

It is enough to choose any representative, ζ of the homology class and deform it in such a way that it does not intersect any of the zero loci of the denominators in the reduction formula. Or one can initially choose such a representative. There are obviously many such choices. On such representatives the reduction formula (3.18) is valid in each point, so it indeed can be integrated.

Eq. (3.18) for the integral can be rewritten as follows

$$Integral = \sum_{e_i, j^i_s\in E_i} \prod_{i\in I} T^{e_i}_{j^i_1,\ldots,j^i_d}(p_{e'_i}) \int_\zeta (dq) \prod_{i\in I} \frac{1}{(q_i + p_{e_i})^2 + m^2_{e_i}} \tag{3.20}$$
$$\times \prod_{s=1\ldots d} \frac{1}{2q_i\cdot(p_{j^i_s} - p_{e_i}) + (p_{j^i_s})^2 + (m_{j^i_s})^2 - (p_{e_i})^2 - m^2_{e_i}} \ ,$$

with the single sum over all possible choices of the d-tuples of external lines that emanate from each bubble line i, in a sufficiently dressed diagram. The rightmost operations are done first. The indices $j^i_1, ..., j^i_d$ of the $T^{e_i}_{j^i_1,\ldots,j^i_d}(p_{e'_i})$ are the same as the indices of the vectors $p_{j^i_s}$ in the second product under the integral sign.

In summary, we see that an arbitrary sufficiently dressed integral can be reduced to a linear combination of integrals of simpler type, with one quadratic factor and exactly d linear factors for each bubble line. It might be that this form of the integral is useful in applications, especially because of the reduced number of poles in each integrand. One must keep in mind that there is still significant freedom in choosing the contour ζ, if one for instance desires to do numeric evaluation of this integral, or relate it to physical amplitudes.

3.3 Extension to theories with spin.

In this section it is shown how to extend the reduction method to theories with arbitrary spinor or vector numerators. It will be demonstrated that an arbitrary integrand can be reduced to a sum of terms such that there is one quadratic factor per bubble line, up to d

linear factors in the denominator and up to $d+1$ linear factors in the numerator. Thus, the conclusion that the number of elements in this basis for integrals grows linearly with the number of loops and is independent of the number of external lines still holds.

We start with the observation that for a product of propagators like the left-hand side of Eq. (3.1), the number of quadratic factors in the denominator can still be decreased to one through the identity (3.1) without changing numerator momenta at all. It remains to reduce the products of the form

$$I = \frac{\prod_{e=1}^{E-r}(k_e \cdot q + b_e)}{\prod_{e=1}^{E}(l_e \cdot q + a_e)} \ , \tag{3.21}$$

where q is a loop momentum, l_e are linear combinations of momenta flowing into the line and k_e are arbitrary momenta, not necessarily related to the l_e. This generality of the choice for k_e includes open vector indices, so one can choose for instance $k_{e,\mu} = \delta_{\mu\nu}$. The denominator terms a_e are expressed through external momenta and masses, and the q-dependent numerator terms b_e are arbitrary. As above, the integer E is one less the number of propagators that correspond to the bubble line. Integer r is a free parameter of the formula that accounts for the number of linear factors of q in the numerator, ranging from 0 to $E+1$. The final case can be realised when all the external lines are attached to the bubble line through a vertex that is linear in momenta, such as a triple gauge boson coupling. Thus, $r = -1, ..., E$.

If $r \geq d$ then a direct generalization of the scalar formula, Eq. (3.5), holds

$$I = \sum_{f_1,...,f_d} M_{f_1,...,f_d} \frac{1}{\prod_{s=1}^{d}(l_{f_s} \cdot q + a_{f_s})} \ , \tag{3.22}$$

with

$$M_{f_1,...,f_d} = \frac{\prod_{e=1}^{E-r}(k_e \cdot Q + b_e)}{\prod_{e \neq f_1,...,f_d}(l_e \cdot Q + a_e)} \ , \tag{3.23}$$

where Q is the solution of a system of equations that is analogous to (3.7) and is constructed from the vectors k_{f_s}. Therefore, in this case the basis of intergals is the same as in the scalar case.

In the proof of Eq. (3.22), the following generalization of the identity (3.2) will be used

$$\frac{\prod_{e=1}^{F}(f_e x + a_e)}{\prod_{e=1}^{E}(g_e x + b_e)} = \sum_{e=1}^{E} \frac{1}{g_e x + b_e} \left(\frac{\prod_{f=1}^{F}(f_f x + a_f)}{\prod_{f=1,\neq e}^{E}(g_f x + b_f)}\right)|_{x=-b_e/g_e} \ , \tag{3.24}$$

which is valid at a generic point in the space of complex variables f_e, a_e, g_e, b_e, x, and for all integers $F < E$. The proof involves the same residue argument as before and we omit it.

The proof of (3.22) now parallels the proof of (3.5). Consider the quantity

$$G_{F,E}(\{l\},\{k\},\{a\},\{b\},q) = \frac{\prod_{e=1}^{F}(k_e \cdot q + b_e)}{\prod_{e=1}^{E}(l_e \cdot q + a_e)} \ , \tag{3.25}$$

where $l_e, k_e, q \in C^d, a_e, b_e \in C$ and $F \leq E - d$. Application of the identity (3.24) to the variable q_d gives

$$G_{F,E}(\{l\},\{k\},\{a\},\{b\},q) = \sum_{e_d=1}^{E} \frac{1}{l_{e_d}\cdot q + a_{e_d}} \times (\frac{\prod_{f=1}^{F}(k_f\cdot q + b_f)}{\prod_{f=1,\neq e_d}^{E}(l_f\cdot q + a_f)}|_{q_d=Q_d^{e_d}}) \ . \tag{3.26}$$

with $Q_d^{e_d} = Q_d^{e_d}(\{l\},\{a\},q_{d-1},...,q_1)$ the solution for q_d of the equation $l_{e_d}\cdot q + a_{e_d} = 0$. The identity (3.24) can be applied again to the product inside the sum, with q_{d-1} taken as x. The result, analogous to (3.12), is

$$\begin{aligned} G_{F,E}(\{l\},\{k\},\{a\},\{b\},q) = \sum_{e_d=1}^{E} \frac{1}{l_{e_d}\cdot q + a_{e_d}} \\ \times \sum_{e_{d-1}=1,\neq e_d}^{E} (\frac{1}{l_{e_{d-1}}\cdot q + a_{e_{d-1}}}|_{q_d=Q_d^{e_d}}) \\ \times (\frac{\prod_{f=1}^{F}(k_f\cdot q + b_f)}{\prod_{f=1,\neq e_d,e_{d-1}}^{E}(l_f\cdot q + a_f)}|_{q_r=Q_r^{e_d,e_{d-1}},r=d,d-1}) \ , \end{aligned} \tag{3.27}$$

with $Q_r^{e_d,e_{d-1}} = Q_r^{e_d,e_{d-1}}(\{l\},\{a\},q_{d-2},...,q_1)$ being the solution for q_d, q_{d-1} of the system $l_t\cdot q + a_t = 0, t = e_d, e_{d-1}$. After the application of the basic identity (3.24) s more times the result takes the form

$$\begin{aligned} G_{F,E}(\{l\},\{k\},\{a\},\{b\},q) = \sum_{e_d=1}^{E} \frac{1}{l_{e_d}\cdot q + a_{e_d}} \times \cdots \times \\ \times \sum_{e_{d-s}=1,\neq e_d,...,e_{d-s+1}}^{E} (\frac{1}{l_{e_{d-s+1}}\cdot q + a_{e_{d-s+1}}}|_{q_r=Q_r^{e_d,...,e_{d-s+1}},,r=d,...,d-s+1}) \\ \times (\frac{\prod_{f=1}^{F}(k_f\cdot q + b_f)}{\prod_{f=1,\neq e_d,...,e_{d-s}}^{E}(l_f\cdot q + a_f)}|_{q_r=Q_r^{e_d,...,e_{d-s}},r=d,...,d-s}) \ . \end{aligned} \tag{3.28}$$

As in the scalar case for $s = d - 1$ can be rewritten as

$$\begin{aligned} G_{F,E}(\{l\},\{k\},\{a\},\{b\},q) = \sum_{f_1\neq...\neq f_d} M_{f_d,...,f_1}(\{k\},\{l\},\{a\},\{b\}) \\ \times \sum_{\{e_1,...,e_d\}=\{f_1,...,f_d\}} \frac{1}{l_{e_d}\cdot q + a_{e_d}} (\frac{1}{l_{e_{d-1}}\cdot q + a_{e_{d-1}}}|_{q_d=Q_d^{e_d}}) \\ \times \cdots \times (\frac{1}{l_{e_1}\cdot q + a_{e_1}}|_{q_r=Q_r^{e_d,...,e_2},r=d,..,2}) \ , \end{aligned} \tag{3.29}$$

with M given by Eq. (3.23). The sum that multiplies $M_{f_d,...,f_1}$ is precisely $F_d(l_{e_d},...,l_{e_1},a_{e_d},...,a_{e_1},q)$. This proves the identity (3.22).

In case $r < d$, I can be represented in the form

$$I = \sum_{f_1,...,f_d} M_{f_1,...,f_d} \frac{1}{\prod_{s=1}^{d}(l_{f_s} \cdot q + a_{f_s})} \prod_{f=E-d+1,...,E-r} (k_f \cdot q + b_f) \ , \tag{3.30}$$

with M the same as above, Eq. (3.23). This proves the assertion made in the beginning of this section.

Equation (3.30) can be simplified and recast in the invariant terms, again by partial fractioning. We do it here in the case $r = d - 1$, where for Eq. (3.30),

$$I = \sum_{f_1,...,f_d} M_{f_1,...,f_d} \frac{(k_{E-d+1} \cdot q + b_{E-d+1})}{\prod_{s=1}^{d}(l_{f_s} \cdot q + a_{f_s})} \ . \tag{3.31}$$

Momenta l_{f_s} are linearly independent, so $k_{E-d+1} = \sum_s \alpha_s l_{f_s}$ for some α_s. Therefore,

$$I = \sum_{f_1,...,f_{d-1}} M^{(d-1)}_{f_1,...,f_{d-1}} \frac{1}{\prod_{s=1}^{d-1}(l_{f_s} \cdot q + a_{f_s})} + \sum_{f_1,...,f_d} M^{(d)}_{f_1,...,f_d} \frac{1}{\prod_{s=1}^{d}(l_{f_s} \cdot q + a_{f_s})} \ , \tag{3.32}$$

for some $M^{(d-1)}, M^{(d)}$.

It is possible to determine the coefficients $M^{(d-1)}, M^{(d)}$. The $M^{(d)}$ are given by the same formula (3.23), as can be seen by studying the asymptotics near d-tuple denominator poles. It remains to find $M^{(d-1)}$. In order to do this, consider the line defined by

$$\begin{gathered} l_{f_1} \cdot q + a_{f_1} = 0 \\ .... \\ l_{f_{d-1}} \cdot q + a_{f_{d-1}} = 0 \ . \end{gathered} \tag{3.33}$$

Its equation can be written as

$$L = \{q_\mu = A_\mu + B_\mu t | t \in C\} \ . \tag{3.34}$$

We multiply Eq. (3.32) by the factors $l_{f_1} \cdot q + a_{f_1}, ..., l_{f_{d-1}} \cdot q + a_{f_{d-1}}$ and consider the result near the line L. It is

$$\frac{\prod_{f=1,...,E-d+1}(k_f \cdot (A + Bt) + b_f)}{\prod_{f \neq f_1,...,f_{d-1}}(l_f \cdot (A + Bt) + a_f)} = M^{(d-1)}_{f_1,..,f_{d-1}} + \sum \frac{M^{(d)}_{f_1,...,f_d}}{l_f \cdot (A + Bt) + a_f} \ . \tag{3.35}$$

It follows from this formula that

$$M^{(d-1)}_{f_1,...,f_{d-1}} = \frac{\prod_{f=1,...,E-d+1} k_f \cdot B}{\prod_{f \neq f_1,...,f_{d-1}} l_f \cdot B} \ . \tag{3.36}$$

Note that B is determined by the $d - 1$ hyperplanes of Eq. (3.33) up to a constant, which cancels in the above fraction.

3.4 Further reduction and symmetries for multiloop integrals.

In this section further partial fractioning in the linear sector of the integrand is discussed for the example of two-loop scalar integrals. This allows one to reduce the number of linear factors further. Also, a symmetry of the resulting integrals is identified. These techniques can be generalized to higher loops.

In Section 2 it was shown that the scalar integral can be reduced to the following sum

$$Integral = \sum_{e_i, j_s^i \in E_i} \prod_i T^{e_i}_{j_1^i,\ldots,j_d^i}(p_{e_i'}) I(p_{e_i}, p_{j_s^i}, a_{j_s^i}) \ , \tag{3.37}$$

where $a_{j_s^i}$ are quadratic functions of masses and momenta that can be read off from the previous formulas. In the two-loop case a generic integral I has the form

$$\begin{aligned} I(p_{e_i}, p_{j_s^i}, a_{e_s^i}) = \int dq_1 dq_2 \frac{1}{(q_1+p_{e_1})^2+m_1^2} \frac{1}{(q_2+p_{e_2})^2+m_2^2} \\ \times \frac{1}{(q_1+q_2+p_{e_3})^2+m_3^2} \prod_{j_s^1 \in E_1} \frac{1}{q_1 \cdot (p_{j_s^1} - p_{e_1}) + a_{j_s^1}} \\ \times \prod_{j_s^2 \in E_2} \frac{1}{q_2 \cdot (p_{j_s^2} - p_{e_2}) + a_{j_s^2}} \prod_{j_s^3 \in E_3} \frac{1}{(q_1+q_2) \cdot (p_{j_s^3} - p_{e_3}) + a_{j_s^3}} \ , \end{aligned} \tag{3.38}$$

where $i \in 1,2,3$, E_i are d-element sets of the indices j_s^i, and $a_{j_s^i}$ are functions of masses and momenta that one can read off from Eq. (10). The change of variables

$$\begin{aligned} q_1' &= q_1 + p_{e_1} \ , \\ q_2' &= q_2 + p_{e_2} \ , \end{aligned} \tag{3.39}$$

will eliminate the dependence of the two quadratic factors on the external momenta. The prime in q_i' will be suppressed in the following. In order to simplify the notation, the following change of coordiantes can be made

$$\begin{aligned} r &= p_{e_3} - p_{e_1} - p_{e_2} \ , \\ p_{s_i} &= p_{j_s^i} - p_{e_i} \ , a_{s_i} = a_{j_s^i} - p_{s_i} \cdot p_{e_i} \ , \quad s_i \in E_i \ , i = 1,2,3 \ . \end{aligned} \tag{3.40}$$

In these variables, the integral I, which will still be denoted by the same letter, assumes the form

$$\begin{aligned} I(p_{e_i}, p_{j_s^i}, a_{j_s^i}) = \int dq_1 dq_2 \ \frac{1}{q_1^2+m_1^2} \frac{1}{q_2^2+m_2^2} \frac{1}{(q_1+q_2+r)^2+m_3^2} \\ \times \prod_{s_1 \in E_1} \frac{1}{q_1 \cdot p_{s_1} + a_{s_1}} \prod_{s_2 \in E_2} \frac{1}{q_2 \cdot p_{s_2} + a_{s_2}} \prod_{s_3 \in E_3} \frac{1}{(q_1+q_2+r) \cdot p_{s_3} + a_{s_3}} \ . \end{aligned} \tag{3.41}$$

In the general two-loop integral, Eq. (3.41), there are exactly $2d$ linear factors that have q_2 dependence, namely

$$P_2 = \prod_{s_2 \in E_2} \frac{1}{q_2 \cdot p_{s_2} + a_{s_2}} \prod_{s_3 \in E_3} \frac{1}{(q_1+q_2+r) \cdot p_{s_3} + a_{s_3}} \ . \tag{3.42}$$

where E_i are d-element sets of indices. The same partial fractioning as in Eq. (2) for products of linear denominators can be done on these factors with the result

$$P_2 = \sum_{|E_2'|+|E_3'|=d} T'_{E_2',E_3'} \prod_{s_2\in E_2'} \frac{1}{q_2\cdot p_{s_2}+a_{s_2}} \prod_{s_3\in E_3'} \frac{1}{(q_1+q_2+r)\cdot p_{s_3}+a_{s_3}} \ , \tag{3.43}$$

where we have introduced the subsets E_1' and E_2' whose union has d elements, as indicated by the first summation over all such subsets. The functions $T'_{E_1',E_2'}$ are the analogs of the functions T in Eq. (2),

$$T'_{E_2',E_3'} = \prod_{s_2\notin E_2'} \frac{1}{Q'\cdot p_{s_2}+a_{s_2}} \prod_{s_3\notin E_3'} \frac{1}{(Q'+q_1+r)\cdot p_{s_3}+a_{s_3}} \ , \tag{3.44}$$

where Q' is the solution of the following linear system

$$\begin{aligned} Q'\cdot p_{s_2}+a_{s_2} &= 0, s_2\in E_2' \\ (Q'+q_1+r)\cdot p_{s_3}+a_{s_3} &= 0, s_3\in E_3' \ . \end{aligned} \tag{3.45}$$

The solution of this linear sysytem can be found by inverting the $d\times d$ matrix whose rows are the d vectors p_{s_2} and p_{s_3} in Eq. (3.45), which we assume to be linearly independent. It can thus be written

$$Q'_\mu = f_\mu + e_{\mu\nu} q_{1,\nu} \ , \tag{3.46}$$

where f, e are rational functions of all external momenta and are independent of q_1. The functions $T'_{E_2',E_3'}$ in Eq. (3.44) can thus be written as

$$T'_{E_2',E_3'} = \prod_{f_i\in F} \frac{1}{q_1\cdot v_{f_i}+d_{f_i}} \ , \tag{3.47}$$

where $F = (E_2 - E_2')\cup(E_3-E_3')$ is a d-element set. We thus have from Eq. (3.43),

$$P_2 = \sum_{|E_2'|+|E_3'|=d} \prod_{f_i\in F} \frac{1}{q_1\cdot v_{f_i}+d_{f_i}} \prod_{s_2\in E_2'} \frac{1}{q_2\cdot p_{s_2}+a_{s_2}} \prod_{s_3\in E_3'} \frac{1}{(q_1+q_2+r)\cdot p_{s_3}+a_{s_3}} \ . \tag{3.48}$$

Explicit expressions for v and d are obtained by substituting the solutions (3.46) in Eq. (3.44). In the resulting form, the $2d$ q_2-dependent denominators P_2 in Eq. (3.43) are transformed to a sum of terms with d linear factors in q_1 and q_2, times d linear factors in q_1 alone. So far, the total number of q_i-dependent denominators is still the same as in Eq. (3.43).

Partial fractioning can now be applied to the $2d$ remaining denominators that depend on q_1 but not q_2,

$$\begin{aligned} P_1 &= \prod_{s_1\in E_1} \frac{1}{q_1\cdot p_{s_1}+a_{s_1}} T'_{E_2',E_3'} \\ &= \prod_{s_1\in E_1} \frac{1}{q_1\cdot p_{s_1}+a_{s_1}} \prod_{f_i\in F} \frac{1}{q_1\cdot v_{f_i}+d_{f_i}} \ , \end{aligned} \tag{3.49}$$

where F is the d-element set in (3.48). Going through the same steps of partial fractioning that led to (3.43) this quantity can be reduced to a linear combination of d linear factors in q_1 times products of fractions that depend only on external momenta,

$$P_1 = \sum_{E_1'} T_{E_1'}(p,a) \prod_{s_1 \in E_1'} \frac{1}{q_1 \cdot \tilde{p}_{s_1} + \tilde{a}_{s_1}} \ , \tag{3.50}$$

where $T_{E_1'}(p,a)$ are the familiar T-functions, which in this case are obtained from partial fractioning of (3.49), and the solution of a system of equations, as in (3.45).

Thus, the original integral I, Eq. (3.42), can be reduced to linear combinations of a new set of integrals with $2d$ loop momentum-dependent denominators, reduced from $3d$,

$$I(p_{e_i}, p_{j_s^i}, a_{j_s^i}) = \sum_{|E_1'|=d, |E_2'|+|E_3'|=d} I'(r, \tilde{p}_{s_i}, \tilde{a}_{s_i}) \ T_{E_1'}(p,a) \ , \tag{3.51}$$

where $T_{E_1'}(p,a)$ is a function of external momenta only and where

$$I'(r, \tilde{p}_{s_i}, \tilde{a}_{s_i}) = \int dq_1 dq_2 \frac{1}{q_1^2 + m_1^2} \frac{1}{q_2^2 + m_2^2} \frac{1}{(q_1+q_2+r)^2 + m_3^2} \tag{3.52}$$
$$\times \prod_{s_1 \in E_1'} \frac{1}{q_1 \cdot \tilde{p}_{s_1} + \tilde{a}_{s_1}} \prod_{s_2 \in E_2'} \frac{1}{q_2 \cdot p_{s_2} + a_{s_2}} \prod_{s_3 \in E_3'} \frac{1}{(q_1+q_2+r) \cdot p_{s_3} + a_{s_3}} \ .$$

This looks exactly like the original integrals (3.41) with the exception that now the sets E_2', E_3' in total have d elements (while in the original integral they had $2d$ elements). Quantities $m, r, p_{s_2}, a_{s_2}, p_{s_3}, a_{s_3}$ are the same as in the original integral, while the vectors $\tilde{p}_{s_1}$ and the scalars $\tilde{a}_{s_1}$ are rational functions of the variables of the original integral found by solving linear systems of equations, like (3.45). Note that the intergal I' is still overall UV-convergent, and UV-convergent in both q_1, q_2 sectors.

Finally, under the change of variables

$$\begin{aligned} q_2' &= q_2 + q_1 + r \\ q_1' &= -q_1 \end{aligned} \tag{3.53}$$

the function I' transforms as

$$I'(r; p_{s_1}, a_{s_1}; p_{s_2}, a_{s_2}; p_{s_3}, a_{s_3}) = I'(-r; -p_{s_1}, a_{s_1}; p_{s_3}, a_{s_3}; p_{s_2}, a_{s_2}) \ , \tag{3.54}$$

where $s_1 \in E_1', s_2 \in E_2', s_3 \in E_3'$. This identity allows the integral to be reduced to a form with no more than $[d/2]$ linear factors with $q_1 + q_2$, where $[x]$ is the largest integer not greater than x. Indeed, the integrals I' have the property that $|E_2'| + |E_3'| = d$. Therefore, if originally $|E_2'| \geq [d/2]$, then after such change of varibales $|E_2'| \leq [d/2]$.

3.5 Conclusion.

This paper describes a new method for the simplification of one-particle irreducible perturbative diagrams with many external lines. Each set of internal lines that carry the same linear

combination of loop momentum in any diagram is rewritten as a sum of terms with one quadratic and no more that d linear denominators in that momentum. In the case of tensor integrals, there can be up to $d+1$ linear factors in the numerator as well. This reduction is achieved through the use of two elementary identities, both of which are variants of partial fractioning, and which are analogous to propagator identities described in Refs. [68],[69] for tree diagrams. Arbitrary integrals are linear combinations of a basis integrals of this kind, with coefficients that are rational functions of external momenta and masses, which may take on arbitrary complex values. The analytic continuation of correlation functions is thus simplified.

The results of this study may offer a new starting point for studies of the analytic properties of correlation functions in perturbation theory, related to the use of the unitarity method [79],[63]. By writing complex diagrams as sums of integrals with reduced numbers of poles, it may be possible to simplify the study of both asymptotic behavior and analytic structure. These applications will be the subject of future research.

Chapter 4

Amplitudes in (2,2) signature.

4.1 Introduction

Scattering amplitudes are to a large extent determined by their singularity structure in the complex planes of external momenta [74, 75]. This feature has been exploited, for example, to derive a recursive construction for tree amplitudes [76] from singularities at unphysical momenta, and enables the development of unitarity-based techniques [77, 78] for the evaluation of loop integrals [79, 80].

For the construction of scattering amplitudes, any diagram in perturbation theory can be thought of as a multidimensional complex integral, in the first instance by a Wick rotation from Euclidean space. The rotation effectively changes a free Euclidean Green function, $1/(-k_1^2 - \cdots - k_n^2 - m^2)$ to the causal propagator, $1/(k_0^2 - k_1^2 \cdots - k_{n-1}^2 - m^2 + i\epsilon)$. In this sense, the choice of contour corresponds to a change in the signature of the metric, from all minus (or plus) to $(1,3)$.

Thus, the difference between Euclidean and Minkowski Green functions can be thought of as a difference in the choice of contour integration. It is therefore natural to study other signatures, corresponding to other choices of contour, in particular, a $(2,2)$ signature, for which $k^2 = k_0^2 + k_1^2 - k_2^2 - k_3^2$. In this connection, it is of interest to ask how to construct a perturbation theory based on this signature as an analytic continuation of Minkowski, and therefore ultimately Euclidean, perturbation theory.

The symmetries characteristic of $(2,2)$ signature help relate momentum to twistor spaces through a Fourier transform [81]. The relationship between perturbation theory in $(2,2)$ and Minkowski formulations [82], however, appears to be subtle and not yet fully clarified. Toward this goal, we will show below that there exists a non-singular analytic continuation for scalar diagrams, analogous to Wick rotation, from Minkowski to $(2,2)$ signature that crosses no singularities. Perhaps surprisingly, singularities in the rotated integrals are avoided by the same "$i\epsilon$" prescription as with Minkowski signature. Theories with 'two times' have also been studied for their own interest [84, 83], and most of our results below apply when the number of spatial dimensions is greater than two.

In the process of the transformation from $(1,3)$ to $(2,2)$, both internal loop integration contours and external momenta are continued in terms of a single angular variable. This naturally takes off shell any external momenta that are on the light cone for Minkowski sig-

nature, except for momenta with no components in the transverse direction that is rotated. We observe that for such momenta overlapping collinear-infrared singularities survive the rotation, and clarify a subtlety in the use of light cone coordinates that can lead to an apparent vanishing of otherwise nonzero integrals. More generally, for two, three and four-point functions, Lorentz invariance always allows us to choose momenta for which the Minkowski and $(2,2)$ functions are identical. This result holds for massive and massless internal and external lines, on shell and off-shell.

We begin the explicit development of these results in Sec. 4.2, where we show how to construct perturbation theory for $(2,2)$ signature by a Wick-like rotation from Minkowski space, and discuss similarities and differences in the singularity structure of diagrams evaluated in $(1,3)$ and $(2,2)$ signature. In $(2,2)$ signature it is natural to introduce two sets of light cone coordinates, and in Sec. 4.3 we use this approach to show that after integration over the two "minus" components of each loop, the remaining $2L$-dimensional integrals are over a finite region, dependent on the external momenta. We also observe that in $(2,2)$ signature, perturbative unitarity is realized in two different ways. Restricting ourselves to ultraviolet finite diagrams, in Sec. 4.4 we derive a representation for an arbitrary $(2,2)$ scalar diagram as a $2L$-dimensional integral. We go on in Sec. 4.5 to derive a compact representation for one-loop integrals with arbitrary masses and external momenta, and illustrate how infrared singularities manifest themselves in $(2,2)$ signature, using our representation for the box diagram. We close with a summary of our results.

4.2 From Minkowski to $(2,2)$

As indicated above, our guiding criterion for the definition of $(2,2)$ integrals is that they be analytic continuations of corresponding integrals in Minkowski space, constructed so that the continuation manifestly encounters no singularities. In fact, such a construction can be carried out by a direct generalization of Wick rotation. In this discussion, we restrict ourselves to scalar integrals only. Like Wick rotation, the construction turns out to be completely general and rather simple. We give it below, followed by a few consequences.

4.2.1 Defining the integrals

We consider an arbitrary perturbative integral, written in covariant form, with L loops and N lines of arbitrary mass, possibly with positive imaginary parts, and with external momenta p_j, which may or may not be on shell,

$$I_{N,L}(p_j) = (-i)\, i^{L-1} \prod_{\text{loops } a=1}^{L} \int \frac{d^4 l_a}{(2\pi)^4} \prod_{\text{lines } i=1}^{N} \frac{1}{k_i^2(l_a, p_j) - m_i^2 + i\epsilon}\,. \tag{4.1}$$

We take $k^2 = k_0^2 - k_1^2 - k_2^2 - k_3^2$ to start. The first factor of $-i$ on the right hand side normalizes tree diagrams to be real whenever each vertex is associated with a factor $-i$ and each line with an i. Here and below, we set the coupling constant to unity. As indicated in Eq. (4.1), line momenta are themselves determined by the loop and external momenta,

through linear combinations that can by summarized by matrices η_{ia} and ξ_{ij}, respectively,

$$k_i = \eta_{ia} l_a + \xi_{ij} p_j \,, \tag{4.2}$$

with η_{ia}, $\xi_{ij} = \pm 1$, 0. The integration contours are defined, as usual, by the "$i\epsilon$" prescription, in which energy integrals pass above the pole at the larger on shell energy for each propagator, and below the pole at the smaller on shell energy.

We now define a new parameter, θ, and a new function, $I_{N,L}(p_j, \theta)$, constructed so that it equals the original diagrammatic integral, (4.1) at $\theta = 0$,

$$I_{N,L}(p_j, \theta = 0) = I_{N,L}(p_j) \,. \tag{4.3}$$

The new function is defined in terms of momentum components, as a joint rotation of the 'one' components, p_j^1 of all external and l_a^1 of all loop momenta, as illustrated in Fig. 4.1,

$$\begin{aligned} I_{N,L}(p_j, \theta) &= (-i)\, i^{L-1} \prod_{\text{loops } a=1}^{L} \int \frac{dl_a^0 dl_a^3 dl_a^2}{(2\pi)^4} \int_{-\infty}^{\infty} d(l_a^1\, e^{-i\theta}) \\ &\times \prod_{\text{lines } i} \frac{1}{\left(k_i^0(l_a^0, p_j^0)\right)^2 - \left(\eta_{ia} l_a^1 e^{-i\theta} + \xi_{ij} p_j^1 e^{-i\theta}\right)^2 - \left(k_i^2(l_a^2, p_j^2)\right)^2 - \left(k_i^3(l_a^3, p_j^3)\right)^2 - m_i^2 + i\epsilon} \,. \end{aligned} \tag{4.4}$$

At finite θ, the real and imaginary parts of the denominator of propagator i are given by

$$\begin{aligned} \text{Re}(k_i^2 + i\epsilon) &= (k_i^0)^2 - \left(\eta_{ia} l_a^1 + \xi_{ij} p_j^1\right)^2 \cos(2\theta) - (k_i^2)^2 - (k_i^3)^2 \\ \text{Im}(k_i^2 + i\epsilon) &= \left(\eta_{ia} l_a^1 + \xi_{ij} p_j^1\right)^2 \sin(2\theta) \;+\; \epsilon \,. \end{aligned} \tag{4.5}$$

As we vary θ from zero to $\frac{\pi}{2}$, the coefficient of the square of $(k_i^1)^2$ in the real part changes sign, while the imaginary part of each diagram starts at $+i\epsilon$, increases to a maximum at $\theta = \frac{\pi}{4}$, always staying positive, and decreases back down to $+i\epsilon$ at $\theta = \frac{\pi}{2}$. For fixed values of the original momenta, p_j, the integrand is thus finite over the entire continuation in θ, and crosses no singularities. The procedure works for any choice of masses, so long as their imaginary parts are positive.

The result of this procedure, continuation from $\theta = 0$ to $\theta = \frac{\pi}{2}$, is a smooth transition from Minkowski signature, with a single time-like momentum component, to a $(2,2)$ integral, in which the 1 component has joined the 0 component as a positive contribution to the invariant squares of the momenta. This fully-rotated integral is given explicitly by

$$I_{N,L}\left(p_j, \frac{\pi}{2}\right) = - \prod_{\text{loops } a=1}^{L+1} \int \frac{dl_a^0 dl_a^1\, dl_a^2 dl_a^3}{(2\pi)^4} \prod_{\text{lines } i=1}^{N} \frac{1}{\left(k_i^0\right)^2 + \left(k_i^1\right)^2 - \left(k_i^2\right)^2 - \left(k_i^3\right)^2 - m_i^2 + i\epsilon} \,, \tag{4.6}$$

where we have suppressed the linear dependence of line momenta on loops and external lines. We note that the integrals are defined by the same $i\epsilon$-prescription as in Minkowski space, a perhaps surprising result. This definition has (at least) two important consequences for the singularity structure of $(2,2)$ diagrams, which we develop in the following two subsections.

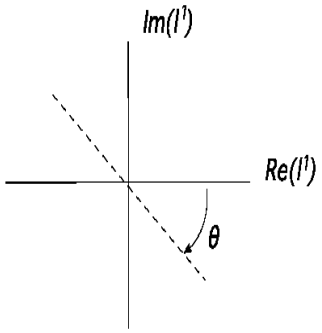

Figure 4.1: Rotation of the l^1 contour.

4.2.2 Signature-invariance of two, three and four-point functions

For two- three- and four-point functions in Minkowski space, we can always go to a frame where at least one component of spatial momentum is zero for all external lines. For $2 \to 2$ scattering, for example, this is the normal to the scattering plane. If we choose this direction as the 'one' direction above, all $p_j^1 = 0$, and the rotations of loop momenta can be carried out for fixed (Minkowskian) external momenta without crossing singularities. Indeed, if the momentum integrals are convergent, Cauchy's theorem ensures that the integrals are independent of θ, because the rotation can be treated as the change of a contour that can be closed at infinity. As a result, for such diagrams, we have

$$A_n^{(3,1)}(p_1 \dots p_n) = A_n^{(2,2)}(p_1 \dots p_n)\,, \tag{4.7}$$

for $n \leq 4$, so long as the extra time-like coordinate is chosen perpendicular to the space spanned by the p_i, which remain in a Minkowskian $(1,2)$ subspace. Such a choice is always possible for $n \leq 4$. This result applies to scalar diagrams of all orders, any choices of (real) masses, and for off-shell Green functions as well as on shell amplitudes. Indeed it applies to diagrams with any number of external lines so long as all $p_j^1 = 0$. We note that an analogous invariance applies to Wick rotation for diagrams with all $p_j^0 = 0$.

Although a simple consequence of analytic continuation, the relation (4.7) will enable us to give new representations for loop integrals in $(1,3)$ signature for two-, three- and four-point functions in Minkowski space, as special cases of general representations of n-point functions in $(2,2)$. These representations will follow from the introduction of double light cone coordinates in $(2,2)$ signature, which we will describe in Sec. 4.3. We turn first, however, to a brief investigation of the singularity structure of $(2,2)$ integrals.

4.2.3 Singularities in $(2,2)$

Starting from the defining equation (4.6), we can make quite strong statements about the origin of the singularities of perturbative integrals in $(2,2)$ signature. In particular, because they share the same $i\epsilon$ prescription with their $(1,3)$ counterparts, the Landau equations [74, 85, 86] that help determine singularities in perturbative integrals take the same form for $(1,3)$ and $(2,2)$ signatures, Eqs. (4.1) and (4.6). This is most easily confirmed by reviewing

the use of Feynman parameterization to identify possible pinches in loop integrals [74], to emphasize its signature independence. For the $(2,2)$ case, for example, we have simply

$$I_{N,L}\left(p_j,\frac{\pi}{2}\right) = -\Gamma(N-1)\prod_{\text{loops }a=1}^{L}\int\frac{dl_a^0 dl_a^1\,dl_a^2 dl_a^3}{(2\pi)^4}\prod_{\text{lines }i=1}^{N}\int_0^1 d\alpha_i\;\delta\left(1-\sum_{i=1}^{N}\alpha_i\right) \times\frac{1}{\left[\sum_{i'=1}^{N}\alpha_{i'}\left[k_{i'}^2(l_a,p_j)-m_{i'}^2\right]+i\epsilon\right]^N}\,, \tag{4.8}$$

the difference from $(1,3)$ being entirely in the definition of the k_i^2 on the right hand side, and the argument on the left. Because line momenta $k_{i'}$ are linear in loop momenta l_a, the single, parameterized denominator is quadratic in every loop momentum component l_a^ν, while being linear in the parameters $\alpha_{i'}$. We note that the relative signs of the denominator terms in this expression are determined uniquely by requiring that the coefficient of the imaginary term $i\epsilon$ be α_i-independent. This ensures that whatever component integral we do first has one Nth order pole in the upper half plane, and one in the lower half plane.

Necessary conditions for the presence of a singularity in (4.8) are then that those line momenta $k_{i'}$ whose coefficients $\alpha_{i'}$ are nonzero must satisfy

$$\frac{\partial}{\partial l_a^\nu}\left[\sum_{i'=1}^{N}\alpha_{i'}\left(k_{i'}(l_a,p_j)\right)^2+i\epsilon\right]=2\sum_{i'=1}^{N}\alpha_{i'}\eta_{ai'}k_{i'}^\nu(l_a,p_j)=0\,, \tag{4.9}$$

for every component ν of every loop l_a, with η_{ai} the matrix that relates loop to line momenta in Eq. (4.2) above. These are the same (Landau) equations, whether in $(1,3)$ or $(2,2)$. A singularity also requires, of course, that $k_i^2=m_i^2$ for the relevant lines. Thus, given the differences in the signatures that define k_i^2 for $(1,3)$ and $(2,2)$, there is no immediate correspondence between momentum configurations found in the two cases for the same diagrams. In particular, it is not obvious whether there is an analog in $(2,2)$ of the Coleman-Norton criterion for singularities [87] in $(1,3)$, that on shell momenta at a singularity correspond to a physical scattering process. This would at least require us to develop intuition on what "physical scattering" means in $(2,2)$ signature. Nevertheless, although we do not have such a general criterion for singularities in $(2,2)$, we can make some significant observations, finding a wide range of both similarities and differences from $(1,3)$.

In this connection, we note a simple result on singularity surfaces for Green function integrals like $I_{N,L}(p_j,\theta)$, Eq. (4.8). When the external lines of a diagram are restricted to a subspace where one component vanishes for all lines,

$$p_j^\nu=0\,,\quad \text{all } j\,, \tag{4.10}$$

the corresponding component of all *internal* on-shell lines must vanish at any pinch singularity. To see this, consider an arbitrary "candidate" pinch surface with a set of on shell lines, k_l, $k_l^2=m_l^2$, some of which have nonzero component k_l^ν. Starting with any line momentum $k_i\in\{k_l\}$ with $k_i^\nu\neq 0$, we can follow the flow of positive (or negative) k_i^ν, from line i into some unique vertex of the diagram, which we label as, say, v_0. Let us consider the combination k_i, v_0 as the beginning of a path (a "chain") through the diagram. We continue the

path by picking any line attached to vertex v_0 that carries positive ν component out of v_0 to some other vertex v_1. By momentum conservation, there must be at least one such line. In this way, we continue the path through the diagram. Because of our assumption (4.10), the ν component can never flow out of the diagram, and therefore the path will stay inside the diagram at each step. If the diagram is of finite order, the path will eventually intersect itself, by connecting a sequence of vertices,

$$v_0 \to v_1 \to \cdots \to v_n \to v_0 \,. \tag{4.11}$$

In general, there is more than one such path if the diagram has more than one loop, but in any case we can pick a loop momentum l_a that flows precisely around the loop specified by the sequence of vertices (4.11). For this loop, all the factors η_{ia} and all the ν components of lines k_i are positive, and the Landau equations (4.9) cannot be satisfied for nonzero α_i. Therefore, this set of lines, and since they are arbitrary any set of lines with nonzero k_i^ν, cannot satisfy the Landau equations and cannot be pinched on shell.

This result shows us that a kinematic range where the two signatures give a similar singularity structure can be found for $2 \to 2$ on shell scattering amplitudes,

$$p_1 + p_2 \to p_3 + p_4 \,, \quad p_i^1 \;=\; 0 \,, \quad p_i^0 \;>\; 0 \,. \tag{4.12}$$

For such a process, no pinch surface can have internal lines with a one component, and the classification of pinch singularities follows the same reasoning as in Minkowski space [89, 90, 91]. It is worth pointing out that in Minkowski space, because the scattering is planar in the center-of-mass, pinch surfaces are always restricted to a three-dimensional subspace here as well. Recall that we have observed above that the continuation can be carried out without changing external momenta in this frame. The only difference in $(2,2)$ compared to $(1,3)$ is that the "normal" to this subspace is now a time-like rather than a space-like variable. In particular, for fixed angle scattering in massless theories [89, 90, 91], pinch surfaces in $(2,2)$ reduce to the same "jet", "soft" and "hard" subdiagrams long known to characterize these amplitudes in Minkowski space. We will not pursue a further investigation of this case here, but only note that there is every reason to believe that for gauge theories the basic factorization properties and infrared structure of massless Minkowski $2 \to 2$ amplitudes [90, 91] are the same in $(2,2)$.

The fundamental similarity between $(1,3)$ and $(2,2)$ singularity structure for $2 \to 2$ amplitudes is certainly the exception, and we need not look far for fundamental differences, once we relax the condition $p_j^1 = 0$, for external lines. Indeed, once the number of external lines exceeds four, this condition restricts us to a subspace of their full momentum space. In the new signature, a general amplitude has many singularities that are qualitatively different from those found in Minkowski signature.

A fundamental property of light-like lines in Minkowski space is that the sum of two positive energy light-like momenta has a positive semi-definite invariant mass, which vanishes only when the momenta are proportional, that is to say, the lines are collinear. For $(2,2)$ signature, in contrast, every light-like momentum, v^μ, $v^0 > 0$ defines a one dimensional subspace of light-like vectors $\bar{v}^\mu$ with $\bar{v}^2 = \bar{v} \cdot v = 0$, found by making equal $SO(2)$ rotations

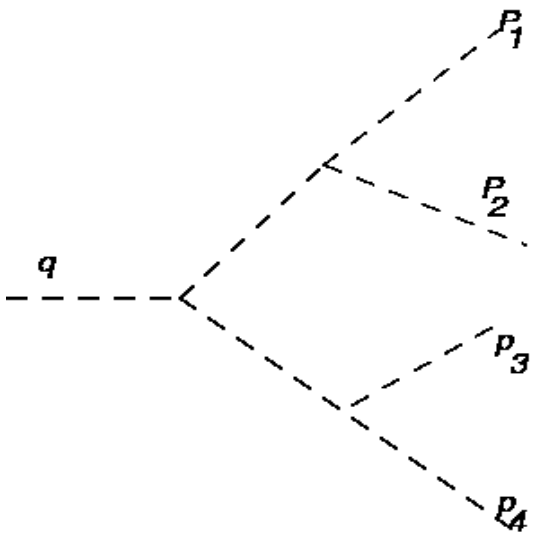

Figure 4.2: One-to-four scalar process discussed in the text.

on the pairs (v^0, v^1) and (v^2, v^3),

$$\bar{v}^\mu = \begin{pmatrix} R & 0 \\ 0 & R \end{pmatrix} \begin{pmatrix} v^0 \\ v^1 \\ v^2 \\ v^3 \end{pmatrix}, \; R \in SO(2)\,. \tag{4.13}$$

As a result, in $(2,2)$, the sum of two, non-collinear light-like momenta can also be light-like. This has consequences for the singularity structure even of tree diagrams, as illustrated by Fig. 4.2. Here we start with the generalized "rest" momentum, $q^\mu = (Q, Q', 0, 0)$ in $(2,2)$ signature, and we show a lowest-order diagram that produces four lines of momenta

$$\begin{aligned} p_1 &= \left(\frac{Q}{2}\,, 0\,, 0\,, \frac{Q}{2}\right), \\ p_2 &= \left(0\,, \frac{Q'}{2}\,, \frac{Q'}{2}\,, 0\right), \\ p_3 &= \left(\frac{Q}{2}\,, 0\,, 0\,, -\frac{Q}{2}\right), \\ p_4 &= \left(0\,, \frac{Q'}{2}\,, -\frac{Q'}{2}\,, 0\right). \end{aligned} \tag{4.14}$$

For this set of "outgoing particles", the virtual lines have $(p_1+p_2)^2 = (p_3+p_4)^2 = 0$, in sharp contrast to the corresponding diagrams of Minkowski space whenever the outgoing lines are noncollinear. This suggests that beyond the simplest amplitudes, the concept of "jets", for example, would have to be generalized in any complete picture of $(2,2)$ scattering.

4.3 Light Cone Variables

We now turn to another interesting feature of $(2,2)$ integrals that are ultraviolet convergent. In the rotated integral, $I_{N,L}(p_j, \frac{\pi}{2})$, Eq. (4.6), there is a nice symmetry between the pairs of components, $0,3$ and $1,2$, and it is natural to introduce two pairs of light cone loop momentum variables,

$$\begin{aligned} k^{\tilde{\pm}} &\equiv k^1 \pm k^2 \,, \\ k^{\pm} &= k^0 \pm k^3 \,, \end{aligned} \tag{4.15}$$

where we have chosen a normalization for which

$$\begin{aligned} k^2 &= k^+ k^- + k^{\tilde{+}} k^{\tilde{-}} \,, \\ 2k \cdot k' &= k^+ k'^- + k^- k'^+ + k^{\tilde{+}} k'^{\tilde{-}} + k^{\tilde{-}} k'^{\tilde{+}} \,, \\ d^4k &= \frac{1}{4} dk^+ dk^{\tilde{+}} dk^- dk^{\tilde{-}} \,. \end{aligned} \tag{4.16}$$

We use these variables below to develop a procedure for doing $2L$ integrals in an arbitrary ultraviolet finite L-loop diagram. Before doing so, we point out one subtle point in making such a change of variables. This observation applies as well to the use of light cone variables in $(1,3)$ to develop, for example, light cone ordered perturbation theory [92].

4.3.1 Convergence and light cone variables

Consider the manifestly finite two-dimensional integral, of a self-energy form,

$$\begin{aligned} I_2\left(p, m^2\right) &= -i \int_{-\infty}^{\infty} \frac{dk_1 dk_0}{(2\pi)^2} \, \frac{1}{[(k_0+p)^2 - (k_1-p)^2 - m^2 + i\epsilon]} \, \frac{1}{[k_0^2 - k_1^2 - m^2 + i\epsilon]} \\ &= \frac{1}{4\pi\, m^2} \,. \end{aligned} \tag{4.17}$$

Here the two-dimensional "external" momentum is $P = (P_0, P_1) = (p, -p)$, with $p > 0$. The result of this integral is independent of parameter p because $P^2 = 0$, and readily follows from standard formulas based on Feynman parameterization and Wick rotation. We can also evaluate (4.17) as a pair of complex integrals explicitly in terms of its poles. Each of the two variables, k_0 and k_1 encounters four poles, two in each half plane, and we can perform the integral by closing one contour in either the upper or lower half plane without Wick rotation.

Now let us try to re-express the integral, Eq. (4.17) in terms of light cone coordinates, $k^{\pm} \equiv k_0 \pm k_1$, as in Eq. (4.15). In this notation, the vector P has $P^- = 2p$ and $P^+ = 0$. This, however, gives

$$I_2\left(m^2\right) = \frac{-i}{2} \int_{-\infty}^{\infty} \frac{dk^+ dk^-}{(2\pi)^2} \, \frac{1}{[k^+(k^- + 2p) - m^2 + i\epsilon]} \, \frac{1}{[k^+ k^- - m^2 + i\epsilon]} \,, \tag{4.18}$$

which vanishes because the two poles in the k^- integral are always on the same side of the contour, regardless of the value of k^+. This would seem to imply that the self energy vanishes

whenever $P^+ = 0$, a paradoxical result that would extend to four dimensions. On the other hand, if we do the k^+ integral first, the result is nonzero, because the two poles in k^+ are on opposite sides of the contour for $-P^- < k^- < 0$.

The reason for this inconsistency is that the change from Cartesian to light cone variables involves an exchange of integrals that are not uniformly convergent in this case. To be specific, suppose we wish to do the k^- integral first at fixed k^+. We would then first change variables from (say) k_0 to k^+ in the original k_0, k_1 form, Eq. (4.17) at fixed k_1, giving

$$\begin{aligned} I_2\left(m^2\right) &= \frac{-i}{(2\pi)^2}\int_{-\infty}^{\infty} dk_1 \int_{-\infty}^{\infty} dk^+ \, \frac{1}{[(k^+ - k_1 + p)^2 - (k_1 - p)^2 - m^2 + i\epsilon]} \\ &\qquad \times \frac{1}{[(k^+ - k_1)^2 - k_1^2 + i\epsilon]} \, . \end{aligned} \tag{4.19}$$

The next step would be to exchange the k_1 and k^+ integrals, and then change variables from k_1 to k^- at fixed k^+, giving (4.18), but this is not possible because the unbounded k_1 integral diverges badly for $k^+ = 0$. We may note, however, that this pitfall does not prevent us from carrying out rotations in Cartesian coordinates from $(1,3)$ to $(2,2)$ as above. The transition to light cone coordinates is a separate issue.

4.3.2 Finite volume

Having pointed out a subtlety associated with the vanishing of external plus momenta, we can limit ourselves to all nonzero external plus momenta. In this case, we can do all the minus loop integrals in a given diagram, to get a sum of terms given by the rules of light cone ordered perturbation theory (LCOPT) [92]. This procedure does not depend at all on whether or not we have carried out the rotation that takes us from $(1,3)$ to $(2,2)$ signature. For a scalar diagram $\mathcal{G}$ (normalized as above so that tree graphs are real) the LCOPT expression found by integration over minus momenta is related to the covariant form by

$$\begin{aligned} \mathcal{G}(\{p_a\}) &\equiv (-i)\, i^{L-1} \sum_{\text{orderings } T} \int \prod_{\text{loops}\,\{l\}} \frac{d^4 l}{4(2\pi)^4} \prod_{\text{lines}\,k} \frac{1}{k^2 - m_k^2 + i\epsilon} \\ &= -\int \prod_{\text{loops}\,\{l\}} \frac{d\tilde{l}^+ d\tilde{l}^- dl^+}{4(2\pi)^3} \prod_{\text{lines}\,\{k\}} \frac{\theta(k^+)}{k^+} \prod_{\text{states}\,\{i\}\ \text{in}\ T} \frac{1}{P_i^- - s_i\left([k]\right) + i\epsilon} \ , \end{aligned} \tag{4.20}$$

where $P_i^- = \sum_{a \in i} p_a^-$ is the algebraic sum of total incoming and outgoing minus momenta up to state i, and where

$$\begin{aligned} s_i\left([k]\right) &= \sum_{\text{lines}\,\{k\} \in \text{state}\, i} [k]^- \\ &= \sum_{k \in i} \frac{-k^{\tilde{+}} k^{\tilde{-}} + m_k^2}{k^+} \\ &\equiv \sum_{k \in i} \Big(- k^{\tilde{-}} r_k + \mu_k \Big) \ , \end{aligned} \tag{4.21}$$

is the sum of all the on shell minus momenta in a specific state. We have written the result in terms of the $(2,2)$ signature transverse 'light cone' variables formed from $k_T = (k^1, k^2)$ in Eq. (4.15), and we define

$$\begin{aligned} r_k &\equiv \frac{k^{\tilde{+}}}{k^+} \\ \mu_k &\equiv \frac{m_k^2}{k^+}\,, \end{aligned} \tag{4.22}$$

where the label k identifies both the line momentum and the corresponding mass. The transition to $(2,2)$ signature can be carried out before the minus integrals that lead to the second equality in Eq. (4.20), or after.

We will first use the invariant integral representation of an arbitrary ultraviolet finite diagram in Eq. (4.20) to show that the volume of the l^+ integrals is finite after the l^- integrals at fixed $l^{\tilde{+}}$ and $l^{\tilde{-}}$. We will go on to use the light cone ordered form to show that the $l^{\tilde{+}}$ integrals also have a finite volume after the integration over the $l^{\tilde{-}}$ for diagrams that are ultraviolet finite.

Assume, then, that some plus loop momentum grows without bound in such a way that it is much larger than the corresponding components of all external momenta. As we shall see, it is then possible to find a minus loop integral such that all of its poles are in the same half-plane, either upper or lower. Such an integral gives zero, and because we assume that the diagrams are well-behaved at infinity, we can choose to do this minus integral first. We conclude that the integral is non-zero only in a bounded region in plus momentum. To be specific, let us provide an explicit construction of the loop in question, by an argument similar to that of Sec. 4.2.3 above.

The construction begins by identifying the internal line with the largest plus momentum, which we may call $K_1^+ > 0$. We can choose the orientation of momentum flow so that this quantity is positive. Momentum K_1^+ then flows into a unique vertex of the diagram, which we may call V_1, and out of a unique vertex V_0. Suppose that vertex V_1 is an a-point vertex. Since momentum K_1^+ flows in to V_1 at least one line must carry a momentum $K_2^+ \geq K_1^+/(a-1)$ out of V_1. If K_1^+ is sufficiently large, this line cannot flow out of the diagram, but must flow to another vertex, V_2, internal to the diagram. Assuming for simplicity that this is also an a-point vertex, at least one line must carry plus momentum $K_3^+ \geq K_1^+/(a-1)^2$ out of V_2. We repeat the process, following the largest flow of plus momentum, and in each case, we find a momentum that flows out of the next vertex that is proportional to K_1^+, and which therefore cannot carry momentum onto an external line when K_1^+ is large enough. For any diagram of finite order, we will eventually encounter a vertex $V_m = V_k$, with $k = 0 \ldots m-2$ ($m = 2$ is not possible for a diagram with no ultraviolet-divergent subdiagrams in four dimensions). This is the loop we are after.

Exactly the same reasoning would apply to show that the $l^{\tilde{+}}$ integrals also have a finite volume at fixed l^+ and l^-. We show next, however, that the $l^{\tilde{+}}$ integration regions are limited even *after* the l^- integrals are performed. For this, we apply a similar reasoning to the light cone ordered expression, the second equality in Eq. (4.20). That is, we assume that some set of loop momenta, $\{l_a^{\tilde{+}}\}$ become large enough that it is possible to find a loop around which every line carries plus tilde momentum in the direction of the loop. We claim that in this case, the momentum $l_b^{\tilde{-}}$ that flows around this loop sees poles only in the lower (or upper)

half plane in Eq. (4.20), so that its integral vanishes. To show this, we consider the on shell momentum of the ith line in this loop, of momentum k_i. Neglecting external momenta and masses for large loop momenta, we have

$$[k_i]^- = -k_i^{\tilde{-}} \frac{k_i^{\tilde{+}}}{k^+} = -\left(\eta_{ib} l_b^{\tilde{-}} + \sum_{a\neq b} \eta_{ia} l_a^{\tilde{-}}\right) \frac{\left(\eta_{ib} l^{\tilde{+}} + \sum_{a\neq b} \eta_{ia} l_a^{\tilde{+}}\right)}{k_i^+}, \tag{4.23}$$

where as in Eq. (4.2), $\eta_{bi} = \pm 1$ around the loop, depending on whether loop l_b flows with or against the defining direction of line momentum k_i, and where the sum over a includes all loop momenta with the exception of l_b. To be definite, suppose $l_b^{\tilde{+}}$ is large and positive. The condition that each component $k_i^{\tilde{+}}$ flows in the same direction as loop momentum l_b can then be written as

$$\eta_{ib} l_b^{\tilde{+}} + \sum_{a\neq b} \eta_{ia} l_a^{\tilde{+}} = \eta_{ib} \left| l_b^{\tilde{+}} + \frac{1}{\eta_{ib}} \sum_{a\neq b} \eta_{ia} l_a^{\tilde{+}} \right|. \tag{4.24}$$

We then have

$$[k_i]^- = -\left(\eta_{ib}^2 l_b^{\tilde{-}} + \eta_{ib} \sum_{a\neq b} \eta_{ia} l_a^{\tilde{-}}\right) \frac{\left| l_b^{\tilde{+}} + \frac{1}{\eta_{ib}} \sum_{a\neq b} \eta_{ia} l_a^{\tilde{+}} \right|}{k_i^+}, \tag{4.25}$$

and the coefficient of $l_b^{\tilde{-}}$ is always positive for every term in which it appears in the LCOPT denominators of Eq. (4.20), since k_i^+ is also always positive. All $l_b^{\tilde{-}}$ poles are thus in the same half plane (lower for $l_b^{\tilde{+}}$ positive), and the integrals vanish so long as the loop appears in at least two states. This, however, is ensured by our assumption of an ultraviolet-finite scalar diagram.

4.3.3 Unitarity(ies)

The light cone ordered expression (4.20) for an arbitrary diagram implies the order-by-order unitarity of perturbation theory, a relation that has been used extensively in showing the cancellation of infrared divergences in inclusive cross sections [88, 93, 94]. Here we note only the fundamental identity at the basis of this connection. We consider an arbitrary diagram $\mathcal{G}^{(T)}$, with a specific light cone order T, and sum over the terms found by setting each state, s_i of T on shell in turn, replacing its light cone denominator by a delta function. Each such substitution we refer to as a "cut" of the diagram. All states before (to the left of) the cut retain a $+i\epsilon$ prescription, and those after the cut (to the right) are given a $-i\epsilon$ prescription. See the left hand side of Fig. 4.3.

Each cut in the figure splits the ordered diagram into two ordered sub-amplitudes, $\mathcal{G}_{j,l}^{(T)}$ and $\mathcal{G}_{j,r}^{(T)}$, at fixed loop momenta to the "left" and "right" of the cut, respectively. The

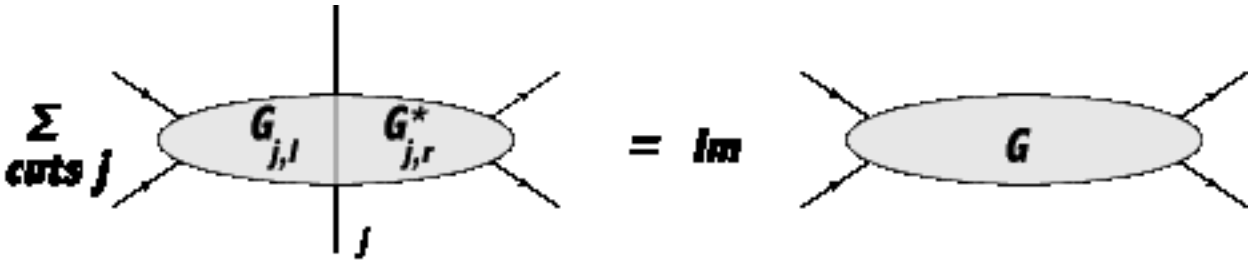

Figure 4.3: A representation of perturbative unitarity, Eq. (4.26) for an arbitrary diagram G. As shown in the text, after an integral over loop l^- integrals, this relation holds for each light cone ordering of diagram G at fixed values of all loop l^+, and l^1, l^2 or $l^{\tilde{+}}$ and $l^{\tilde{-}}$. A similar result holds when all $l^{\tilde{-}}$ integrals are carried out at fixed $l^{\tilde{+}}$, l^+ and l^-.

fundamental identity, which holds at fixed values of the all loop momenta l_a^+, $l_a^{\tilde{+}}$ and $l_a^{\tilde{-}}$, is

$$\begin{aligned}
\mathcal{G}_{j,r}^{(T)*}\mathcal{G}_{j,l}^{(T)} &= \sum_{j=1}^{V_{\mathcal{G}}-1}\left(\prod_{i'=j+1}^{V_{\mathcal{G}}-1}\frac{1}{P_{i'}^- - s_{i'} - i\epsilon}\right) 2\pi\delta\left(P_j^- - s_j\right)\left(\prod_{i=1}^{j-1}\frac{1}{P_i^- - s_i + i\epsilon}\right) \\
&= -i\left[\left(\prod_{i'=1}^{V_{\mathcal{G}}-1}\frac{1}{P_{i'}^- - s_{i'} - i\epsilon}\right) - \left(\prod_{i=1}^{V_{\mathcal{G}}-1}\frac{1}{P_i^- - s_i + i\epsilon}\right)\right] \\
&= -i\left[\mathcal{G}^* - \mathcal{G}\right] , \qquad (4.26)
\end{aligned}$$

where $\mathcal{G}$ is the uncut diagram at fixed remaining components of loop momenta and $V_{\mathcal{G}}$ the number of vertices in $\mathcal{G}$. The on shell value of minus momentum for state i is s_i. The proof of this relation follows easily from repeated use of the distribution identity, $2\pi i\delta(x) = 1/(x - i\epsilon) - 1/(x + i\epsilon)$. In this form the integrand of the sum of cut diagrams is related to the imaginary part of the integrand for the uncut diagram, a generalized form of the optical theorem, as illustrated by Fig. 4.3.

At the level of the fundamental identity, Eq. (4.26), then, unitarity is a property of perturbation theory in $(2, 2)$ signature as much as in Minkowski space. In fact, we can derive light cone ordered perturbation theory just as well by performing the $l^{\tilde{-}}$ integrals as the l^- integrals, deriving an identity of exactly the same form as Eq. (4.26) for an arbitrary diagram, but now at fixed loop momenta l^+, l^- and $l^{\tilde{+}}$. In a sense, then, there is an extra unitarity relation for $(2, 2)$ compared to $(1, 3)$. We do not have a practical application of this result to propose at this time.

4.4 $2L$-dimensional representation

The double set of light cone coordinates of Eq. (4.15) can be used to derive a new representation for diagrammatic integrals, based on the linearity of all propagators in the minus and minus tilde variables. We start with the general scalar integral, Eq. (4.6), in $(2, 2)$ signature for an arbitrary diagram with L loops and N lines, assuming that $L_g > 2N_g$ for any

subgraph, g, so that all subintegrals are convergent,

$$I_{N,L}(p_j) \equiv - \int \prod_{i=1}^{L} \frac{dl_i^+ \, dl_i^{\tilde{+}}}{2(2\pi)^2} \, \frac{dl_i^{\tilde{-}} \, dl_i^-}{2(2\pi)^2} \, \prod_{\alpha=1}^{N} \frac{1}{D_\alpha} \, . \tag{4.27}$$

In the defining normalizations of Eq. (4.15), the denominators are given by

$$\begin{aligned} D_\alpha &= (l_\alpha - p_\alpha)^2 - m_\alpha^2 + i\epsilon \\ &\equiv \left(l_\alpha^+ - p_\alpha^+\right)\left(l_\alpha^- - p_\alpha^-\right) + \left(l_\alpha^{\tilde{+}} - p_\alpha^{\tilde{+}}\right)\left(l_\alpha^{\tilde{-}} - p_\alpha^{\tilde{-}}\right) - m_\alpha^2 + i\epsilon \, . \end{aligned} \tag{4.28}$$

Here l_α and p_α are the combinations of loop momenta l_i and external momenta p_j, respectively, flowing along internal line line α, with momentum k_α. In the notation of Eq. (4.2),

$$l_\alpha = \eta_{\alpha i} l_i \, , \quad p_\alpha = \xi_{\alpha j} p_j \, , \tag{4.29}$$

with $\eta_{\alpha i}, \ \xi_{\alpha j} = \pm 1, 0$. Making the minus and minus-tilde loop momentum dependence explicit, we write the denominators as

$$D_\alpha = A_{\alpha i}^+ l_i^- \ + \ A_{\alpha i}^{\tilde{+}} l_i^{\tilde{-}} + B_\alpha \, , \tag{4.30}$$

in terms of coefficients A and B, defined by

$$\begin{aligned} A_{\alpha i}^+ &= (l_\alpha^+ - p_\alpha^+)\eta_{\alpha i} \, , \\ A_{\alpha i}^{\tilde{+}} &= (l_\alpha^{\tilde{+}} - p_\alpha^{\tilde{+}})\eta_{\alpha i} \, , \\ B_\alpha &= (p_\alpha^+ - l_\alpha^+)p_\alpha^- \ + \ (p_\alpha^{\tilde{+}} - l_\alpha^{\tilde{+}})p_\alpha^{\tilde{-}} - m_\alpha^2 \\ &= p_\alpha^2 - m_\alpha^2 - 2\hat{p}_\alpha \cdot l \, , \end{aligned} \tag{4.31}$$

where in the second relation for B_α, we define a vector with only minus and minus tilde components,

$$\hat{p}_\alpha^\mu \equiv \left(0^+, p_\alpha^-, 0^{\tilde{+}}, p_\alpha^{\tilde{-}}\right) \, . \tag{4.32}$$

The linearity of all denominators, (4.28) in both sets of integration variables $\{l_i^-\}$ and $\{l_i^{\tilde{-}}\}$ will allow us to derive an explicit form for each integral $I_{N,L}$ as a sum over choices of $2L$ on shell ('cut') lines.

Our integrals can be put into a more compact form by introducing a single index to cover the sum over components *and* loops,

$$I_{N,L}(p_j) = - \left(\frac{1}{4(2\pi)^4}\right)^L \int \prod_{k=1}^{2L} dy_k \int \frac{\prod_{j=1}^{2L} dx_j}{\prod_{\alpha=1}^{N} (\sum_{j=1}^{2L} A_{\alpha j} x_j + B_\alpha + i\epsilon)} \, , \tag{4.33}$$

where $\{x_j\} \equiv \{l_i^-, l_i^{\tilde{-}}\}$, runs over the minus and minus tilde components of all loops and α over the set of lines. To make our result as explicit as possible, we are free to define

$$\begin{aligned} x_{2i-1} &= l_i^- \, , \\ x_{2i} &= l_i^{\tilde{-}} \, , \end{aligned} \tag{4.34}$$

where i runs from 1 to L. Correspondingly, we may define the remaining $2L$ integration variables as

$$\begin{aligned} y_{2i-1} &= l_i^{\tilde{+}}\,, \\ y_{2i} &= l_i^{+}\,, \end{aligned} \tag{4.35}$$

for the set y_k. The relabeled coefficients $A_{\alpha i}$ are then linear functions of parameters y and can be thought of as defining a matrix. To be explicit, in terms of the coefficients of Eq. (4.31), we define

$$\begin{aligned} A_{\alpha,2i-1} &\equiv A_{\alpha i}^{+}\,, \\ A_{\alpha,2i} &\equiv A_{\alpha i}^{\tilde{+}}\,. \end{aligned} \tag{4.36}$$

We may choose to do the integrals in the order $y_1 \cdots y_{2L}$, and as we will see, individual terms in our results depend in a structured manner on the order of integration. The final result, however, cannot depend on the order.

The essential observation regarding the integral in Eq. (4.33) is that the singularity structure of the integrand for each x_j is simple poles at every step in the integration procedure, and that closing on these poles does not affect the limits of the remaining x_j, only the y_j. We will choose to perform these integrals by closing contours in each lower half complex x_j-plane. The choice of each pole sets one line on shell, and at the end of $2L$ integrations we have a sum of terms in which $2L$ lines are "cut" in this fashion. Let an arbitrary sequence of k lines found in this way be labelled $\mathcal{A}_k$, where $k = 1$ labels the first line set on shell, and $\mathcal{A}_{2L}$ the full set for the sequence. Each set $\mathcal{A}_k$ must be such that: (i) its lines carry k linearly independent loop momenta, and (ii) after any m integrals $x_1 \ldots x_m$, $m \leq k-1$, there must be a lower half-plane pole in the next integration variable, x_{m+1}. Let us denote by $A^{(\mathcal{A}_k)}$ the $k \times k$ matrix whose elements are $A_{\alpha j}$, such that $j = 1 \ldots k$ and $\alpha \in \mathcal{A}_k$.

The result we are after clearly depends on the values of the x_j when k, $k = 1 \ldots 2L$, lines are set on shell, that is on solutions to a system of $2L$ linear equations in $2L$ variables. For any choice of k lines, where k need not be an even number, these equations are

$$A_\alpha^{(\mathcal{A}_k)} \cdot x + B_\alpha^{(\mathcal{A}_k)} + i\epsilon \equiv \sum_{j=1}^{k} A_{\alpha j}^{(\mathcal{A}_k)} x_j + B_\alpha^{(\mathcal{A}_k)} + i\epsilon = 0\,, \quad \alpha \in \mathcal{A}_k\,, \tag{4.37}$$

where, again, the superscripts identify $A^{(\mathcal{A}_k)}$ as a $k \times k$ matrix and $B^{(\mathcal{A}_k)}$ as a k-component vector. The matrix, of course, must be non-singular, which is to say that we will find k independent poles only if the momenta of these lines are linearly independent. The solution to Eq. (4.37) can be represented in terms of its real and imaginary parts $x_j = X_j^{(\mathcal{A}_k)} + i\epsilon Y_j^{(\mathcal{A}_k)}$, $j = 1 \ldots k$ as [1]

$$\begin{aligned} X_j^{(\mathcal{A}_k)} &= -\sum_{\alpha'} \left(A^{(\mathcal{A}_k)}\right)^{-1}_{j\alpha'} B_{\alpha'}^{(\mathcal{A}_k)}\,, \\ Y_j^{(\mathcal{A}_k)} &= -\sum_{\alpha'} \left(A^{(\mathcal{A}_k)}\right)^{-1}_{j\alpha'}\,, \end{aligned} \tag{4.38}$$

[1] Here we assume that all masses are real. The generalization to masses with positive imaginary parts is immediate.

in terms of the inverse of matrix $A^{(\mathcal{A}_k)}$. Note the sum over unrepeated index α' in the expression for the imaginary part. The solutions in (4.38) determine the values of the remaining denominators when all $k \to 2L$ denominators are replaced by delta functions. This result alone does not determine the integral, however, because of theta functions that result from closing each contour in the lower half-plane in turn. The arguments of these step functions depend, in general, on the order in which the integrals are carried out.

We will now show that in the notation of Eq. (4.38), the result of doing the $2L$ x_j integrals in (4.33) is given by

$$\begin{aligned} I_{N,L} &= -\left(\frac{-1}{4(2\pi)^2}\right)^L \sum_{\mathcal{A}_{2L}} \int \prod_{k=1}^{2L} dy_k \; \theta\left(\frac{\det A^{(\mathcal{A}_{k-1})}\; F_{\alpha_k}^{(\mathcal{A}_k)}(y_1 \dots y_k)}{\det A^{(\mathcal{A}_k)}(y_1 \dots y_k)}\right) \\ &\quad \times \frac{1}{\det(A^{(\mathcal{A}_{2L})})} \frac{1}{\prod_{\beta \notin \mathcal{A}_{2L}} (A_\beta \cdot X^{(\mathcal{A}_{2L})} + B_\beta + i\epsilon(1 + A_\beta \cdot Y^{(\mathcal{A}_{2L})}))} \,. \end{aligned} \tag{4.39}$$

The product of theta functions depends, as suggested above, on the order of integration. For the kth integration, we find

$$F_{\alpha_k}^{(\mathcal{A}_k)} = 1 + \sum_{j=1}^{k-1} A_{\alpha_k j}^{(\mathcal{A}_k)}\, Y_j^{(\mathcal{A}_{k-1})} \,, \tag{4.40}$$

where α_k is the index of the kth line put on shell, as above $A^{(\mathcal{A}_k)}$ is the $k \times k$ matrix associated with the first k lines, and where $Y_j^{(\mathcal{A}_{k-1})}$ is the solution for the imaginary part of x_j given in (4.38) when the first $k-1$ lines are put on shell. It should be noted that in the sum over sequences $\mathcal{A}_{2L}$ there are many terms that differ only in sign and integration region. The sign comes from the determinant of $A^{(\mathcal{A}_{2L})}$. Note the response of the imaginary parts to the selection of poles, as analyzed in the context of "loop-tree" dualities for Minkowski integrals [95, 96, 97].

For an inductive proof of Eq. (4.39), we start by noting that that the role of the y_j is entirely passive. We need therefore only consider the proof of

$$\begin{aligned} J_{N,l}\,(A_{\alpha i}, B_\alpha) &\equiv \int \frac{\prod_{j=1}^{l} dx_j}{\prod_{\alpha=1}^{N} (\sum_{j=1}^{l} A_{\alpha j} x_j + B_\alpha + i\epsilon)} \\ &= -(-2\pi i)^l \sum_{\mathcal{A}_l} \prod_{k=1}^{l} \theta\left(\frac{\det A^{(\mathcal{A}_{k-1})}\; F_{\alpha_k}^{(\mathcal{A}_k)}(y_1 \dots y_l)}{\det A^{(\mathcal{A}_k)}(y_1 \dots y_l)}\right) \\ &\quad \times \frac{1}{\det(A^{(\mathcal{A}_l)})} \frac{1}{\prod_{\beta \notin \mathcal{A}_l} (A_\beta \cdot X^{(\mathcal{A}_l)} + B_\beta + i\epsilon(1 + A_\beta \cdot Y^{(\mathcal{A}_l)}))} \,, \end{aligned} \tag{4.41}$$

for arbitrary l. The case of $l = 1$, $J_{N,1}$ is easily verified, and for any l, we can use the relation

$$J_{N,l}\,(A_{\alpha i}, B_\alpha) = \int dx_l \; J_{N,l-1}\,(A_{\alpha i}, B_\alpha + A_{\alpha l} x_l) \;, \tag{4.42}$$

in which the x_l integral of $J_{N,l}$ is absorbed into the B's for $J_{N,l-1}$. Now assuming the result (4.41) for $l-1$, and using (4.38), we have

$$\begin{aligned} J_{N,l}\left(A_{\alpha i}, B_\alpha\right) &= -\left(-2\pi i\right)^{l-1} \int dx_l \sum_{\mathcal{A}_l} \prod_{k=1}^{l-1} \theta\left(\frac{detA^{(\mathcal{A}_{k-1})}\, F_{\alpha_k}(y_1 \ldots y_k)}{\det A^{(\mathcal{A}_k)}(y_1 \ldots y_k)}\right) \frac{1}{\det(A^{(\mathcal{A}_l)})} \\ &\times \prod_{\beta \notin \mathcal{A}_{l-1}} \Bigg[\left(A_{\beta l} - A_{\beta j}\left(A^{(\mathcal{A}_{l-1})}\right)^{-1}_{j\alpha'} A_{\alpha' l}\right) x_l \\ &\quad + B_\beta - A_{\beta j}\left(A^{(\mathcal{A}_{l-1})}\right)^{-1}_{j\alpha'} B^{(\mathcal{A}_{l-1})}_{\alpha'} + i\epsilon\left(1 - A_{\beta j}\sum_{\alpha'}\left(A^{(\mathcal{A}_{l-1})}\right)^{-1}_{j\alpha'}\right)\Bigg]^{-1}. \end{aligned} \tag{4.43}$$

To this expression, we apply an elementary identity, applicable to any nonsingular, $(n+1)\times(n+1)$ matrix, $M^{(n+1)}$ defined by $M_{i,j}$, $i,j = 1\ldots n+1$ in terms of its submatrix $M^{(n)}_{a,b} \equiv M_{a,b}$, $a,b = 1\ldots n$,

$$\frac{\det M^{(n+1)}}{\det M^{(n)}} = M_{n+1,n+1} - \sum_{i=1}^{n}\sum_{j=1}^{n} M_{n+1,i}\left(M^{(n)}\right)^{-1}_{i,j} M_{j,n+1}\,. \tag{4.44}$$

This is readily proved using the relation of the inverse of a matrix to minors of its determinant. Applying Eq. (4.44) to the coefficient of x_l in (4.43), the form of Eq. (4.41) for $J_{N,l}$ is then simply the sum of residues found by closing the x_l integral in the lower half plane. By identifying l with $2L$, Eq. (4.39) follows directly.

In fact, the identity (4.44) can be applied again, to the imaginary and real parts of (4.39), to provide an alternative expression for the integrand in eq. (4.39) entirely in turns of the matrices $A_{\alpha i}$ and vectors B_α. For each sequence $\mathcal{A}_k$, we find in the remaining denominators, β,

$$A_\beta \cdot X^{(\mathcal{A}_k)} + B_\beta = \frac{1}{\det A^{(\mathcal{A}_k)}}\begin{vmatrix} A^{(\mathcal{A}_k)}_{\alpha_1 1} & \cdots A^{(\mathcal{A}_k)}_{\alpha_1 n} & B_{\alpha_1} \\ \vdots & \vdots & \vdots \\ A^{(\mathcal{A}_k)}_{\alpha_k 1} & \cdots A^{(\mathcal{A}_k)}_{\alpha_k k} & B_{\alpha_n} \\ A_{\beta 1} & \cdots A_{\beta k} & B_\beta \end{vmatrix} \equiv \frac{G^{(\mathcal{A}_{k+1})}_\beta}{\det A^{(\mathcal{A}_k)}}\,. \tag{4.45}$$

We have a similar form for the arguments of the theta functions in Eq. (4.39),

$$F^{(\mathcal{A}_{k+1})}_\beta = \frac{1}{\det A^{(\mathcal{A}_k)}}\begin{vmatrix} A^{(\mathcal{A}_k)}_{\alpha_1 1} & \cdots A^{(\mathcal{A}_k)}_{\alpha_1 k-1} & 1 \\ \vdots & \vdots & \vdots \\ A^{(\mathcal{A}_k)}_{\alpha_k 1} & \cdots A^{(\mathcal{A}_k)}_{\alpha_k k} & 1 \\ A_{\beta 1} & \cdots A_{\beta k} & 1 \end{vmatrix} \equiv \frac{H^{(\mathcal{A}_{k+1})}_\beta}{\det A^{(\mathcal{A}_k)}}\,. \tag{4.46}$$

We can thus reinterpret the result of the x_i integrals, Eq. (4.39) as

$$\begin{aligned} I_{N,L} &= -\left(\frac{-1}{4(2\pi)^2}\right)^L \sum_{\mathcal{A}_{2L}} \int \prod_{k=1}^{2L} dy_k\, \theta\left(\frac{H^{(\mathcal{A}_k)}_{\alpha_k}}{\det A^{(\mathcal{A}_k)}}\right)\left(\det A^{(\mathcal{A}_{2L})}\right)^{N-2L-1} \\ &\quad \times \prod_{\beta \notin \mathcal{A}_{2L}} \frac{1}{G^{(\mathcal{A}_{2L+1})}_\beta + i\epsilon H^{(\mathcal{A}_{2L+1})}_\beta}\,, \end{aligned} \tag{4.47}$$

where, as the notation indicates, the determinants G and H are of $(2L+1)\times(2L+1)$ matrices, determined in each case by the coefficients of on shell lines, and of each remaining, uncut line β. In this expression the entire integrand is specified by determinants of elements $A_{\alpha i}$ and B_α. These coefficients, in turn, given in (4.31), are linear functions of the plus and plus tilde loop momentum components in addition to external momenta and masses. Note that for $k=1$, the theta function corresponds to the condition that the pole in the first integral, over loop momentum l_1^-, be in the lower half-plane, so that, because the set $\mathcal{A}_1$ consists of one line only, say i, we have

$$\begin{aligned} H_{\alpha_1}^{(A_1)} &\equiv 1\,, \\ \det A^{(A_1)} &= \left(l_i^+ - p_i^+\right)\eta_{i1}\,, \end{aligned} \tag{4.48}$$

with no sum on i in the second expression. The integrand in Eq. (4.47) is a rational function of the remaining $2L$ components, y_j. Individual denominators labelled by index β may involve powers of up to order $2L+1$ in these variables, although by examining the one-loop case below, we will see that the power can be lower.

Eq. (4.47) is our final result for ultraviolet finite scalar integrals in $(2,2)$. For any such diagram, $2L < N-1$, so that the number of integrations remaining is fewer than the number of Feynman parameter integrals for the corresponding diagram, at the price of having a sum of terms. In these expressions, the finiteness of the remaining integration regions, shown in Sec. 4.3.2 above, is not manifest. It results from cancellations between different terms at each stage in the integration. We will give an example in the next section, where we study the one-loop case.

4.5 One Loop Diagrams

We now turn to the application of our basic result, (4.47) to one loop diagrams. We begin with a one loop diagram of any order, with completely arbitrary real masses and external momenta. We will not attempt to perform the remaining two integrals, but will be able to identify certain interesting general features. Following this, we confirm the presence of double-logarithmic behavior in a sample $(2,2)$ box diagram.

4.5.1 The general one loop diagram in (2,2) notation

For the case $L=1$ in Eq. (4.47), the sum over sets of cut lines, $\mathcal{A}_1$ and $\mathcal{A}_2$ is simply a sum of ordered choices of lines, say $\alpha_1 = i$ and $\alpha_2 = j$, which we will denote by $\mathcal{A}_1 = \mathcal{A}_i$ and $\mathcal{A}_2 = \mathcal{A}_{(ij)}$. With the labeling of momenta specified in Eq. (4.31), the first index, $\alpha_1 = i$ denotes the line set on shell by the integral over loop component $x_1 = l^-$, while $\alpha_2 = j$ identifies the line set on shell by the integral over $x_2 = \tilde{l^-}$, in the notation of Eq. (4.34). In these terms, we find, using (4.48), for $L=1$,

$$\begin{aligned} I_{N,1} &= \frac{1}{4(2\pi)^2}\sum_{i,j}\int dl^+\;\theta\left(\frac{1}{l^+ - p_i^+}\right)\int d\tilde{l^+}\theta\left(\frac{H_{\alpha_j}^{(\mathcal{A}_{(ij)})}}{\det A^{(\mathcal{A}_{ij})}}\right) \\ &\qquad \times\left(\det A^{(\mathcal{A}_{(ij)})}\right)^{N-3}\;\prod_{\beta\neq i,j}\frac{1}{G_\beta^{(\mathcal{A}_{(ij\beta)})} + i\epsilon H_\beta^{(\mathcal{A}_{(ij\beta)})}}\,, \end{aligned} \tag{4.49}$$

where $\mathcal{A}_{(ij\beta)}$ in the superscripts of determinants G and H corresponds to $\mathcal{A}_{2L+1}$ in (4.47). To illustrate the method, we evaluate the remaining determinants in the expression. These are from the 2×2 matrices, $A^{(\mathcal{A}_{(ij)})}$,

$$\det A^{(\mathcal{A}_{(ij)})} = \begin{vmatrix} l^+ - p_i^+ & l^{\tilde{+}} - p_i^{\tilde{+}} \\ l^+ - p_j^+ & l^{\tilde{+}} - p_j^{\tilde{+}} \end{vmatrix} = (\boldsymbol{l}^+ - p_i^+)(p_i^{\tilde{+}} - p_j^{\tilde{+}}) - (l^{\tilde{+}} - p_i^{\tilde{+}})(p_i^+ - p_j^+)\,, \tag{4.50}$$

and $H_{\alpha_j}^{(\mathcal{A}_{(ij)})}$,

$$H_{\alpha_j}^{(\mathcal{A}_{(ij)})} = \begin{vmatrix} l^+ - p_i^+ & 1 \\ l^+ - p_j^+ & 1 \end{vmatrix} = p_j^+ - p_i^+\,, \tag{4.51}$$

and the two 3×3 matrices, $G_\beta^{(\mathcal{A}_{(ij)})}$,

$$\begin{aligned} \det G_\beta^{(\mathcal{A}_{(ij)})} &= \begin{vmatrix} l^+ - p_i^+ & l^{\tilde{+}} - p_i^{\tilde{+}} & B_i \\ l^+ - p_j^+ & l^{\tilde{+}} - p_j^{\tilde{+}} & B_j \\ l^+ - p_\beta^+ & l^{\tilde{+}} - p_\beta^{\tilde{+}} & B_\beta \end{vmatrix} \\ &= B_i \det A^{(\mathcal{A}_{(j\beta)})} - B_j \det A^{(\mathcal{A}_{(i\beta)})} + B_\beta \det A^{(\mathcal{A}_{(ij)})}\,, \end{aligned} \tag{4.52}$$

and $H_\beta^{(\mathcal{A}_{(ij)})}$,

$$\det H_\beta^{(\mathcal{A}_{(ij)})} = \begin{vmatrix} l^+ - p_i^+ & l^{\tilde{+}} - p_i^{\tilde{+}} & 1 \\ l^+ - p_j^+ & l^{\tilde{+}} - p_j^{\tilde{+}} & 1 \\ l^+ - p_\beta^+ & l^{\tilde{+}} - p_\beta^{\tilde{+}} & 1 \end{vmatrix} = (p_\beta^+ - p_i^+)(p_\beta^{\tilde{+}} - p_j^{\tilde{+}}) - (p_\beta^+ - p_j^+)(p_\beta^{\tilde{+}} - p_i^{\tilde{+}})\,. \tag{4.53}$$

Recalling that the B_i are linear in loop momenta, we see that the denominators β in Eq. (4.49) are of power two jointly in l^+ and $l^{\tilde{+}}$, rather than three.

In order to write our result in a more compact form, we introduce an antisymmetric product

$$\{v, w\} \equiv v^+ w^{\tilde{+}} - w^+ v^{\tilde{+}}\,. \tag{4.54}$$

In this notation, the general one-loop scalar integral becomes

$$\begin{aligned} I_{N,1} &= \frac{1}{4(2\pi)^2} \sum_{i,j} \int dl^+ \; \theta\left(l^+ - p_i^+\right) \int dl^{\tilde{+}} \theta \left(\frac{\{l, p_i - p_j\} + \{p_i, p_j\}}{p_j^+ - p_i^+} \right) \; (\{l, p_i - p_j\} + \{p_i, p_j\})^{N-3} \\ &\qquad \times \prod_{\beta \neq i,j} \frac{1}{\frac{1}{2} \sum_{\{a,b,c\}=\{i,j,\beta\}} \epsilon_{abc} B_a \left(\{l, p_b - p_c\} + \{p_b, p_c\}\right) + i\epsilon \{p_\beta - p_i, p_\beta - p_j\}} \\ &\equiv \frac{1}{4(2\pi)^2} \sum_{i,j} \int dl^+ \; \theta\left(l^+ - p_i^+\right) \int dl^{\tilde{+}} \theta \left(l^{\tilde{+}} - l^+ r_{p_i - p_j} + \frac{\{p_i, p_j\}}{p_j^+ - p_i^+} \right) \; \omega_{ji}(l^+, l^{\tilde{+}})\,, \end{aligned} \tag{4.55}$$

where in the second equality we have evaluated the theta function for the $l^{\tilde{+}}$ integral, using the notation of Eq. (4.22), and have defined ω_{ji} as the integrand that results from taking the

ith pole for the l^- integral, and the jth pole for $l^{\tilde{-}}$. The ϵ symbol reflects the antisymmetry of determinant $G_\beta^{(\mathcal{A}_{(ij)})}$, Eq. (4.52), in indices i, j and β, corresponding to line momenta k_i, k_j and k_β. We now note that for fixed i, the subsequent $l^{\tilde{+}}$ integral vanishes if all its poles are in the lower half plane, which leads to the identity,

$$\sum_{j\neq i} \omega_{ji}(l^+, l^{\tilde{+}}) = 0\,. \tag{4.56}$$

This enables us to rewrite $I_{N,1}$, (4.49) as

$$\begin{aligned} I_{N,1} &= \frac{1}{4(2\pi)^2}\sum_i \int_{p_i^+}^{\infty} dl^+ \sum_{j\neq i} \left(\int_{l^+ r_{p_i-p_j} - \frac{\{p_i,p_j\}}{p_i^+ - p_j^+}}^{\infty} dl^{\tilde{+}}\ \omega_{ji}(l^+, l^{\tilde{+}}) \ -\ \int_{\sigma(l^+)}^{\infty} dl^{\tilde{+}} \omega_{ji}(l^+, l^{\tilde{+}}) \right) \\ &= \frac{1}{4(2\pi)^2}\sum_i \sum_{j\neq i} \int_{p_i^+}^{\infty} dl^+ \int_{l^+ r_{p_i-p_j} - \frac{\{p_i,p_j\}}{p_i^+ - p_j^+}}^{\sigma(l^+)} dl^{\tilde{+}}\ \omega_{ji}(l^+, l^{\tilde{+}})\,, \end{aligned} \tag{4.57}$$

where $\sigma(l^+)$ is a completely arbitrary function of l^+ (possibly a constant), which must be chosen the same for every pair i, j.

We can simplify this expression further by using that in Eq. (4.57), the integrand ω_{ji} is fully antisymmetric under the exchange of p_i and p_j, that is,

$$\omega_{ji}(l^+, l^{\tilde{+}}) = -\omega_{ij}(l^+, l^{\tilde{+}})\,. \tag{4.58}$$

Equation (4.57) can thus be rewritten as a sum over $(1/2)N(N-1)$ ordered pairs of terms, with fixed limits on the l^+ integrals, and linear one-sided limits for the $l^{\tilde{+}}$ integrals,

$$\begin{aligned} I_{N,1} &= \frac{1}{4(2\pi)^2}\sum_i \sum_{j\neq i} \theta(p_j^+ - p_i^+) \int_{p_i^+}^{p_j^+} dl^+ \ \int_{\sigma(l^+)}^{l^+ r_{p_i-p_j} - \frac{\{p_i,p_j\}}{p_i^+ - p_j^+}} dl^{\tilde{+}} \\ &\quad \times \frac{(\{l, p_i - p_j\} + \{p_i, p_j\})^{N-3}}{\prod_{\beta\neq i,j} \left[\frac{1}{2} \sum_{\{a,b,c\}=\{i,j,\beta\}} \epsilon_{abc} B_a \left(\{l, p_b - p_c\} + \{p_b, p_\beta\}\right) + i\epsilon\{p_\beta - p_i, p_\beta - p_j\} \right]}\,, \end{aligned} \tag{4.59}$$

where we observe again that because of the identity (4.56), the result is independent of our choice of $\sigma(l^+)$. The integration region is illustrated in Fig. 4.4.

In principle, Eq. (4.59) could be the starting point of an explicit calculation, but in any case an arbitrary one-loop diagram can be reduced to box diagrams [98]-[102], which are known for any choices of masses [103]-[8]. Our emphasis here is rather on the extension of the formalism to the new signature.

4.5.2 Double logs in a (2,2) box

We have already argued that four-point amplitudes are insensitive to the choice of Minkowski or $(2,2)$ signature. To illustrate this point, let us show how double-logarithmic integrals arise

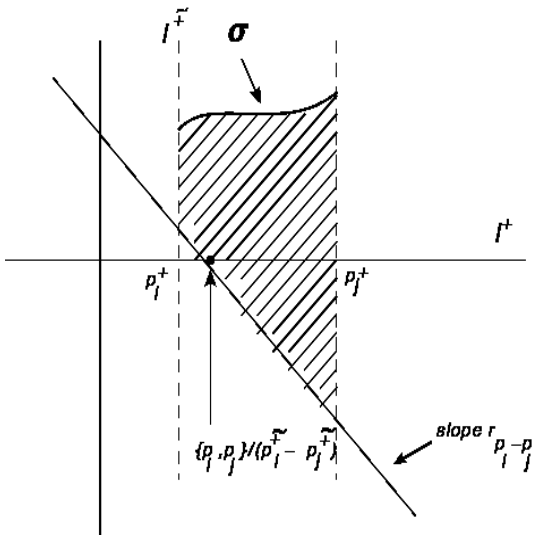

Figure 4.4: Region of integration (shaded) corresponding to Eq. (4.59) in the $l^+, l^{\tilde{+}}$ plane. For the case shown, the parameter $r_{p_i-p_j}$ is negative, corresponding to a negative slope in the lower limit of the $l^{\tilde{+}}$ integral. Positive slopes and negative intercepts are also possible. As explained in the text, the boundary σ is arbitrary.

in the one-loop box with a suitable choice of massless internal and external lines, directly from the $(2,2)$ result, Eq. (4.59) with $N = 4$.

We consider the scalar box, Fig. 4.5 describing a pair production process in "deep-inelastic scattering" kinematics,

$$p + q \to K_1 + K_2\,, \tag{4.60}$$

where incoming line p is massless, two outgoing lines are massive,

$$\begin{aligned} p^2 &= 0\,, \\ q^2 &< 0\,, \\ K_1^2 &= K_2^2 = M^2, \end{aligned} \tag{4.61}$$

and where the process is initiated by a space-like momentum transfer, q. In the notation of Eq. (4.28) and Fig. 4.5, we have we have four line momenta, $l - p_i$, with

$$\begin{aligned} p_1 &= 0\,, \\ p_2 &= p\,, \\ p_3 &= p + q\,, \\ p_4 &= K_1\,. \end{aligned} \tag{4.62}$$

We assign a mass M to the propagator carrying momentum $l - K_1$, while other propagators are taken as massless,

$$I_{4,1}(\{p_i\}, M) = -i \int \frac{d^4l}{(2\pi)^4} \frac{1}{l^2 + i\epsilon} \frac{1}{(l-p)^2 + i\epsilon} \frac{1}{(l-p-q)^2 + i\epsilon} \frac{1}{(l-K_1)^2 - M^2 + i\epsilon}\,. \tag{4.63}$$

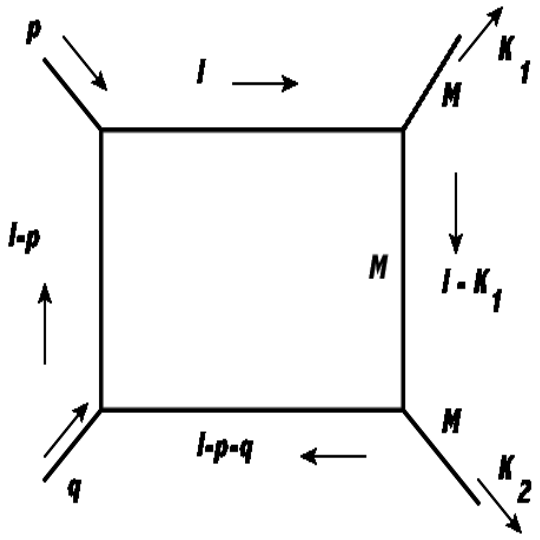

Figure 4.5: Box diagram

In Minkowski space and with the momenta chosen as above, this integral has a double-logarithmic infrared behavior when the loop momentum l becomes proportional to p (collinear singularity) with vanishing energy (soft singularity), and no other sources of double logarithms. Without fully evaluating the diagram, Fig. 4.5, let us see how a double-logarithmic behavior emerges in the $(2,2)$ integral.

The term that has double-logarithmic behavior in Eq. (4.59) for this diagram in $(2,2)$ signature is the choice $k_i = l$, $k_j = l - p$, that is, the term with the mass shell poles of the two lines that become parallel. To be definite, we label $k_{\beta_1} = l - p - q$, $k_{\beta_2} = l - K_1$. With the routing of momenta shown in the figure, $B_i = 0$ and $p_i = 0$, so that the relevant term in (4.59) is

$$\begin{aligned} I_{4,1}^{(l,l-p)} &= \frac{1}{4(2\pi)^2} \int_0^{l_1^+} dl^+ \int dl^{\tilde{+}} \theta\left(\{l,p\}\right) \; \{l,-p\} \\ &\quad \times \frac{1}{-B_{l-p}\{l,l-K_1\} + B_{l-K_1}\{l,l-p\} + i\epsilon\{p,K_1\}} \\ &\quad \times \frac{1}{-B_{l-p}\{l,l+q\} + B_{l-q-p}\{l,q-p\} + i\epsilon\{p,p+q\}} \,, \end{aligned} \tag{4.64}$$

where we have replaced indices d on the B_d by the corresponding momenta, k_d. The coefficients of the B_{k_d} are given by

$$\begin{aligned} \{l, p_i - p_j\} &= \{l,-p\} \\ &= p^+ l^{\tilde{+}} \; - \; l^+ p^{\tilde{+}} \\ &= l^+ p^+ \left(r_l \; - \; r_p\right) \,, \end{aligned} \tag{4.65}$$

where we have have used the notation of Eq. (4.22) for r_l and r_p. This antisymmetric combination vanishes both when loop momentum l is proportional to the massless momentum p, so that $r_l = r_p$, and when l^+ vanishes. These are the collinear and soft limits from

Minkowski analysis, and the limits for l^+ and $l^{\tilde{+}}$ are just at these points. The numerator factor vanishes linearly in both the collinear and soft limits, but the denominators with momenta $l - K_1$ and $l - p - q$ behave as

$$\begin{aligned} - B_{l-p}\{l, -K_1\} \; + \; B_{l-K_1}\{l, -p\} \;\; &= \;\; - \, u_1 \, (l^+)^2 \, (r_l - r_p) + \cdots \\ - B_{l-p}\{l, -p-q\} \; + \; B_{l,-p-q}\{l, l-p\} \;\; &= \;\; s \, p^+ l^+ (r_l - r_p) + \cdots \; , \end{aligned} \tag{4.66}$$

respectively, with $s \equiv (p+q)^2$ and $u_1 \equiv 2p \cdot K_1$, where neglected terms are higher order in l^+ and/or $r_l - r_p$. In deriving these results, we have used that $p^2 = 0$ implies $p^{\tilde{+}}/p^+ = -p^-/p^{\tilde{-}}$. Now changing variables from $l^{\tilde{+}}$ to r_l, we find near the end-points a double-logarithmic integral,

$$I_{4,1}^{(l,l-p)} \;\; = \;\; - \, \frac{1}{4(2\pi)^2} \, \frac{1}{u_1 \, s} \, \int_0 \frac{dl^+}{l^+} \, \int_{r_p} \frac{dr_l}{r_l - r_p} \, . \tag{4.67}$$

It is straightforward to check that no other term in the sum over poles has an end-point singularity at $r_l = r_p$, and hence a collinear singularity.

We can compare the result (4.67) to the double-logarithmic integral in Minkowski signature, which appears by taking the energy pole at $l^0 = \sqrt{|\vec{l}|^2}$ in Fig. 4.5. In that case, in the limit that $\cos\theta_{pl} \to 1$, where θ_{pl} is the angle between $\vec{l}$ and $\vec{p}$, we find

$$I_{DL} = - \, \frac{1}{4(2\pi)^2} \, \frac{1}{u_1 \, s} \, \int_0 \frac{d|\vec{l}|}{|\vec{l}|} \, \int^1 \frac{d\cos\theta_{pl}}{1 - \cos\theta_{pl}} \, , \tag{4.68}$$

with the same double-logarithmic behavior as (4.67) up to a change of variables.

In the above calculation, we have not discussed regulation of infrared-divergent integrals. The simplest regulation for the example above is to take $p_1^2 < 0$, but with gauge theories in mind it is natural to ask whether dimensional regularization is possible. Although our approach to $(2,2)$ signature is closely linked to four dimensions, there is in fact nothing to keep us from dimensionally regulating. The interpretation is particularly straightforward for infrared regulation, which requires $\varepsilon = 2 - D/2 < 0$, with D the number of dimensions, taken greater than four. We thus imagine adding -2ε dimensions to the four dimensions spanned by our coordinates $l^{\pm}$ and $l^{\tilde{\pm}}$.

While a full discussion of dimensional regularization for multi loop diagrams would take an extensive analysis, we will content ourselves here with the observation that if we label the momenta of the extra dimensions as $l_\perp$, and keep the external momenta in four dimensions, all of the analysis leading to our one loop result, Eq. (4.59), for example, is unchanged. The effect of dimensional regularization is simply to add a term $-l_\perp^2$ to every squared mass term in the denominators of (4.59), $B_\alpha \to B_\alpha - l_\perp^2$ in Eq. (4.31), and to introduce an overall integration over the "extra" dimensions of the form

$$\frac{2\pi^\varepsilon}{\Gamma(\varepsilon)} \, \int_0^\infty dl_\perp \, l_\perp^{-2\varepsilon - 1} \, , \tag{4.69}$$

acting on the modified integrand, where the prefactor represents the angular volume. In the limit $\varepsilon \to 0$, the zero of the angular integration is balanced by the (infrared) pole from the radial integral. For infrared finite integrands, the net result is unity for $\varepsilon = 0$, but for divergent integrals as in Eq. (4.67), the result is infrared regulated after the $l_\perp$ integration.

4.6 Summary and Conclusions

We have studied scalar perturbation theory in $(2,2)$ signature, and have identified a natural analytic continuation from Minkowski signature, which crosses no singularities and can be used to define diagrams with arbitrary external momenta. The resulting integrals have a standard "$i\epsilon$" prescription for the definition of contours in the presence of propagator singularities. This enables us to appeal to standard Landau analysis to identify pinches of momentum integrals, and singularities in external momenta. The singularities in $(2,2)$ are in general quite different than those in $(1,3)$ signature. An exception is when external momenta are restricted to a plane in Minkowski space; in this case the contour rotation to $(2,2)$ signature does not change the integral.

For diagrams that are fully ultraviolet finite (in all subdiagrams), we can introduce two sets of light cone variables, all four of which are linear in all denominators. We have derived a general expression for such an L-loop N-line integral as the sum of $2L$-dimensional integrals using $(2,2)$ integration. Whether these expressions can be of use in the practical evaluation of higher-loop scalar integrals is a subject for further investigation.

Chapter 5

Conclusions.

The dynamics of QCD is very complicated. It is probably true that it occurs in an infinite dimensional functional space, and only projects down to what is seen in our asymptotically 4-dimensional world. We see tracks of stable particles in the detector, which are probably something like ends of geometric 4-dimensional manifolds, embedded in a topological space-time. The fact that there are visible thresholds, and other real pieces of Landau varieties, is quite remarkable in that it suggests that space-time is a topological manifold, rather than differentiable one, and our observables are sensitive to its topological structure, that differentiability is lost for some observables. It might be that dimensionality and specific properties of 4-maifolds, and pseudomanifolds of their homeomorphisms, are crusial for QCD, but the theory that was developed in this thesis is oblivious of the dimensionality. In fact, the conclusions drawn in chapters 2 and 3 are valid in other dimensions as well.

Withing the framework of perturbative correlation functions, it became clear that the functions should be considered as sections of flat bundles over the compliment of Landau varieties, in suitably compactified space of external momenta. Thus, the probelm is essentily about the study of fundamental group of these compliments. This is itself very difficult problem [113], and is a subject of research in math community. Fundamental groups are notoriously difficult to compute [111], and the methods of computation are very sensitive to the presence of singularities in the varieties. Thus, the first logical step in the problem of calculating the Green's functions is the very detailed understanding of Landau varieties and their intersections. Very little is known about this topic today. It is not known if they posess singularities. One very promising way of analysing this problem involves the algebraic technique of elimination theory [114]. This technique allows in principle to derive the explicit ideals that correspond to Landau varieties. It is applicable right away to the problem where there is no relation on the coefficients of the polynomials in the denominator, but can in principle be generalized to the situation where there is injective map into the parameter set from some other algebraic variety - the situation that we have in QFT. However, deriving equations for the intersections of Landau varieties, and especially understanding their intersection, is well beyond reach in this advanced algebraic formalism. For example, extending this formalism to the problem of deriving equations for the substratum in the discriminant where there is one-dimensional singularity locus in the projective hypersurface is already a research problem, considered hard by the experts (private communication, M.Kapranov).

However, it might be possible to use specific structure of the denominators to understand

the stratification by the singularity type of the system of Feynman denominators. It is observed in the second chapter of this thesis, that this singularity type is captured by a system of degenerate projective quadrics of very specific type, together with a system of hyperplanes. There is a large dimensional singularity locus of the quadric, which is independent of the parameters. On the quotient of this locus, the quadric is just the standard 3-dimensional complex quadric. Thus the parameter space of perturbative QFT is quite similar to the Grassmanian, with its natural stratification by Schubert strata. In fact, the subsystem that corrsponds to the linear factors, can be exactly captured by a subvariety of the Garassmanian of the corresponding dimension, that respects Schubert stratification, if one reparametrizes the terms $p^2 + m_i^2$ into new variables (this is probably the reason why on-shell methods undergo such a boom, and why different sorts of Grassmanians arise in this context [112]).

Despite this plethora of algebro-geometric and number-theoretic questions that are more or less within reach, QCD can be considered rather as source of problems in functional analysis, topology and geometry of function spaces. Not much is known in these areas, in fact, even the notion of submanifold of a function space still awaits definition. There is a variety of Frechet polynormed structures, that respect analytic notions not captured by topological functors, that seem to be relevant for classical YM equations, not to mention the quantum world we are studying. It is probably true that understanding the spectral theorem in the context of tangent spaces to the space of YM fields in the Minkowski space is relevant to understanding low energy scattering in QCD. Probably the configuration spaces of momenta of hadrons produced in a collision should be viewed as dimension theories of these tangent spaces, a fascinating topic for future research.

Bibliography

[1] D. Hanneke, S. F. Hoogerheide and G. Gabrielse, arXiv:1009.4831 [physics.atom-ph].

[2] K. Hagiwara, A. D. Martin, D. Nomura and T. Teubner, Phys. Lett. B **649**, 173 (2007) [hep-ph/0611102].

[3] J. Beringer *et al.* [Particle Data Group Collaboration], Phys. Rev. D **86**, 010001 (2012).

[4] T. Lappi, S. Srednyak and R. Venugopalan, JHEP **1001**, 066 (2010) [arXiv:0911.2068 [hep-ph]].

[5] S. Srednyak, arXiv:1112.5648 [hep-ph].

[6] S. Srednyak and G. Sterman, Phys. Rev. D **87**, no. 10, 105017 (2013) [arXiv:1302.4290 [hep-th]].

[7] M. Eides, H. Grotch, V. Shelyuto, " Theory of Light Hydrogenic Bound States.".

[8] A. Denner and S. Dittmaier, Nucl. Phys. B **844**, 199 (2011) [arXiv:1005.2076 [hep-ph]].

[9] G. 't Hooft and M. J. G. Veltman, Nucl. Phys. B **44**, 189 (1972). .

[10] L. D. Faddeev and V. N. Popov, Phys. Lett. B **25**, 29 (1967).

[11] G. F. Sterman, In *Boulder 1995, QCD and beyond* 327-406 [hep-ph/9606312].

[12] J. L. Albacete and C. Marquet, Prog. Part. Nucl. Phys. **76**, 1 (2014) [arXiv:1401.4866 [hep-ph]].

[13] L. D. McLerran and R. Venugopalan, *Phys. Rev.* **D49** (1994) 2233 [arXiv:hep-ph/9309289]; L. D. McLerran and R. Venugopalan, *Phys. Rev.* **D49** (1994) 3352 [arXiv:hep-ph/9311205]; L. D. McLerran and R. Venugopalan, *Phys. Rev.* **D50** (1994) 2225 [arXiv:hep-ph/9402335].

[14] J. Jalilian-Marian, A. Kovner, L. D. McLerran and H. Weigert, *Phys. Rev.* **D55** (1997) 5414 [arXiv:hep-ph/9606337]; J. Jalilian-Marian, A. Kovner, A. Leonidov and H. Weigert, *Nucl. Phys.* **B504** (1997) 415 [arXiv:hep-ph/9701284]; J. Jalilian-Marian, A. Kovner, A. Leonidov and H. Weigert, *Phys. Rev.* **D59** (1999) 014014 [arXiv:hep-ph/9706377]; J. Jalilian-Marian, A. Kovner and H. Weigert, *Phys. Rev.* **D59** (1999) 014015 [arXiv:hep-ph/9709432]; J. Jalilian-Marian, A. Kovner, A. Leonidov and H. Weigert, *Phys. Rev.* **D59** (1999)

034007 [arXiv:hep-ph/9807462]; H. Weigert, *Nucl. Phys.* **A703** (2002) 823 [arXiv:hep-ph/0004044]; E. Iancu, A. Leonidov and L. D. McLerran, *Nucl. Phys.* **A692** (2001) 583 [arXiv:hep-ph/0011241]; E. Iancu and L. D. McLerran, *Phys. Lett.* **B510** (2001) 145 [arXiv:hep-ph/0103032]; E. Ferreiro, E. Iancu, A. Leonidov and L. McLerran, *Nucl. Phys.* **A703** (2002) 489 [arXiv:hep-ph/0109115]; E. Iancu, A. Leonidov and L. D. McLerran, *Phys. Lett.* **B510** (2001) 133 [arXiv:hep-ph/0102009]; A. H. Mueller, *Phys. Lett.* **B523** (2001) 243 [arXiv:hep-ph/0110169].

[15] E. Iancu and R. Venugopalan in *Quark gluon plasma* (R. Hwa and X. N. Wang, eds.). World Scientific, 2003. arXiv:hep-ph/0303204; H. Weigert, *Prog. Part. Nucl. Phys.* **55** (2005) 461 [arXiv:hep-ph/0501087].

[16] F. Gelis and R. Venugopalan, *Nucl. Phys.* **A776** (2006) 135 [arXiv:hep-ph/0601209]; F. Gelis and R. Venugopalan, *Nucl. Phys.* **A779** (2006) 177 [arXiv:hep-ph/0605246].

[17] A. Kovner, L. D. McLerran and H. Weigert, *Phys. Rev.* **D52** (1995) 3809 [arXiv:hep-ph/9505320].

[18] D. Kharzeev, A. Krasnitz and R. Venugopalan, *Phys. Lett.* **B545** (2002) 298 [arXiv:hep-ph/0109253].

[19] T. Lappi and L. McLerran, *Nucl. Phys.* **A772** (2006) 200 [arXiv:hep-ph/0602189].

[20] F. Gelis and R. Venugopalan, *Acta Phys. Polon.* **B37** (2006) 3253 [arXiv:hep-ph/0611157]; F. Gelis, T. Lappi and R. Venugopalan, *Int. J. Mod. Phys.* **E16** (2007) 2595 [arXiv:0708.0047 [hep-ph]].

[21] F. Gelis, T. Lappi and R. Venugopalan, *Phys. Rev.* **D78** (2008) 054019 [arXiv:0804.2630 [hep-ph]].

[22] F. Gelis, T. Lappi and R. Venugopalan, *Phys. Rev.* **D78** (2008) 054020 [arXiv:0807.1306 [hep-ph]].

[23] I. Balitsky, *Nucl. Phys.* **B463** (1996) 99 [arXiv:hep-ph/9509348]; I. Balitsky, *Phys. Rev. Lett.* **81** (1998) 2024 [arXiv:hep-ph/9807434]; I. Balitsky, *Phys. Rev.* **D60** (1999) 014020 [arXiv:hep-ph/9812311]; Y. V. Kovchegov, *Phys. Rev.* **D60** (1999) 034008 [arXiv:hep-ph/9901281]; Y. V. Kovchegov, *Phys. Rev.* **D61** (2000) 074018 [arXiv:hep-ph/9905214]; I. Balitsky, *Phys. Lett.* **B518** (2001) 235 [arXiv:hep-ph/0105334].

[24] J. P. Blaizot, F. Gelis and R. Venugopalan, *Nucl. Phys.* **A743** (2004) 57 [arXiv:hep-ph/0402257].

[25] F. Gelis, T. Lappi and R. Venugopalan, *Phys. Rev.* **D79** (2008) 094017 [arXiv:0810.4829 [hep-ph]]; T. Lappi, *Acta Phys. Polon.* **B40** (2009) 1997 [arXiv:0904.1670 [hep-ph]].

[26] A. Krasnitz and R. Venugopalan, *Nucl. Phys.* **B557** (1999) 237 [arXiv:hep-ph/9809433]; A. Krasnitz and R. Venugopalan, *Phys. Rev. Lett.* **84** (2000) 4309 [arXiv:hep-ph/9909203]; A. Krasnitz and R. Venugopalan, *Phys. Rev. Lett.* **86** (2001) 1717 [arXiv:hep-ph/0007108].

[27] A. Krasnitz, Y. Nara and R. Venugopalan, *Phys. Rev. Lett.* **87** (2001) 192302 [arXiv:hep-ph/0108092].

[28] A. Krasnitz, Y. Nara and R. Venugopalan, *Nucl. Phys.* **A727** (2003) 427 [arXiv:hep-ph/0305112].

[29] T. Lappi, *Phys. Rev.* **C67** (2003) 054903 [arXiv:hep-ph/0303076]; T. Lappi, *Phys. Lett.* **B643** (2006) 11 [arXiv:hep-ph/0606207].

[30] A. Krasnitz, Y. Nara and R. Venugopalan, *Phys. Lett.* **B554** (2003) 21 [arXiv:hep-ph/0204361]; A. Krasnitz, Y. Nara and R. Venugopalan, *Nucl. Phys.* **A717** (2003) 268 [arXiv:hep-ph/0209269]; T. Lappi and R. Venugopalan, *Phys. Rev.* **C74** (2006) 054905 [arXiv:nucl-th/0609021].

[31] D. E. Kharzeev, L. D. McLerran and H. J. Warringa, *Nucl. Phys.* **A803** (2008) 227 [arXiv:0711.0950 [hep-ph]].

[32] S. A. Voloshin, *Phys. Lett.* **B632** (2006) 490 [arXiv:nucl-th/0312065].

[33] E. V. Shuryak, *Phys. Rev.* **C76** (2007) 047901 [arXiv:0706.3531 [nucl-th]].

[34] A. Dumitru, F. Gelis, L. McLerran and R. Venugopalan, *Nucl. Phys.* **A810** (2008) 91 [arXiv:0804.3858 [hep-ph]].

[35] S. Gavin, L. McLerran and G. Moschelli, *Phys. Rev.* **C79** (2009) 051902 [arXiv:0806.4718 [nucl-th]]; G. Moschelli and S. Gavin, arXiv:0910.3590 [nucl-th].

[36] **STAR** collaboration, J. Adams *et. al.*, *Phys. Rev. Lett.* **95** (2005) 152301 [arXiv:nucl-ex/0501016].

[37] **STAR** collaboration, F. Wang, *J. Phys.* **G30** (2004) S1299 [arXiv:nucl-ex/0404010]; **PHENIX** collaboration, A. Adare *et. al.*, *Phys. Rev.* **C78** (2008) 014901 [arXiv:0801.4545 [nucl-ex]]; **PHOBOS** collaboration, B. Alver *et. al.*, arXiv:0812.1172 [nucl-ex].

[38] **STAR** collaboration, P. K. Netrakanti, *J. Phys.* **G35** (2008) 104010 [arXiv:0804.4417 [nucl-ex]]; **STAR** collaboration, B. I. Abelev *et. al.*, *Phys. Rev. Lett.* **102** (2009) 052302 [arXiv:0805.0622 [nucl-ex]].

[39] **STAR** collaboration, L. Molnar, *J. Phys.* **G34** (2007) S593 [arXiv:nucl-ex/0701061]; **PHOBOS** collaboration, B. Alver *et. al.*, *J. Phys.* **G35** (2008) 104080 [arXiv:0804.3038 [nucl-ex]].

[40] **STAR** collaboration, J. Adams *et. al.*, *Phys. Rev.* **C73** (2006) 064907 [arXiv:nucl-ex/0411003]; **STAR** collaboration, B. I. Abelev *et. al.*, *Phys. Rev.* **C80** (2009) 064912 [arXiv:0909.0191 [nucl-ex]].

[41] **STAR** collaboration, M. Daugherity, *J. Phys.* **G35** (2008) 104090 [arXiv:0806.2121 [nucl-ex]].

[42] N. Armesto, C. A. Salgado and U. A. Wiedemann, *Phys. Rev. Lett.* **93** (2004) 242301 [arXiv:hep-ph/0405301]; A. Majumder, B. Muller and S. A. Bass, *Phys. Rev. Lett.* **99** (2007) 042301 [arXiv:hep-ph/0611135]; V. S. Pantuev, arXiv:0710.1882 [hep-ph]; C.-Y. Wong, *Phys. Rev.* **C78** (2008) 064905 [arXiv:0806.2154 [hep-ph]]; C. B. Chiu and R. C. Hwa, *Phys. Rev.* **C79** (2009) 034901 [arXiv:0809.3018 [nucl-th]].

[43] J. L. Nagle, *Nucl. Phys.* **A830** (2009) 147c [arXiv:0907.2707 [nucl-ex]].

[44] K. Dusling, D. Fernandez-Fraile and R. Venugopalan, *Nucl. Phys.* **A828** (2009) 161 [arXiv:0902.4435 [nucl-th]].

[45] F. Gelis, T. Lappi and L. McLerran, *Nucl. Phys.* **A828** (2009) 149 [arXiv:0905.3234 [hep-ph]].

[46] **PHENIX** collaboration, A. Adare *et. al.*, *Phys. Rev.* **C78** (2008) 044902 [arXiv:0805.1521 [nucl-ex]].

[47] A. Kovner, L. D. McLerran and H. Weigert, *Phys. Rev.* **D52** (1995) 6231 [arXiv:hep-ph/9502289].

[48] A. Dumitru and L. D. McLerran, *Nucl. Phys.* **A700** (2002) 492 [arXiv:hep-ph/0105268].

[49] J. P. Blaizot, F. Gelis and R. Venugopalan, *Nucl. Phys.* **A743** (2004) 13 [arXiv:hep-ph/0402256].

[50] Y. V. Kovchegov, *Phys. Rev.* **D54** (1996) 5463 [arXiv:hep-ph/9605446].

[51] H. Fujii, F. Gelis and R. Venugopalan, *Nucl. Phys.* **A780** (2006) 146 [arXiv:hep-ph/0603099].

[52] J. F. Gunion and G. Bertsch, *Phys. Rev.* **D25** (1982) 746.

[53] Y. V. Kovchegov and D. H. Rischke, *Phys. Rev.* **C56** (1997) 1084 [arXiv:hep-ph/9704201].

[54] M. Gyulassy and L. D. McLerran, *Phys. Rev.* **C56** (1997) 2219 [arXiv:nucl-th/9704034].

[55] T. Lappi, *Eur. Phys. J.* **C55** (2008) 285 [arXiv:0711.3039 [hep-ph]].

[56] K. J. Golec-Biernat and M. Wusthoff, *Phys. Rev.* **D59** (1999) 014017 [arXiv:hep-ph/9807513]; K. J. Golec-Biernat and M. Wusthoff, *Phys. Rev.* **D60** (1999) 114023 [arXiv:hep-ph/9903358]; A. M. Stasto, K. J. Golec-Biernat and J. Kwiecinski, *Phys. Rev. Lett.* **86** (2001) 596 [arXiv:hep-ph/0007192].

[57] J. Bartels, K. J. Golec-Biernat and H. Kowalski, *Phys. Rev.* **D66** (2002) 014001 [arXiv:hep-ph/0203258].

[58] H. Kowalski, T. Lappi and R. Venugopalan, *Phys. Rev. Lett.* **100** (2008) 022303 [arXiv:0705.3047 [hep-ph]].

[59] K. Fukushima, *Phys. Rev.* **D77** (2008) 074005 [arXiv:0711.2364 [hep-ph]].

[60] E. Iancu, K. Itakura and L. McLerran, *Nucl. Phys.* **A724** (2003) 181 [arXiv:hep-ph/0212123]; A. H. Mueller, *Nucl. Phys.* **B643** (2002) 501 [arXiv:hep-ph/0206216].

[61] J. Takahashi *et. al.*, *Phys. Rev. Lett.* **103** (2009) 242301 [arXiv:0902.4870 [nucl-th]].

[62] R. Britto, J. Phys. A A **44**, 454006 (2011) [arXiv:1012.4493 [hep-th]].

[63] L. J. Dixon, J. Phys. A A **44**, 454001 (2011) [arXiv:1105.0771 [hep-th]].

[64] J. R. Andersen *et al.* [SM and NLO Multileg Working Group], arXiv:1003.1241 [hep-ph].

[65] R. Hwa, V. Toeplitz "Homology and Feynman integrals", (Benjamin, New York 1966), Eden R. J., Landshoff P.V., Olive D. I., Polkinghorne J. C., "The Analytic S-Matrix", (Cambridge University Press 1966).

[66] M. Argeri and P. Mastrolia, Int. J. Mod. Phys. A **22**, 4375 (2007) [arXiv:0707.4037 [hep-ph]].

[67] S. Laporta, Int. J. Mod. Phys. A **15**, 5087 (2000) [arXiv:hep-ph/0102033].

[68] D. Vaman and Y. P. Yao, JHEP **0604**, 030 (2006) [arXiv:hep-th/0512031].

[69] P. D. Draggiotis, R. H. P. Kleiss, A. Lazopoulos and C. G. Papadopoulos, Eur. Phys. J. C **46**, 741 (2006) [arXiv:hep-ph/0511288].

[70] D. B. Melrose, Nuovo Cim. **40**, 181-213 (1965).

[71] W. L. van Neerven and J. A. M. Vermaseren, Phys. Lett. B **137**, 241 (1984).

[72] Z. Bern, L. J. Dixon and D. A. Kosower, Phys. Lett. B **302**, 299 (1993) [Erratum-ibid. B **318**, 649 (1993)] [hep-ph/9212308].

[73] R. Britto, F. Cachazo, B. Feng, E. Witten, Phys. Rev. Lett. **94**, 181602 (2005). [hep-th/0501052].

[74] R. J. Eden, P. V. Landshoff, D. I. Olive, and J. C. Polkinghorne, *The Analytic S-Matrix*, Cambridge University Press, 1966.

[75] R. Hwa, V. Toeplitz "Homology and Feynman integrals", (Benjamin, New York 1966).

[76] R. Britto, F. Cachazo, B. Feng, E. Witten, "Direct proof of tree-level recursion relation in Yang-Mills theory," Phys. Rev. Lett. **94**, 181602 (2005). [hep-th/0501052].

[77] Z. Bern, L. J. Dixon, D. C. Dunbar and D. A. Kosower, "One loop n point gauge theory amplitudes, unitarity and collinear limits," Nucl. Phys. B **425**, 217 (1994) [hep-ph/9403226].

[78] Z. Bern, L. J. Dixon, D. C. Dunbar and D. A. Kosower, "Fusing gauge theory tree amplitudes into loop amplitudes," Nucl. Phys. B **435**, 59 (1995) [hep-ph/9409265].

[79] R. Britto, "Loop Amplitudes in Gauge Theories: Modern Analytic Approaches," J. Phys. A **44**, 454006 (2011) [arXiv:1012.4493 [hep-th]].

[80] R. K. Ellis, Z. Kunszt, K. Melnikov and G. Zanderighi, "One-loop calculations in quantum field theory: from Feynman diagrams to unitarity cuts," Phys. Rept. **518**, 141 (2012) [arXiv:1105.4319 [hep-ph]].

[81] E. Witten, "Perturbative gauge theory as a string theory in twistor space," Commun. Math. Phys. **252**, 189 (2004) [hep-th/0312171].

[82] N. Arkani-Hamed, F. Cachazo, C. Cheung and J. Kaplan, "The S-Matrix in Twistor Space," JHEP **1003**, 110 (2010) [arXiv:0903.2110 [hep-th]].

[83] I. Bars and S. -H. Chen, "Geometry and Symmetry Structures in 2T Gravity," Phys. Rev. D **79**, 085021 (2009) [arXiv:0811.2510 [hep-th]].

[84] I. Bars, "Survey of two time physics," Class. Quant. Grav. **18**, 3113 (2001) [hep-th/0008164].

[85] L. D. Landau, "On analytic properties of vertex parts in quantum field theory," Nucl. Phys. **13**, 181 (1959).

[86] J. D. Bjorken and S. D. Drell, "Relativistic quantum fields," ISBN-0070054940, McGraw Hill (New York) 1965; J. D. Bjorken, doctoral dissertation, Stanford University, 1959.

[87] S. Coleman and R. E. Norton, "Singularities in the physical region," Nuovo Cim. **38**, 438 (1965).

[88] G. F. Sterman, "Mass Divergences in Annihilation Processes. 1. Origin and Nature of Divergences in Cut Vacuum Polarization Diagrams," Phys. Rev. D **17**, 2773 (1978).

[89] R. Akhoury, "Mass Divergences Of Wide Angle Scattering Amplitudes," Phys. Rev. **D19**, 1250 (1979).

[90] A. Sen, "Asymptotic Behavior Of The Wide Angle On-Shell Quark Scattering Amplitudes In Nonabelian Gauge Theories," Phys. Rev. **D28**, 860 (1983).

[91] J. Botts and G. F. Sterman, Nucl. Phys. B **325**, 62 (1989).

[92] S. -J. Chang and S. -K. Ma, "Feynman rules and quantum electrodynamics at infinite momentum," Phys. Rev. **180**, 1506 (1969).

[93] T. D. Lee and M. Nauenberg, "Degenerate Systems and Mass Singularities," Phys. Rev. **133**, B1549 (1964).

[94] J. C. Collins, D. E. Soper and G. F. Sterman, "Factorization of Hard Processes in QCD," Adv. Ser. Direct. High Energy Phys. **5**, 1 (1988) [hep-ph/0409313].

[95] S. Catani, T. Gleisberg, F. Krauss, G. Rodrigo and J. -C. Winter, "From loops to trees by-passing Feynman's theorem," JHEP **0809**, 065 (2008) [arXiv:0804.3170 [hep-ph]].

[96] I. Bierenbaum, S. Catani, P. Draggiotis and G. Rodrigo, "Feynman's Tree Theorem and Loop-Tree Dualities," PoS LC **2010**, 034 (2010) [arXiv:1011.0585 [hep-ph]].

[97] S. Caron-Huot, "Loops and trees," JHEP **1105**, 080 (2011) [arXiv:1007.3224 [hep-ph]].

[98] L. M. Brown and R. P. Feynman, "Radiative corrections to Compton scattering," Phys. Rev. **85**, 231 (1952).

[99] D.B. Melrose, "Reduction of Feynman diagrams," Il Nuovo Cimento, 40A (1965) 181..

[100] W. L. van Neerven and J. A. M. Vermaseren, "Large Loop Integrals," Phys. Lett. B **137**, 241 (1984).

[101] Z. Bern, L. J. Dixon and D. A. Kosower, "Dimensionally Regulated One Loop Integrals," Phys. Lett. B **302**, 299 (1993) [Erratum-ibid. B **318**, 649 (1993)] [arXiv:hep-ph/9212308].

[102] Z. Bern, L. J. Dixon and D. A. Kosower, "Dimensionally regulated pentagon integrals," Nucl. Phys. B **412**, 751 (1994) [arXiv:hep-ph/9306240].

[103] G. 't Hooft and M. J. G. Veltman, "Scalar One Loop Integrals," Nucl. Phys. B **153**, 365 (1979).

[104] G. J. van Oldenborgh and J. A. M. Vermaseren, "New Algorithms for One Loop Integrals," Z. Phys. C **46**, 425 (1990).

[105] A. Denner, U. Nierste and R. Scharf, "A Compact expression for the scalar one loop four point function," Nucl. Phys. B **367**, 637 (1991).

[106] G. J. van Oldenborgh, "FF: A Package to evaluate one loop Feynman diagrams," Comput. Phys. Commun. **66**, 1 (1991).

[107] T. Hahn and M. Perez-Victoria, "Automatized one-loop calculations in four and D dimensions," Comput. Phys. Commun. **118**, 153 (1999) [arXiv:hep-ph/9807565].

[108] W. Beenakker and A. Denner, "Infrared divergent scalar box integrals with applications in the electroweak standard model," Nucl. Phys. B **338**, 349 (1990).

[109] J. Fleischer, F. Jegerlehner and O. V. Tarasov, dimensions," Nucl. Phys. B **672**, 303 (2003) [arXiv:hep-ph/0307113].

[110] R. K. Ellis and G. Zanderighi, "Scalar one-loop integrals for QCD," JHEP **0802**, 002 (2008) [arXiv:0712.1851 [hep-ph]].

[111] I. Dolgachev, A. Libgober, "On the fundamental group of the complement to a discriminant variety," Algebraic geometry (Chicago, Ill., 1980), pp. 125, Lecture Notes in Math., 862, Springer, Berlin-New York, 1981.

[112] N. Arkani-Hamed, J. L. Bourjaily, F. Cachazo, A. B. Goncharov, A. Postnikov and J. Trnka, arXiv:1212.5605 [hep-th].

[113] A. Libgober "Lectures on topology of complements and fundamental groups".

[114] I. Gelfand, A. Zelevinsky, M. Kapranov, "Discriminants, Resultants, and Multidimensional Determinants".